DOCUMENT RELEASE AND CHANGE FORM

Prepared For the U.S. Department of Energy, Assistant Secretary for Environmental Management
By Washington River Protection Solutions, LLC., PO Box 850, Richland, WA 99352
Contractor For U.S. Department of Energy, Office of River Protection, under Contract DE-AC27-08RV14800

TRADEMARK DISCLAIMER: Reference herein to any specific commercial product, process, or service by trade name, trademark, manufacturer, or otherwise, does not necessarily constitute or imply its endorsement, recommendation, or favoring by the United States government or any agency thereof or its contractors or subcontractors. Printed in the United States of America.

Release Stamp

DATE: Nov 01, 2016

HANFORD RELEASE

1. **Doc No:** RPP-RPT-59344 **Rev.** 00A

2. **Title:** Integrated Disposal Facility Model Package Report: Vadose and Saturated Zone Flow and Transport

3. **Project Number:** T2C24 ☐ N/A

4. **Design Verification Required:** ☐ Yes ☒ No

5. **USQ Number:** ☒ N/A RPP-27195

6. **PrHA Number** **Rev.** ☒ N/A

Clearance Review Restriction Type: undefined

7. **Approvals**

Title	Name	Signature	Date
Clearance Review	RAYMER, JULIA R	*RAYMER, JULIA R*	10/31/2016
Document Control Approval	PARK, ALISON	*PARK, ALISON*	11/01/2016
Originator	LEE, KEARN	*LEE, KEARN*	10/20/2016
Responsible Manager	RUTLAND, PAUL L	*RUTLAND, PAUL L*	10/20/2016

8. **Description of Change and Justification**

Initial Revision – Prepared and checked by INTERA for WRPS
Rev 00A: Remove display of computer and network subdirectory pathways. Fix section numbering in Appendix C. Fix figure call outs in Appendices C & D.

9. **TBDs or Holds** ☒ N/A

10. **Related Structures, Systems, and Components**

a. **Related Building/Facilities** ☒ N/A	b. **Related Systems** ☒ N/A	c. **Related Equipment ID Nos. (EIN)** ☒ N/A

11. **Impacted Documents – Engineering** ☒ N/A

Document Number	Rev.	Title

12. **Impacted Documents (Outside SPF):**

N/A

13. **Related Documents** ☐ N/A

Document Number	Rev.	Title
RPP-RPT-59341	00	Integrated Disposal Facility Model Package Report: ILAW Glass Release
RPP-RPT-59342	00	Integrated Disposal Facility Model Package Report: Non-Glass Release
RPP-RPT-59343	00	Integrated Disposal Facility Model Package Report: Geologic Framework

14. **Distribution**

Name	Organization
BERGERON, MARCEL P	CLOSURE & CORRECTIVE MEASURES
DUNBAR, KATHI J	
LEE, KEARN	HANFORD TOC
RUTLAND, PAUL L	ONE SYSTEM/CTO

EXECUTIVE SUMMARY

The primary mission of *Resource Conservation and Recovery Act of 1976*-permitted Integrated Disposal Facility (IDF) in the 200 East Area is disposal of U.S. Department of Energy low-level wastes and mixed low-level wastes. Following U.S. Department of Energy Order 435.1, *Radioactive Waste Management*, a detailed IDF-specific performance assessment (PA) must be prepared to support the IDF disposal action. This model package report (MPR) documents the development of the three-dimensional (3-D) saturated-unsaturated numerical flow and transport model and its implementation. The MPR, RPP-RPT-59343 "*Model Package Report: Geologic Framework Model for the Integrated Disposal Facility",* serves as the predecessor for development and numerical discretization of the 3-D combined vadose zone/saturated zone model domain. The conceptual model framework for the IDF PA can be divided into key conceptual model components, which include descriptions of the subsystems and associated features, events, and processes as well as assumptions that are important for description of the engineered and natural system. The features, events, and processes applicable to vadose zone and saturated zone flow and transport model are identified, and representative initial estimates for various parameters are documented. Note that the parameter estimates presented in this MPR are for illustration purposes, and may or may not reflect values selected for 2017 IDF PA. Several key topical discussions (i.e., basis for recharge estimates, basis for vadose zone modeling, basis for saturated zone model development and calibration) are included which serve as the groundwork for confidence building and model validation for the groundwater pathway modeling and results. Numerical simulation results based on an example test case are included to illustrate the use of the combined saturated-unsaturated model in PA calculations. Sensitivity and uncertainty results are not included in this MPR, and are part of environmental calculation files that will be prepared in future.

The STOMP (Subsurface Transport Over Multiple Phases)[1] computer code will be used to implement the integrated vadose zone and saturated zone flow and transport model. All inputs and outputs for the development of IDF PA models are required to be submitted to the CH2M HILL Plateau Remediation Company Environmental Model Management Archive to maintain and preserve configuration managed models. Inputs include the input files used in the STOMP simulations and the files called by the input files such as the zonation and boundary node list files. Basis information (the information collected to form the basis for model input parameterization) is also stored in the Environmental Model Management Archive for traceability purposes. Control of all software used to implement the model is directed by the requirements of PRC-PRO-IRM-309, *Controlled Software Management*.

[1] http://stomp.pnnl.gov/index.stm

CONTENTS

1.0 PURPOSE 1-1
1.1 NEED 1-1
1.2 BACKGROUND 1-3
1.3 DOCUMENT ORGANIZATION 1-4
2.0 MODEL OBJECTIVES 2-1
3.0 MODEL CONCEPTUALIZATION 3-1
3.1 Features, Events, and Processes 3-1
3.1.1 Infiltration and Recharge 3-2
3.1.2 Impacts due to vegetation and climate changes. 3-7
3.1.3 Vadose Zone Stratigraphy beneath IDF 3-8
3.1.4 Model Domain and Boundary Conditions 3-9
3.1.5 Vadose Zone and Saturated Zone Flow and Transport 3-9
3.1.6 Geochemistry and Sorption 3-16
3.1.7 Groundwater Concentration, Point(s) of Calculation, Protectiveness Metric, and Timeframe Considerations 3-16
3.2 NATURE AND EXTENT OF CONTAMINATION 3-17
4.0 MODEL IMPLEMENTATION 4-1
4.1 SOFTWARE 4-1
4.2 DISCRETIZATION 4-1
4.2.1 Numerical Model Stability Considerations. 4-4
4.3 PARAMETERIZATION 4-10
4.4 MODEL VALIDATION AND MODEL CALIBRATION 4-16
4.4.1 Basis for Recharge Estimates 4-16
4.4.2 Basis for Vadose Zone Model Development and Its Evaluation 4-16
4.4.3 Basis for Saturated Media Model Development and its Calibration 4-21
4.5 MODEL SENSITIVITY, UNCERTAINTY, AND SCREENING ANALYSES 4-24
4.5.1 Sensitivity Analysis 4-25
4.5.2 Uncertainty Analysis 4-32
4.5.3 Screening Analysis 4-32
5.0 STOMP SOFTWARE 5-1
5.1 STOMP SOFTWARE QUALITY ASSURANCE 5-2
5.2 STOMP CONTROLLED CALCULATION SOFTWARE 5-2
5.3 SOFTWARE INSTALLATION AND CHECKOUT 5-3

5.4 STATEMENT OF VALID SOFTWARE APPLICATION 5-3
6.0 MODEL CONFIGURATION MANAGEMENT 6-1
7.0 MODEL LIMITATIONS.....7-1
8.0 MODEL RECOMMENDATIONS.....8-1
9.0 REFERENCES.....9-1

APPENDICES

Appendix A Features, Events, and Processes .....A-i
Appendix B Vadose Zone Hydraulic Properties and Variable Anisotropy Modeling .....B-i
Appendix C Vadose Zone Macrodispersivity Estimates.....C-i
Appendix D Model Implementation Example Test Case.....D-1

FIGURES

Figure 1-1. Integrated Disposal Facility Current Configuration.....1-2
Figure 1-2. Integrated Disposal Facility Planned Layout Configuration.....1-3
Figure 3-1. IDF Surface Conditions and Conceptual Framework for Recharge Estimation 3-3
Figure 3-2. Schematic Illustrating the Upscaling Concept 3-10
Figure 3-3. Schematic Illustrating Unsaturated Flow Conditions for Low Fluxes in Coarse-Textured Gravelly Media 3-13
Figure 3-4. Measured Saturated Hydraulic Conductivity as a Function of Evolving Length Scale.....3-14
Figure 3-5. Variability of Saturated K Based on Permeameter Tests, Slug Tests, Pumping Tests, and Modeling.....3-15
Figure 4-1. Lateral (X-Y) Model Domain for the Three-Dimensional STOMP Grid. 4-2
Figure 4-2. Hydrostratigraphic Units for the Three-Dimensional STOMP Grid.....4-3
Figure 4-3. West-East and North-South Cross-Sections through IDF Excavation for the Three-Dimensional STOMP Grid.....4-5
Figure 4-4. West-East Cross-Sections for the Three-Dimensional STOMP Grid. 4-6
Figure 4-5. North-South Cross-Sections for the Three-Dimensional STOMP Grid. 4-7
Figure 4-6a. Distribution of H3 and RE Formation at (a) 119.5 m Elevation (b) 114.5 m Elevation (1 of 2 sheets). 4-8
Figure 4-7. Location of the Sisson and Lu Injection Test Site and the Integrated Disposal Facility in 200 East Area.....4-18

Figure 4-8. The Observed and Simulated Center of Mass in the Vertical (z) Direction. 4-20

Figure 4-9. The Observed and Simulated Center of Mass in the Vertical (z) Direction. 4-21

Figure 4-10. The Observed and Simulated Center of Mass in the Vertical (z) Direction. 4-22

Figure 4-11. Spreading of the Moisture Plume in (a) x (Easting), (b) y (Northing), and (c) z (Vertical) Directions Based on the Diagonal Components of the Second Moments.....4-23

Figure 4-11. Location of the Paleochannel Associated with the Ancestral Columbia River near the IDF Site. 4-26

Figure 4-12. Digital Photo Log for Borehole 299-E27-4 with an Expansion Showing the Open-Framework Gravel above and below the Water Table. 4-27

Figure 4-13. Model-Calibrated Saturated Hydraulic Conductivity Values using the Central Plateau Groundwater Model Version 6.3.3. 4-28

Figure 4-14. Comparison of (a) Measured versus Simulated Water Levels, and (b) Probability Density of Water Elevation Misfits for the Central Plateau Groundwater Model. 4-29

Figure 4-15. Location of Wells near IDF site for Comparison of Measured versus Simulated Water Levels. 4-29

Figure 4-16. Comparison of Measured versus Simulated Water Levels for Wells near the IDF Site. 4-30

Figure 4-17. Comparison of Groundwater Mounding Effects from Discharges in the 200 West Area and 200 East Area. 4-31

Figure 4-18. Simulated Moisture Difference Between Cap Drainage Simulation and Background Recharge Simulation at 0.9 mm/y with High Anisotropy (West-East Section). 4-33

Figure 4-19. Simulated Moisture Difference Between Cap Drainage Simulation and Background Recharge Simulation at 0.9 mm/y with High Anisotropy (North-South Section). 4-34

Figure 4-20. Simulated Moisture Difference Between Cap Drainage Simulation and Background Recharge Simulation at 5.0 mm/y with High Anisotropy (West-East Section). 4-35

Figure 4-21. Simulated Moisture Difference Between Cap Drainage Simulation and Background Recharge Simulation at 5.0 mm/y with High Anisotropy (North-South Section). 4-36

TABLE

Table 4-1. Summary of Key Elements and Representative Parameters Associated with Site-Specific Model Components for IDF PA (6 sheets).....4-10

TERMS

2-D	two dimensional
3-D	three dimensional
BTC	breakthrough curves
CFR	*Code of Federal Regulations*
CHPRC	CH2M HILL Plateau Remediation Company
COPC	constituent of potential concern
CPGWM	Central Plateau Groundwater Model
DOE	U. S. Department of Energy
EHM	equivalent homogeneous media
EIS	environmental impact statement
EMCF	environmental model calculation file
EMMA	environmental model management archive
EPA	U. S. Environmental Protection Agency
ERDF	Environmental Restoration Disposal Facility
FEP	feature, event, or process
GFM	geologic framework model
GOSPL	geographic and operational site parameters list
H1	Hanford formation facies
HA	high anisotropy
HSU	hydrostratigraphic unit
IA	Intermediate Anisotropy
IAEA	International Atomic Energy Agency
IDF	Integrated Disposal Facility
ILAW	immobilized low-activity waste
ISO	isotropic
K_d	distribution coefficient
LA	low anisotropy
MPR	model package report
NAVD88	North American Vertical Datum of 1988
ORP	Office of River Protection
PA	performance assessment

PA-TCT	power averaging-tensorial connectivity tortuosity
PHB	prototype Hanford barrier
PNL	Pacific National Laboratory
PNNL	Pacific Northwest National Laboratory
QA/QC	quality assurance/quality control
RCRA	Resource Conservation and Recovery Act
RE	Ringold E
RETC	retention curve (software)
ROD	record of decision
STOMP	Subsurface Transport Over Multiple Phases (software)
SZ	saturated zone
TC&WM EIS	Tank Closure & Waste Management Environmental Impact Statement
TCT	tensorial-connectivity tortuosity
VZ	vadose zone
WCH	Washington Closure Hanford
WRPS	waste treatment plant
WRPS	Washington River Protection Solutions, LLC

1.0 PURPOSE

The Integrated Disposal Facility (IDF) vadose and saturated zone flow and transport model evaluates the movement of water, radionuclides, and chemicals released from the near-surface disposal facility to a point of regulatory compliance. The model will be used to perform the vadose zone and saturated zone flow and transport calculations for the performance assessment (PA) for the facility. U.S. Department of Energy (DOE) Order 435.1, *Radioactive Waste Management,* dictates that the DOE radioactive waste management activities shall protect the public from exposure to radiation from radioactive materials, protect the environment, and comply with applicable Federal, State, and local laws and regulations, and to any applicable Executive Orders and other DOE directives. The PA is the modeling activity used to assess whether or not there is reasonable assurance that the facility will provide the necessary levels of protection. DOE M 435.1-1, *Radioactive Waste Management Manual*, identifies specific performance objectives as well as other performance-related factors that need to be considered in the PA.

This model package report (MPR) describes the flow and transport models for the vadose and saturated zones beneath the IDF. This MPR complements three other MPRs supporting the 2017 IDF PA. Together, the four MPRs address the Immobilized Low-Activity Waste (ILAW) glass source term, the non-glass source term, the hydrostratigraphy in the vadose and saturated zones beneath the IDF, and flow and transport in the vadose and saturated zones beneath the IDF to the accessible environment. The suite of MPRs being developed for the 2017 IDF PA include the following:

- RPP-RPT-59341, *Integrated Disposal Facility Model Package Report: ILAW Glass Release*
- RPP-RPT-59342, *Integrated Disposal Facility Model Package Report: Non-Glass Release*
- RPP-RPT-59343, *Integrated Disposal Facility Model Package Report: Geologic Framework*
- RPP-RPT-59344, *Integrated Disposal Facility Model Package Report: Vadose and Saturated Zone Flow and Transport*

The PA will be developed using the models described in these MPRs and the calculations that will be documented in Environmental Model Calculation Files (EMCF).

1.1 NEED

The primary mission of the *Resource Conservation and Recovery Act of 1976* (RCRA)-permitted IDF (Figure 1-1) in the 200 East Area is disposal of DOE low-level wastes and mixed low-level wastes. Following DOE Order 435.1, a detailed IDF-specific PA must be prepared to support the IDF disposal action. An initial PA for an ILAW disposal facility was developed in 1998 (DOE/RL-97-69, *Hanford Immobilized Low-Activity Tank Waste Performance Assessment*) and revised in 2001 (DOE/ORP-2000-24, *Hanford Immobilized Low-Activity Tank Waste Performance Assessment: 2001 Version*). A related risk assessment was completed in 2003 (RPP-17675, *Risk Assessment Supporting the Decision on the Initial Selection of Supplemental ILAW Technologies*). The 2001 PA has been maintained under an approved maintenance plan (DOE/ORP-2000-01, *Maintenance Plan for the Hanford Integrated Disposal Facility*

Performance Assessment) as required by DOE M 435.1-1 and through annual status reports (e.g., DOE/RL-2012-57, *Annual Summary of the Integrated Disposal Facility Performance Assessment 2012*).

Figure 1-1. Integrated Disposal Facility Current Configuration.

Source: RPP-20691, *Facility Data for the Hanford Integrated Disposal Facility Performance Assessment*

Note: View is to the south. The current configuration represents Phase 1 of the IDF with future expansion planned to the south (upper portion of figure). Cell 1 is to the west (right side of figure) and Cell 2 is to the east (left side of figure). Cell 1 is included in the current IDF permit (WA7 89000 8967, Part III Operating Unit 11). The two circular features on the north of the facility are the storage tanks for the leak collection and recovery systems associated with Cell 1 and Cell 2. The shine berm to shine berm east to west width of the current configuration 421.8 m while the width at the floor of the facility is 330 m. Plans for future expansion of the facility are to the south in the direction of the east-west trending inactive longitudinal sand dunes.

Revision of the ILAW PA has been deferred since 2005, pending issuance of the Final Tank Closure and Waste Management Environmental Impact Statement (TC&WM EIS), which was issued in 2012 (DOE/EIS-0391, *Final Tank Closure and Waste Management Environmental Impact Statement for the Hanford Site, Richland, Washington*). The associated Record of Decision for TC&WM EIS (78 FR 75913, "Record of Decision: Final Tank Closure and Waste Management Environmental Impact Statement for the Hanford Site, Richland, Washington") was issued on December 6, 2013. Based on guidance from DOE to ensure consistency with the modeling work reported in the TC&WM EIS, work on a revised PA can now be performed following the phased approach provided in Memorandum DOE 2012, "Modeling to Support Regulatory Decision making at Hanford." Because of changes to the facility mission and design,

as well as new information collected since the previous PA efforts, the 2017 IDF PA will be a new PA, rather than an update to the previous PAs.

1.2 BACKGROUND

Construction of the IDF was initiated in 2004 and the initial phase of construction consisting of the first two cells, including the initially permitted Cell 1, was completed in 2006 (Figure 1-1). The planned build out of the IDF is illustrated in Figure 1-2. The current Dangerous Waste Permit for the IDF (WA7 89000 8967, Part III Operating Unit 11, Rev. 3) and associated amendments restrict the scope of the permit to the landfill construction and operation as necessary to dispose of immobilized low activity waste from the Waste Treatment Plant, and the Demonstration Bulk Vitrification System and IDF operational waste. Future expansion of the RCRA trench, or disposal of other wastes not specified in the current permit, is prohibited unless authorized via modification of the permit (WA7 89000 8967, Part III Operating Unit 11 Unit Specific Conditions II.11.B.3).

To operate IDF, DOE must complete the remaining regulatory steps, including a performance assessment and a waste incidental to reprocessing determination as required by DOE M 435.1, and a permit modification pursuant to the *Resource Conservation and Recovery Act of 1976*.

Figure 1-2. Integrated Disposal Facility Planned Layout Configuration

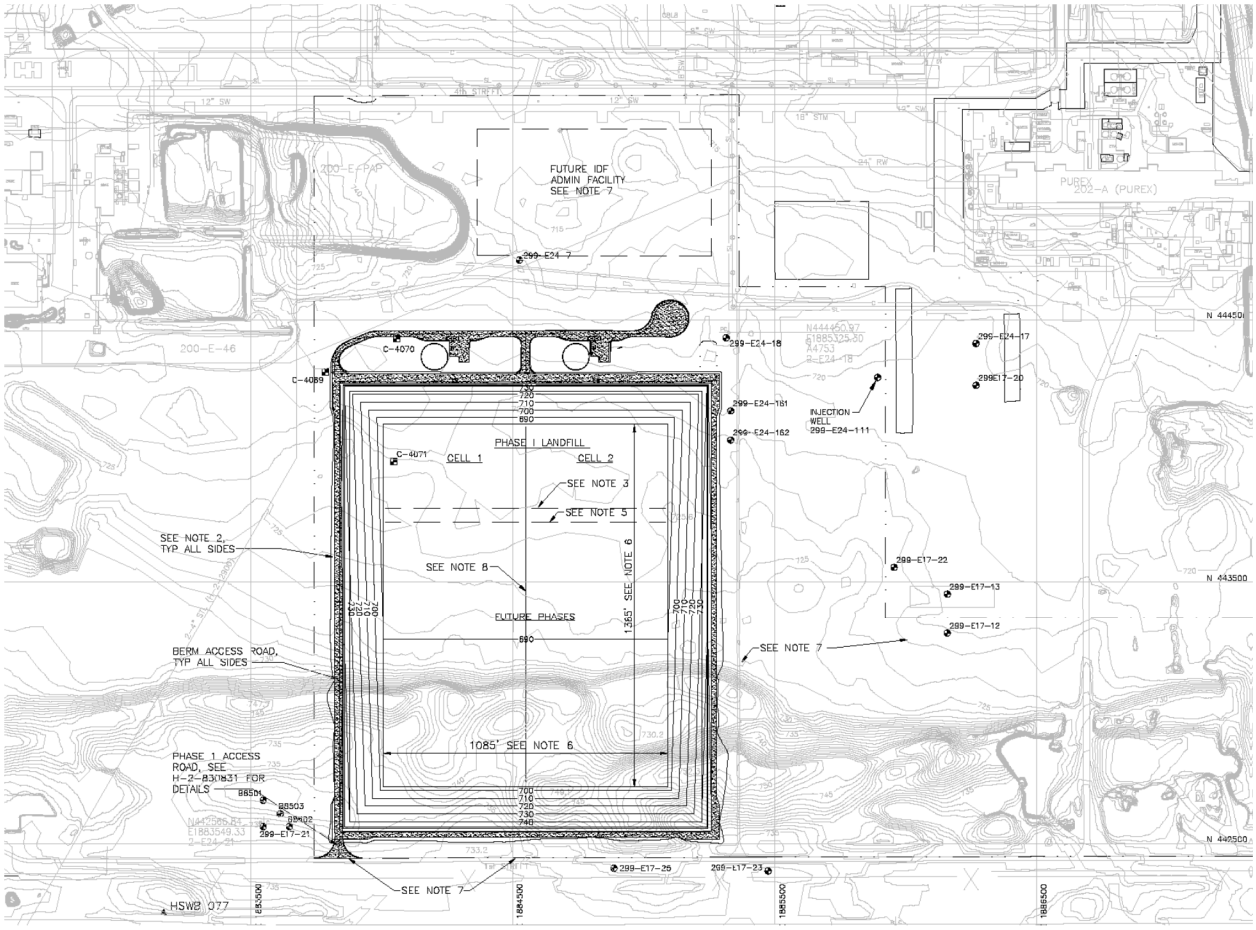

Source: RPP-20691, *Facility Data for the Hanford Integrated Disposal Facility Performance Assessment*

1.3 DOCUMENT ORGANIZATION

The model report package is organized into three basic parts: (1) basis for development of the model, including the identification of objectives; (2) software qualifications; and (3) model implementation. Section 2 presents the modeling objectives. Section 3 presents the model conceptualization and modeling assumptions used in the 3-D combined vadose zone/saturated zone (VZ/SZ) model. Section 4 describes the modeling implementation details, discretization, boundary extents and representative compliance parameter estimates. Section 5 discusses the use of the STOMP (Subsurface Transport Over Multiple Phases)[2] software quality assurance/quality control details. Section 6 identifies the limitations of the model, and the applicability of the results, and Section 7 provides the details related to configuration management of the model inputs and outputs including the software used.

[2] http://stomp.pnnl.gov/index.stm

2.0 MODEL OBJECTIVES

The modeling objectives of the IDF PA are summarized in RPP-PLAN-60324, *Integrated Disposal Facility (IDF) Performance Assessment Project Execution Plan*. As summarized in RPP-PLAN-60324, the 2017 IDF PA process will provide an integrated set of analyses to support regulatory decision making by the relevant cooperating agencies. The PA will provide decision makers with information about the potential future impacts of various waste disposal configurations for the IDF as well as to prioritize additional engineering and scientific studies to address the uncertainty in the forecast performance. The 2017 IDF PA will use and build upon the existing knowledge base and supplement the existing knowledge base with new, updated information relevant to modeling the long-term performance of the IDF. As additional information is developed, future revisions will provide the basis for ongoing regulatory compliance and eventual closure actions. In addition to evaluating the long-term performance of the IDF, the 2017 IDF PA will develop the risk assessment information needed to support the modification of RCRA Permit (WA7 89000 8967, *Hanford Facility Resource Conservation and Recovery Act Permit, Dangerous Waste Portion Revision 8C for the Treatment, Storage, and Disposal of Dangerous Waste*).

This model package focuses on the conceptual framework of the three-dimensional (3-D) combined saturated/unsaturated numerical flow and transport model and its implementation. The following IDF PA model components provide input to the VZ/SZ model.

- The Leapfrog[3] Geo 3D modeling software framework model providing the hydrostratigraphic features in the VZ and SZ within the IDF and the vicinity
- The near field hydrology model provides input on recharge at the base of IDF liner and around margins of IDF cap; these are expected to change with time due to degradation of features in cap and liner
- The ILAW glass release model and the non-glass release model providing contaminant fluxes at the base of the liner
- The Central Plateau groundwater flow model providing time-dependent groundwater fluxes and hydraulic heads which may change with time.

The 3-D combined VZ/SZ modeling results to be provided include, for example:

- Spatial and temporal variation of moisture content within the VZ
- Spatial and temporal variation of Darcian flux within the VZ
- Advective-dispersive transport within the VZ based on releases to VZ provided by near-field release models
- Spatial and temporal variation of specific discharge within the SZ
- Advective-dispersive transport in the SZ to 100 m point of calculation

[3] Leapfrog is a registered trademark of ARANZ Geo Limited, LLC, Christchurch 8140, New Zealand. http://www.leapfrog3d.com

Type of uncertainties to be addressed include, for example:

- Net infiltration/recharge through base of liner/top of VZ, around boundaries of IDF closure surface barrier (cap), and in undisturbed areas beyond cap
- Releases from near-field model
- VZ hydraulic properties
- Clastic dikes and other heterogeneous features (i.e., paleosol) within the VZ
- Specific discharge within the SZ.

3.0 MODEL CONCEPTUALIZATION

3.1 FEATURES, EVENTS, AND PROCESSES

The features, events, and processes (FEP) approach that has been developed in the international community (NEA 02549, *Features, Events, and Processes [FEPs] for Geologic Disposal of Radioactive Waste, an International Database*; and IAEA 2004, *Safety Assessment Methodologies for Near Surface Disposal Facilities, Vols. 1 and 2*) and used for waste management processes in the United States is considered for IDF PA. Appendix A presents the FEPs table; the FEPs applicable to vadose zone and saturated zone flow and transport model are identified (highlighted yellow) in the table. The IDF physical system being conceptualized and modeled is described in RPP-20691, *Facility Data for the Hanford Integrated Disposal Facility Performance Assessment*.

The conceptual model framework for the IDF PA can be divided into key conceptual model components, which include descriptions of the subsystems and associated FEPs and assumptions that are important for description of the engineered and natural system. The key conceptual model components include the following:

- Infiltration and recharge
- Geologic setting
- Model domain and boundary conditions
- Geochemistry and sorption
- Vadose zone and saturated zone flow and transport
- Groundwater concentration
- Post-closure inventory and source term

These conceptual model components are consistent with those identified in EPA guidelines for the evaluation of the protection of groundwater pathway (EPA 402-R-94-012, *A Technical Guide to Ground-water Model Selection at Sites Contaminated with Radioactive Substances*; Luftig and Weinstock 1997, "Establishment of Cleanup Levels for CERCLA Sites with Radioactive Contamination"; HNF-5294, *Computer Code Selection Criteria for Flow and Transport Code(s) to Be Used in Vadose Zone Calculations for Environmental Analyses in the Hanford Site's Central Plateau*). Due to limited data and information pertaining to each model component, certain assumptions have to be made. These assumptions, as appropriate, are discussed below for each model component.

In addition to assumptions, parameter estimates are included in the following discussion in order to provide the reader with a sense of some of the key inputs to the VZ/SZ flow and transport model. Given the temporal and spatial scale of the VZ/SZ flow and transport model and the limited number of nearby boreholes with which to constrain these models, not to mention the effects that the IDF engineered features will impose on the VZ flow regime under and around the IDF, there is considerable uncertainty in the parameter values necessary to populate the VZ/SZ flow and transport model. As a result, the following discussion presents some representative initial parameter ranges as well as a brief discussion of the parameter values used in the TC&WM EIS. However, it should be remembered that final parameter values to be used in the VZ/SZ flow and transport model will be developed and justified in the EMCFs associated with

this MPR along with a range of calculations to illustrate the significance of these uncertainties on the projected performance of the VZ and SZ features of the IDF PA.

3.1.1 Infiltration and Recharge

The recharge conceptual model component typically has a large impact on the results, especially with respect to long-term recharge rates such as those associated with IDF post-closure conditions. The groundwater concentration depends on the mass flux of the contaminant into the groundwater, which depends, in part, on the recharge entering the engineered barrier, the vadose zone, and the underlying aquifer. The primary assumptions associated with the use of recharge rate values concern those values associated with future post-closure conditions for the IDF. For all time periods, net infiltration through the ground surface is represented by an average recharge rate, which is dependent on surface conditions.

A cap or surface barrier (Figure 3-1) is an important engineered component for post-closure conditions at the IDF. Once it is emplaced, the surface barrier performance directly impacts the amount of moisture percolating into the waste and the underlying vadose zone.

The surface barrier is designed to provide containment and long-term hydrologic protection for a period of at least 500 years (DOE/RL-93-33, *Focused Feasibility Study of Engineered Barriers for Waste Management Units in the 200 Areas*). It is assumed that institutional controls prevent intrusion into the waste for at least 100 years and that passive controls prevent intrusion for 500 0years. The design accounts for human and bio-intrusion control and includes a silt loam moisture storage unit, a capillary break to enhance the moisture storage capacity of the silt, and a geomembrane with a geocomposite drainage layer. Furthermore, it is assumed that because the IDF waste is covered with at least 4.6 m of cover materials, intrusion into the waste due to excavation is precluded. It is also assumed that a surface barrier (RCRA barrier) will be degraded after 500 years so that the recharge through the barrier is similar to that through the undisturbed soil.

For time periods with extant liners under the IDF, it is assumed that all leachate is retained by the high-density polyethylene liner and removed by the leachate collection system. The liners and leachate collection system are assumed to be extant during the entire first 100 years post-closure. The liner is assumed to fail after 100 years. The liner failure is assumed to be contiguous through its full areal extent; the impact of such an assumption will be explored with calculations to be presented in EMCFs associated with the VZ/SZ flow and transport model.

The key assumptions associated with the infiltration/recharge component include the following:

- During the construction period, the disturbed zone around the facility has no vegetation cover, but “mature shrub steppe” vegetation will reclaim the surface during the subsequent 100-year institutional control period.

Figure 3-1. IDF Surface Conditions and Conceptual Framework for Recharge Estimation

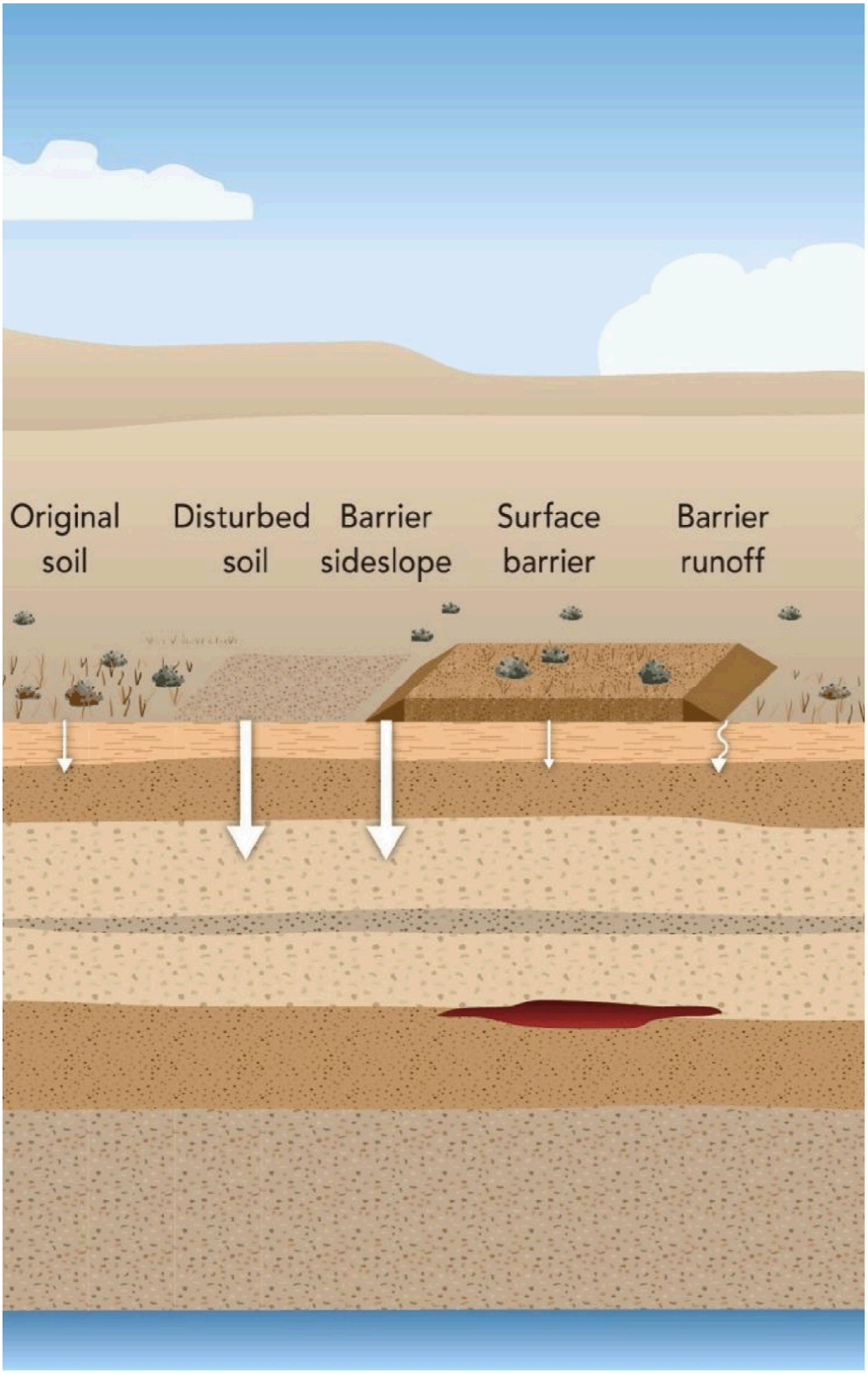

Note: The arrows are indicative of relative magnitude of fluxes.

- During the 500-year design life of the surface barrier, the average net infiltration rate is set at 0.5 mm/yr, and then it is expected to increase for the remainder of the simulation by assuming degraded capability of surface barrier. This is deemed to be a slightly conservative assumption because PNNL-14744, *Recharge Data Package for the 2005 Integrated Disposal Facility Performance Assessment*, indicates that the expected performance for such a barrier is on the order of 0.1 mm/yr for the life of the barrier. They also conclude that, with appropriate design considerations, the possibility of the most likely natural failure mechanisms (i.e., biointrusion of the silt loam layer, wind erosion, and accretion of windblown sand) to occur is quite low, and that the emplaced silt-loam soils are expected to perform as designed indefinitely.
- Side slopes of surface barrier are assumed to be made of compacted silty soil and assumed to have enhanced recharge, compared to top portion of the surface barrier.
- Long-term recharge estimates are primarily based on porewater chloride concentration data from IDF boreholes and other boreholes located in the 200 Area (PNNL-14744). Chloride mass balance calculations factor in variations in past precipitation over long time periods (past several thousand years) and can be used to estimate the future recharge conditions.
- Revegetation of the surface barrier and land impacted by construction with native plants (e.g., sagebrush [Artemisia tridentate] and small bunchgrasses [*Elymus wawawaiensis* and *Poa secunda*]) is assumed to be successful. Revegetation of the land is specifically required, for example, by the Record of Decision (ROD) for the nearby Environmental Restoration Disposal Facility (ERDF), along with other measures to mitigate the ecological impacts caused by construction of the IDF, including restoration of the site. According to the Shrub-Steppe and Grassland Restoration Manual for the Columbia River Basin (Benson et al. 2011), restoration assists the recovery of an ecosystem that has been degraded, damaged, or destroyed, with the intent to return it to its historic condition. The manual includes the technical information necessary to successfully plan and execute habitat restoration projects for shrub-steppe habitat.

3.1.1.1 Spatial and Temporal Recharge Rates at IDF. Results from more than three decades of work are available on meteoric recharge estimates at the Hanford Site. Infiltration (recharge) can vary greatly depending on factors such as climate, vegetation, surface condition, and soil texture. Studies conducted over the last decade at the Hanford Site (Gee et al. 1992, "Variations in Recharge at the Hanford Site;" PNNL-11367, *Hanford Prototype-Barrier Status Report: FY 1996*; Wing and Gee 1994, "Quest for the Perfect Cap"; PNNL 10285, *Estimated Recharge Rates at the Hanford Site*; Fayer et al. 1996, "Estimating Recharge Rates for a Groundwater Model Using a GIS;" PNNL-11463, *A Comprehensive Analysis of Contaminant Transport in the Vadose Zone Beneath Tank SX-109*; PNNL-13033, *Recharge Data Package for the Immobilized Low-Activity Waste 2001 Performance Assessment*) suggest that recharge rates can vary from less than 0.1 mm/yr on a variety of soil and vegetative combinations to greater than 130 mm/yr on bare basalt outcrops or bare, gravel-covered waste sites (Gee et al. 1992). Detailed experimental work has also been performed on infiltration rates through surface barriers (PNNL-14744, *Recharge Data Package for the 2005 Integrated Disposal Facility Performance Assessment*) and discussed in PNNL-16688, *Recharge Data Package for the Hanford Single-Shell Tank Waste Management Areas*.

Recharge is different than most other parameters because the values change in time and space and depend on certain assumptions about decisions made and conditions in the future. For the IDF PA, the recharge rates can be divided into four distinct time periods, noted as follows, representing different surface conditions consistent with the variable conditions expected for the facility. The recommended estimates are based on PNNL-14744, WCH-520, *Performance Assessment for the Environmental Restoration Disposal Facility, Hanford Site, Washington* (hereinafter referred to as ERDF PA), and the preceding supporting studies:

- Recharge Estimates for Pre-Construction Condition
- Recharge Estimates During Construction
- Early Post-Closure and a Functioning Surface Barrier
- Late Post-Closure and a Degraded Surface Barrier

3.1.1.2 Recharge Estimates for Pre-Construction Condition. Recharge estimates for conditions prior to IDF construction are based on correlations of soil types and infiltration characteristics of the native soils. PNNL-14744 and PNNL-16688 provide recharge estimates for areas that remain natural and undisturbed in the central plateau portion (200 Area) of the Hanford Site. Recharge estimates are presented for various soil-vegetation combinations and are based on tracer method (primarily evaluation of chloride profiles from various boreholes), lysimeter data, and detailed numerical simulations. Data supporting these recharge estimates for the 200 East and 200 West Areas soils are also summarized in PNNL 14725, *Geographic and Operational Site Parameters List (GOSPL) for the 2004 Composite Analysis*.

Note that the definition of the “base case” or “compliance case” or “best estimate case” or “reasonably conservative case” for purposes of the 2017 IDF PA document are beyond the scope of this MPR. Although initial parameter estimates are presented, they are for illustration purposes and may or may not reflect values selected for 2017 IDF PA.

For ERDF PA, the compliance case infiltration rate representative of pre-construction conditions was assumed to be 1.7 mm/yr. This was chosen based on the recommended recharge rate by PNNL-16688 for Rupert sand soil type with mature shrub-steppe vegetation cover (representative of IDF).

3.1.1.3 Recharge Estimates During Construction. Because a double liner with leachate collection system is emplaced during the construction phase and gradually extended over the facility to collect any precipitation and dust-suppression water, the recharge rate estimate underneath the IDF cells (construction area) is expected to be negligibly small. Water or recycled leachate is employed to minimize any potential dust generation in IDF during waste placement activities. For an initial estimate, a recharge rate of zero is conceivable for the IDF area during the construction period; however, such an assumption will be evaluated as part of the EMCF calculations. It should be noted, however. that because the first 100-year period is relatively short in comparison to the simulation duration (at least 1,000 years and up to 10,000 years), this input parameter is not likely to have a significant impact on the long-term IDF PA flow and contaminant transport simulations.

3.1.1.4. Early Post-Closure and a Functioning Surface Barrier. Current plans are to use a modified RCRA-compliant closure cover for IDF, which is expected to be at least 4.6 m thick. The current pre-conceptual design for the modified RCRA-compliant surface barrier is based on

DOE/RL 94-47, *Proposed Plan for ERDF at Hanford Site*, and includes cover vegetation, admixture of silt and gravels, geomembrane, and compacted clay admix over the grading fill layer. The silt with gravel admix layer provides for moisture storage and allows evapotranspiration to occur before deep percolation can occur. It also enhances the resistance to burrowing animals and wind erosion. The geomembrane and compacted clay admix layers impede moisture flow across their interfaces.

Extensive laboratory and modeling work and limited field testing of surface barriers have been performed; results are summarized in PNNL-14744. Lysimeter testing has been performed for different surface barrier concepts including a Modified RCRA Subtitle C Barrier with silt loam layers having depths between 1 and 2 m. Lysimeter data from the prototype Hanford barrier (Wing and Gee 1994) have also been collected and analyzed. Finally, modeling has been performed to address potential climate change impacts and no vegetation impacts on surface barrier performance.

The lysimeter drainage data that have been collected since 1989 suggest that the recharge rate beneath surface barriers having at least 1 m of silt loam is zero under ambient precipitation conditions. Most of these lysimeters did not contain an asphalt layer. Simulation results reported in PNNL-14744 investigated the sensitivity of the lysimeter data to climate change, silt loam hydraulic properties, vegetation changes, erosion, and dune formation above the surface barrier. Results indicated that the performance of these surface barriers was robust in that the estimated recharge rates remained below 0.1 mm/yr. For the cases investigated, only in the case of dune formation and no vegetation on the surface barrier were the simulated recharge rates above 0.1 mm/yr.

Based on a review of the results, as stated earlier, PNNL-14744 recommends an expected recharge performance for surface barrier with at least 1 m of silt loam above a gravel layer to be on the order of 0.1 mm/yr for the life of the barrier. This estimate did not take any credit for the asphalt layer that is part of the Modified RCRA Subtitle C Barrier design.

The final design for the IDF surface barrier has not been developed; however, based on the extensive testing reported in PNNL-14744, surface barriers that will limit recharge rates are achievable. For a fully functioning barrier for the early closure period for 500 years, a recharge rate of 0.5 mm/yr is proposed. This is consistent with estimates used in TC&WM EIS and ERDF PA. For the IDF closure barrier undisturbed zone (Rupert sand with vegetation), the initial infiltration rate is proposed as 1.7 mm/yr, as was used in ERDF PA. The compliance value for the barrier side slopes (compacted silt) for ERDF PA was based on the best estimate of 1.9 mm/yr (recommended by PNNL-16688) and rounded to 2 mm/yr.

3.1.1.5 Late Post-Closure and a Degraded Surface Barrier. For a degraded surface barrier, a range of potential recharge rates can be envisioned. PNNL-14744 investigated the possibility of the most likely natural failure mechanisms (i.e., bioturbation of the silt loam layer, wind erosion, and accretion of windblown sand). With appropriate design considerations, PNNL-14744 presents an argument that the failure possibility of these natural systems is quite low, and the emplaced silt-loam soils will continue to perform for as long as they remain in place. Based on these arguments, it is concluded that the long-term effectiveness of the surface barrier would continue to limit recharge rates to less than 0.1 mm/yr for thousands of years (PNNL-14744).

Since the final design for the surface barrier has not been developed and it is difficult to defend the continued performance of a surface barrier for long periods of time, the IDF closure barrier is

expected to maintain the recharge rate (i.e., barrier design goal) at or below 0.5 mm/yr for 500 years. For ERDF PA, at the end of 500 years, the top portion of the closure barrier was assumed to degrade to permit an infiltration rate of 1.0 mm/yr and maintain that infiltration rate for the remainder of the simulation for the compliance case; the degraded side slopes with vegetation were assumed to maintain a compliance value of 2.0 mm/yr. Following PNNL-14744 and ERDF PA, for the closure barrier undisturbed zone (Rupert sand with vegetation), the representative IDF PA infiltration rate is recommended as 1.7 mm/yr. PNNL-14744 suggested 0.9 mm/yr as an upper-bound recharge rate for the degraded surface barrier for IDF. The TC&WM EIS used 0.9 mm/yr for the degraded barrier; this value was chosen to be equivalent to the best estimate for recharge in undisturbed Rupert Sand and Burbank Loamy Sand (PNNL-14744). The underlying assumption was that the upper-bound recharge from the degraded surface barrier would approach the expected recharge of undisturbed soil. Following PNNL-14744, for the IDF PA, the recommended upper range value is 2 mm/yr (0.78 in./yr), which is comparable to the best estimate for undisturbed vegetated Rupert Sand (1.7 mm/yr) and Burbank Loamy Sand (1.9 mm/yr [0.67 in./yr]), as presented in PNNL-16688, based on information from PNNL-14744 and other studies. These upper-bounding values are considered sufficient to accommodate the increased uncertainty in the weather cycles and changes in the fire cycle during the period after the design life of the barrier.

3.1.1.6 Representative Initial Recharge Estimates for IDF PA. Section 4 summarizes various timelines and the corresponding initial estimates of recharge for a variety of surface conditions (e.g., undisturbed, disturbed, cells under construction, fully functional barrier, and degraded barrier).

3.1.2 Impacts due to vegetation and climate changes.

The vegetation on the surface barrier and surrounding area is assumed to remain shrub-steppe indefinitely after closure of the IDF, and exert the same control on recharge that it has in the past. If the estimates of the mean annual precipitation during the past 75,000 years, which range from 50 percent below to 128 percent above modern levels (BHI-00007, *Prototype Hanford Surface Barrier: Design Basis Document*) are indicative and inclusive of future conditions, then the anticipated changes in precipitation rates and patterns resulting from changes in the local climate do not appear to be substantial enough to change the dominant shrub-steppe vegetation or its characteristic ability to control recharge.

Over the period of evaluation considered in this study (1,000 to 10,000 years post-closure), severe climatic change is not expected. The next glaciation period has been estimated to occur tens of thousands of years into the future. The wet and dry cycles that have occurred over the past 10,000 years will likely continue over the next 10,000 years (see Section 2.2.5 of DOE/ORP-2000-24). The variations in the recharge in the future (over next 10,000 years) are therefore expected to be about the same as that of the past. This all assumes that the human disturbances are minimal.

As reported in ERDF PA, the Columbia Basin appears to be in an interglacial cooling period that began approximately 6,000 years ago and is expected to continue for the next 5,000 to 10,000 years (PNL-10788, *The Role of Plants and Animals in Isolation Barriers at Hanford, Washington*). While human activity may influence the change in climate, it cannot prevent the ultimate onset of the next ice age (PNL-10788). A 75,000 plus-year pollen record from Carp Lake (i.e., southwest of the Hanford Site) near Goldendale, Washington, provides evidence for

estimates that the mean annual precipitation in the Columbia River Basin ranged between 0.5 times of modern level and 1.28 times of modern level (BHI-00007). For the majority of the pollen record (almost 65,000 years out of the 75,000 years), the climate in the Columbia Basin was drier (i.e., averaged less than 160 mm/yr) than the present day Hanford climate. Based on the Carp Lake data, it was concluded that there is no evidence that the long-term precipitation average ever reached three times of modern levels, which has been taken as the upper bounding annual amount to test the prototype barrier (BHI-00007).

It should be that the current annual precipitation at the Hanford Site (242 mm) is within the range associated with sagebrush-dominated ecosystems (200 to 500 mm/yr[4]). Therefore, a 1.28 times increase in the annual precipitation increases the annual amount to 310 mm/yr, which is still lower than the average (i.e., 350 mm/yr) of the range (200 to 500 mm/yr). The water usage cycle of sagebrush, its ability to photosynthesize very early in the spring, mine water at depth, and curtail its photosynthetic activity and shed leaves to reduce moisture loss during the summer give it an adaptive advantage over sod-forming grasses. These characteristics also allow it to coexist with Pacific Northwest bunchgrasses that are ideally suited to take advantage of the secondary spring maxima, and then die back during the summer drought (PNL-10788).

3.1.3 Vadose Zone Stratigraphy beneath IDF

The hydrostratigraphic framework, discussed below, for the IDF site and vicinity is based on the Leapfrog framework model described in RPP-RPT-59343.

The H2 (sand-dominated) and H3 (gravel-dominated) units are the two predominant hydrostratigraphic units within the IDF vadose zone; the less extensive gravel-dominated Ringold E is also part of the unsaturated media. Also, clastic dikes (sub-vertical linear features composed of layers of differing particle size distributions), can occur within the vadose zone and can cross cut the major sedimentary units. The hydraulic properties for IDF PA are defined by the hydrostratigraphic units (HSUs) H2, H3, and Ringold E (RE).

3.1.3.1 H2 Sand-dominated facies. This facies consists of fine- to coarse-grained sand and granule gravel with sparse layers of Cascade ash deposits. The sands typically have high basalt content and are commonly referred to as black, gray, or salt-and-pepper sands (DOE/RL-2002-39, *Standardized Stratigraphic Nomenclature for Post-Ringold Formation Sediments Within the Central Pasco Basin*). They may contain small pebbles and rip-up clasts, pebble-gravel interbeds, and silty interbeds less than 1 m thick. The silt content of the sands is variable, but where the silt is low a well-sorted texture is common. The sand facies was deposited adjacent to main flood channel ways during the waning stages of the cataclysmic floods of the Pleistocene age. The facies is transitional between the gravel-dominated facies and the interbedded sand- and silt dominated facies.

3.1.3.2 H3 Gravel-dominated facies. This facies generally consists of coarse-grained basaltic sand and granule to boulder gravel (DOE/RL-2002-39). Many exposures on the Hanford Site (e.g., various burrow pits) show that these deposits typically have an open framework texture, massive bedding, plane to low-angle bedding, and large-scale planar cross bedding in outcrop. The gravel-dominated facies was deposited by high-energy floodwaters in or immediately adjacent to the main cataclysmic flood channel ways.

---

[4] U.S. Department of Agriculture, Natural Resources Conservation Service, *Fact Sheets & Plant Guides, Artemisia tridentata ssp. tridentate.* http://plants.usda.gov/plantguide/pdf/pg_artrt.pdf

The upper gravel dominated Hanford formation facies (H1) is not present at the IDF site and the combined thickness of the sand dominated and lower gravel dominated facies is about 113 m (PNNL-15237, *Geology of the Integrated Disposal Facility Trench*). The geology of the IDF trench consists predominantly of sands to silty sand with clay- to silt-layers and gravel lenses. The trench intersected the uppermost part of the Hanford formation sand dominated facies.

3.1.3.3 Ringold E Unit. The Ringold Formation Unit E is a fluvially deposited pebble-to-cobble gravel with a sandy matrix. It is characterized by complex interstratified beds and lenses of sand and gravel with low to moderate degrees of cementation. The contact between Ringold Unit E and the Hanford formation is important because the saturated hydraulic conductivity for the gravel-dominated sequence of the Hanford formation is typically higher than the more compacted and locally cemented Ringold Unit E.

3.1.4 Model Domain and Boundary Conditions

The IDF measures 457 m wide by 233 m long by 12.8 m deep. The IDF is currently planned as being comprised of two cells, but can be expanded. The facility in its current configuration, referred to as the "first expansion," was completed in April 2006 (Figure 1-1) with a capacity of nearly 165,000 cubic meters.

The thickness of the vadose zone (distance from the ground surface to the top of the water table) across IDF is not uniform; the vadose zone thickness in TC&WM EIS calculations was specified by applying an estimated vadose zone thickness of 100 m at the center of the source to the entire vadose zone model. Details on numerical discretization and extent of the combined VZ/SZ 3-D model are presented in Section 4.

The primary assumptions associated with the model boundary conditions are that the boundaries are chosen far enough away to avoid affecting the results in the area of interest. Boundary conditions applied at the top boundary approximate net infiltration and vary spatially and temporally depending on site conditions, location and physical dimensions of the IDF, and the timeline of barrier functionality. Boundary conditions for the sides of the model domain are assumed to be "no flow" in the vadose zone and prescribed flux in the saturated zone (see Section 4 for details). The bottom boundary of the model in groundwater is defined as a vertical no-flow condition.

3.1.5 Vadose Zone and Saturated Zone Flow and Transport

Averaged and upscaled parameter values for different soil types and geologic units are assumed to adequately represent the bulk flow and transport processes occurring in the vadose zone and saturated zone. Upscaling the parameters incorporates the effects of small-scale textural contrasts that introduce heterogeneity into the flow parameters sufficiently to approximate the bulk flow and transport of contaminants through the vadose zone and saturated zone. A discussion of the upscaling approach and justification is presented in Appendix B.

The equivalent homogeneous medium (EHM) approximation is the cornerstone of flow and transport modeling. With EHM-based upscaling, each heterogeneous geologic unit within the vadose zone is replaced by its homogeneous equivalent, and small-scale measurements are used to predict the large field-scale flow and transport behavior. Each HSU within the vadose zone is assigned its anisotropic, upscaled (effective) hydraulic properties (Figure 3-2).

Figure 3-2. Schematic Illustrating the Upscaling Concept

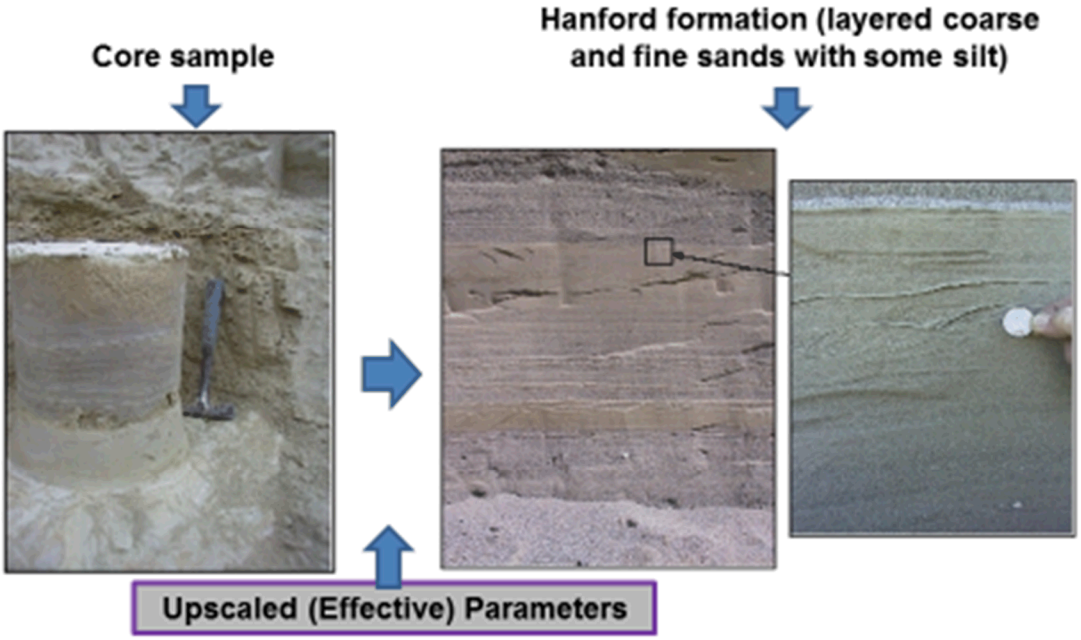

With respect to thickness of the vadose zone, the current water table is assumed to revert to levels comparable to those existing prior to the onset of Hanford Site operations. Changes in offsite land use (e.g., increased agriculture recharge or new reservoirs, or changes in river stage caused by dam breach, dam removal, or renegotiated treaties) are assumed to cause negligible changes to water levels or gradients in the vicinity of IDF.

3.1.5.1 Vadose Zone Modeling. Within the STOMP code, tension-dependent anisotropy provides a framework for upscaling small-scale measurements to the effective (upscaled) properties for the large-scale vadose zone (PNNL-23711, *Physical, Hydraulic, and Transport Properties of Sediments and Engineered Materials Associated with Hanford Immobilized Low-Activity Waste*). Each heterogeneous geologic unit is represented in the model by an equivalent homogeneous media (EHM) with macroscopic flow and transport properties. With each heterogeneous unit assigned its upscaled or effective hydraulic properties, the simulated flow fields predict the bulk or mean flow behavior at the field scale. Upscaling, in effect, accounts for the differences in scale between small, core-scale measurements and large, field-scale modeling. To justify use of the EHM approximation in IDF PA vadose zone modeling, an evaluation of the modeling approach is performed first using a controlled database; Appendix B provides a detailed description of the evaluation.

Tension-dependent anisotropy provides a framework for upscaling small-scale measurements to the effective (upscaled) properties for the large-scale, macroscopic vadose zone. A tensorial connectivity-tortuosity (TCT) model (Zhang et al. 2003, *A Tensorial Connectivity–Tortuosity Concept to Describe the Unsaturated Hydraulic Properties of Anisotropic Soils*) is used to evaluate and apply tension dependent anisotropy for the hydrostratigraphic units at IDF. Details about the development of the tension-dependent anisotropy model and its application to the

hydrostratigraphic units at IDF are presented in PNNL-23711. The parameterization for IDF soil properties and the TCT model are presented in Section 4.3. This is unlike the ERDF PA, for example, wherein a stochastic model (Polmann 1990, *Application of Stochastic Methods to Transient Flow and Transport in Heterogeneous Unsaturated Soils*) was invoked to model the tension-dependent anisotropy and to develop the unscaled (effective) parameter estimates. Compared to the Polmann model, the TCT model used in IDF PA has the advantage that its data requirements are much less stringent, and has unrestricted application over the entire range of saturation. Furthermore, an evaluation of the TCT model using a controlled database has been performed and documented in Appendix B.

3.1.5.2. Alternative Vadose Zone Transport Models. The following two alternative vadose zone transport models are discussed.

- Colloids and colloid-facilitated transport
- Preferential pathways

Colloids and Colloid-Facilitated Transport. The formation of colloids (particles whose sizes range from one nanometer to one micrometer) and occurrence of colloid-facilitated transport of contaminants has often been identified as potentially an important process affecting vadose zone transport. In general, under saturated flow conditions, the potential exists for formation of colloids and their migration. Under unsaturated conditions, however, due to the low water content and significant filtration at the air-water/solid interfaces, conditions are generally not conducive to colloid formation or colloid-facilitated transport. Nonetheless, various interacting mechanisms might be involved simultaneously during colloid transport, but their importance depends on the chemical and physical properties of the colloids and transport media as well as the environmental conditions. Cherrey et al. 2003, "Nitrate and colloid transport through coarse Hanford sediments under steady state, variably saturated flow," studied transport of colloids through Hanford sediments under steady state, unsaturated flow conditions. Colloid breakthrough curves were determined under a series of water contents (i.e., ranging from 0.2 to 1.0 effective saturation). Colloid behavior was described using the mobile-immobile conceptual model, including first-order deposition from the mobile phase only. Colloids were mobile under all water saturations, but the total amount of colloids transported decreased with decreasing water saturation. With decreasing water saturation, the liquid-gas interfacial area increases and the film thickness decreases, and consequently colloids are more likely to be deposited inside the porous matrix. It has been postulated that capillary-based liquid pathways are effective conduits for colloid movement as long these conduits form connected pathways, and that at low water saturations these conduits become discontinuous causing an abrupt decrease in colloid transport (Wan, J. M., and T. K. Tokunaga, 1997, *Film straining of colloids in unsaturated porous media: Conceptual model and experimental testing*); Liu et al., 2013, *Colloid mobilization in an undisturbed sediment core under semiarid recharge rates*) sampled an undisturbed Hanford H2 sand-dominated core (i.d. 50 cm, 59.5 cm high from a depth of 17 m below ground at the nearby ERDF site. The core was set up as a laboratory lysimeter and exposed to an infiltration rate of 18 mm/yr by applying simulated pore water onto the surface. Particle concentrations were quantified in the column outflow, and selected samples were examined microscopically and for elemental composition. During 5.3 years of monitoring, natural colloids like silicates, aluminosilicates, and Fe-oxides were observed in the core outflow, indicating the continuous mobilization of in situ colloids. However, the total amount of particles mobilized during 5.3 years corresponded to 1.1 percent of the total dispersible colloids inside the core. In fact, a

comparison of the amounts of colloids released with weathering rates suggests that mineral weathering can be a major source of the mobilized colloids. The fitted colloid release rate coefficient was 6 to 7 orders of magnitude smaller than coefficients reported from previous studies, where disturbed Hanford sediments and higher flow rates were used. The findings demonstrate that even under low recharge rates and water contents typical for semiarid, deep vadose zone sediments, particles can continuously be mobilized, although the total mass of particles is low (Liu et al. 2013).

Preferential Flow. A variety of preferential flow pathways such as macropores and discontinuities are capable of concentrating or contributing to preferential flow phenomena as well as fingering and funnel flow. Preferential flow has been recognized and widely studied under saturated or near saturated- flow conditions (Nkedi Kizza et al. 1983, "Modeling Tritium and Chloride 36 Transport Through an Aggregated Oxisol"; De Smedt and Wierenga, 1984, "Solute Transfer through Columns of Glass Beads"). Preferential flow is less of an occurrence for arid and semiarid climates or under low moisture fluxes, particularly where sediments are coarse textured, such as those beneath the IDF site. Under natural recharge conditions, precipitation at arid sites is usually too low (in relation to saturated hydraulic conductivity) to invoke preferential flow; much of the water in the dry soils is simply adsorbed onto the grain surfaces as film flow and cannot move along preferred pathways (Figure 3-3). Nonetheless, for IDF PA modeling, the impact of potential preferential pathways such as clastic dikes is considered as part of two-dimensional (2-D) simulations, and results reported in the companion EMCFs.

Saturated Media Modeling. The groundwater in the aquifer system in the vicinity of IDF has been studied extensively as part of the site characterization within the 200 Areas. The groundwater conceptual model for IDF includes the uppermost unconfined aquifer system that exists within a channel eroded by the cataclysmic floods of the Pleistocene age. The base of the aquifer is the underlying basalt surface. The Leapfrog geo framework model in RPP-RPT-59343 is the basis for delineation of saturated Hanford H3 and Ringold E units that comprise the aquifer sediments. The smallest thickness of the uppermost aquifer beneath IDF is ~10 m. As discussed later, the IDF PA simulations represent concentrations in the upper 5 m of the aquifer. The 5 m vertical interval corresponds to the well screen length of a conceptual groundwater monitoring well, and the basis for that delimiter to the groundwater concentrations calculation is presented in upcoming discussion regarding "Point of Calculation, Protectiveness Metric, and Timeframe Considerations."

Groundwater flow beneath IDF has been historically difficult to measure because the hydraulic gradient is very small and the hydraulic conductivity is very high in this region of the Hanford Site. In addition, the water table continues to recover from the operational liquid discharges at the B Pond system near IDF and other large discharge sites in 200 East Area. Nonetheless, the projected equilibrium state is expected to be similar to its pre-Hanford behavior. As a result, the post-closure position of the water table and associated hydraulic gradient can only be evaluated through modeling. Consequently, the groundwater flux in the aquifer beneath IDF is calculated on the basis of the aquifer hydraulic properties, and the hydraulic gradient projected to exist in the future.

Figure 3-3. Schematic Illustrating Unsaturated Flow Conditions for Low Fluxes in Coarse-Textured Gravelly Media

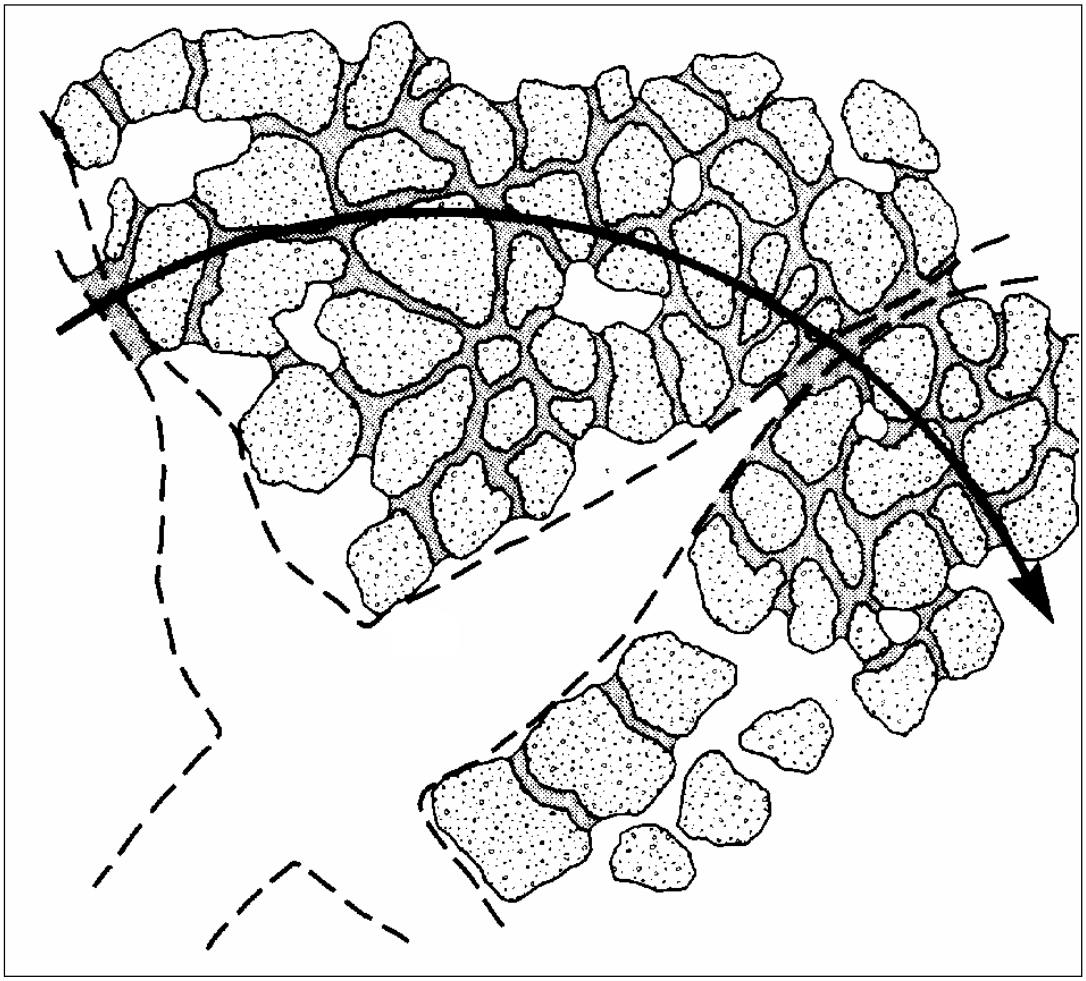

Source: After Wang and Narasimhan, 1985, "Hydrologic Mechanisms Governing Fluid Flow in Saturated, Fractured Porous Media"

The expanded vertical slice illustrates the fact that under unsaturated conditions and low recharge, the bulk flow bypasses the pathway formed by larger pore sizes (i.e., macropores) and essentially follows the pathway formed by the smaller pore size network. The large, open spaces in the figure mimic macropores such as those existing for highly gravelly media.

The hydraulic heads around IDF are expected to continue declining slowly until they stabilize around 119.5 m (Section 4.4.3, Figure 4-14) within 100 years in the future (CP-47631, *Model Package Report: Central Plateau Groundwater Model Version 6.3.3*). The gradient is generally expected to slope from northwest to southeast with a value of about 0.00002 m/m (CP-47631), which is close to the one observed prior to start of Hanford operations. Appreciable changes in hydraulic gradient are not expected in the future once the hydraulic heads stabilize. Thus, the hydraulic gradient is assumed to remain stable for the compliance case analysis.

A fundamental difference exists as to how the large-scale macroscopic parameters are derived for saturated media versus unsaturated media. First, in a highly heterogeneous flow domain such as IDF exists a hierarchy of length scales that needs to be recognized (Figure 3-4) and an increase in parameter estimates with an increase in flow domain scale is noticeable. The evolving heterogeneities at various length scales result in a scale dependence of effective parameters such as saturated hydraulic conductivity and macrodispersivity. For IDF PA saturated media modeling, the flow domain of interest is the "Field Scale," which in Figure 3-4 is to the right (i.e., IDF and Central Plateau scales). Each HSU in the unconfined aquifer is treated as an anisotropic EHM, and equivalent saturated hydraulic conductivity values are estimated for the undifferentiated Hanford gravels and RE). Figure 3-5 shows the saturated K variability for H3 gravel-dominated unit; the values are based on laboratory-scale permeameter experiments, slug tests, pump tests and modeling.

Figure 3-4. Measured Saturated Hydraulic Conductivity as a Function of Evolving Length Scale

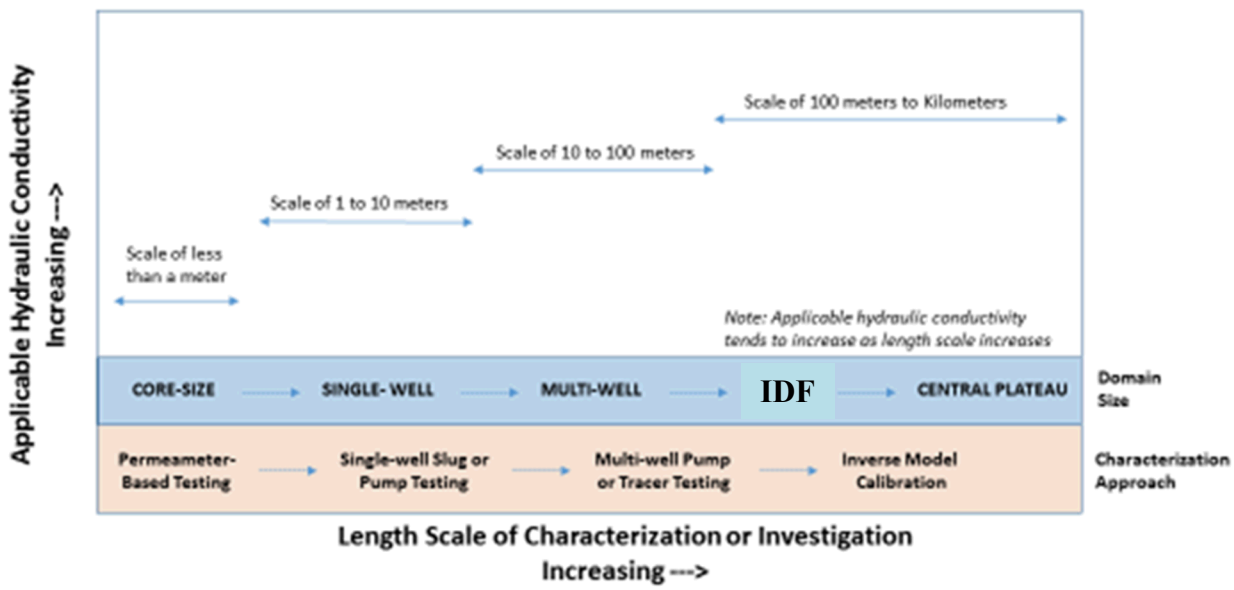

Note: The IDF and Central Plateau length scales represent the "Field Scale."

Figure 3-5. Variability of Saturated K Based on Permeameter Tests, Slug Tests, Pumping Tests, and Modeling

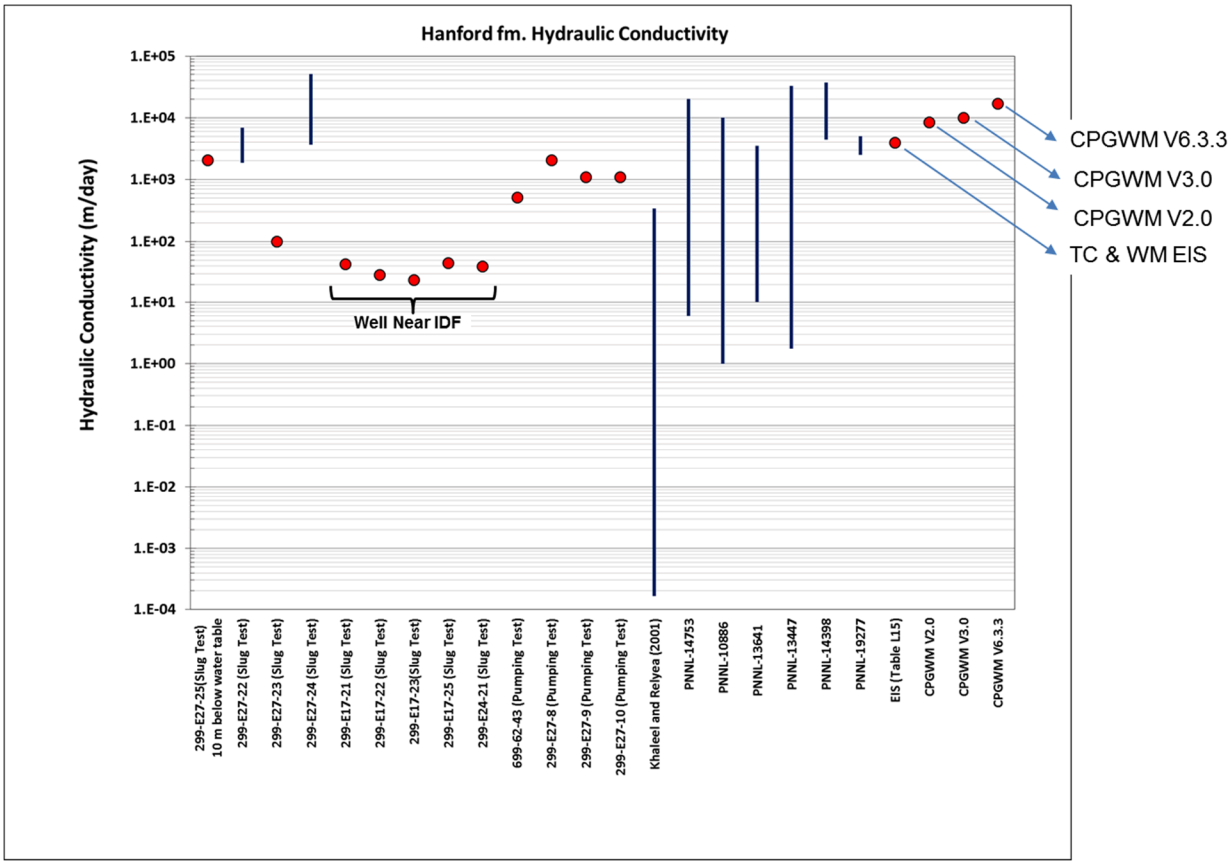

Note: As noted previously, the figure includes slug test data for five wells near IDF. Khaleel and Relyea, 2001, "Variability of Gardner's α for coarse-textured sediments," data are based on laboratory-scale permeameter experiments for gravelly sediments.

Note that, for the large-time, large-scale PA modeling applications, the macro-scale parameterization for saturated media effective parameters depends on the configuration of the heterogeneous media, as well as the establishment and setup of the local boundary conditions. This is unlike the vadose zone parameterization wherein the effective parameters at the large and macro scale are derived from properties at the small and micro scale using upscaling methods. Instead, an effective parameterization for saturated media hydraulic conductivity, for example, is best achieved via a field-scale calibrated groundwater model, which accounts for appropriate local-scale boundary conditions, flow configuration, and history matching. Estimates of hydraulic properties are based on the groundwater flux in the aquifer around IDF according to the Central Plateau groundwater model calibration reported in CP-47631. Flux is a rate measurement defined as the flow through a defined area. It is well suited for the PA because the emphasis of its evaluation is the contaminant mass conveyed through the aquifer to a point of calculation aligned with the direction of groundwater flow. Thus, the hydraulic property values derived from the calibrated Central Plateau groundwater model fluxes are applied to the IDF PA flow model domain.

3.1.6 Geochemistry and Sorption

The geochemical and sorption conceptual model primarily concerns the contaminant release mechanisms in IDF, and the retardation of contaminants within the vadose zone and the unconfined aquifer. For the purpose of the PA analysis, the empirical equilibrium sorption based approach is assumed to approximate contaminant sorption during transport. The focus of the modeling is on far-field transport, away from waste disposal location, as bulk of the residence time of contaminants is likely to be in the thick vadose zone. Concentration dependent sorption/desorption of radionuclides, development of reaction fronts from dissolution and precipitation of mineral phases, and variable soil vapor pressures, are possible at or very close to the source term. But away from the base of IDF, the radionuclide concentrations are likely to be sufficiently low and given large sorption and buffering capacity in the thick vadose zone the leachate ionic strength and pH are expected to become similar to the ambient porewater within a short distance from the base of IDF.

The use of the linear isotherm (constant distribution coefficient [K_d] model) is assumed to be generally applicable under the following conditions:

- When contaminants are present at low concentrations as would be expected away from the source
- When the geochemical environment being modeled is not affected by large spatial or temporal changes
- When the geochemical environment is not considerably different so as to force the adsorption isotherm to become nonlinear

Away from the IDF near-field, far-field K_d values are chosen assuming low-salt, near-neutral waste chemistry. It is acknowledged that the K_d values used in fate and transport models are effective K_d values representing the effective combinations of processes contributing to the overall contaminant retardation and/or release behavior. The utility of the empirical linear adsorption model or K_d approach is that it is a simple, useful, and generally practical approach for modeling contaminant adsorption and transport in geologic systems. The constituents of potential concern (COPC) for IDF PA calculations are listed in Table 4-1. A generic set of K_d values will be used to bracket the COPCs for the PA modeling.

As the majority of the Hanford Site K_d experiments currently available corresponds to measurements performed on fine-grained fraction (<2-mm size fraction) of the sediments, extrapolation of these results to the IDF-specific hydrostratigraphic units requires correction for the presence of gravel (>2-mm size fraction), if any. For units containing a significant amount of gravel (i.e., H3 and RE units), K_d values are typically lower than those determined with <2 mm size material because the surface area and corresponding number of adsorption sites is much lower (PNNL-17154, *Geochemical Characterization Data Package for the Vadose Zone in the Single-Shell Tank Waste Management Areas at the Hanford Site*). Depending on a minimum K_d value, equations (Table 4-1) as recommended by PNNL-17154, are used for gravel correction.

3.1.7 Groundwater Concentration, Point(s) of Calculation, Protectiveness Metric, and Timeframe Considerations

Contamination from the vadose zone that enters the aquifer is expected to be diluted with the groundwater by advective and dispersive processes. Concentrations calculated in the model for a

specified depth, elevation, or interval in the aquifer are assumed to be comparable to concentrations that would be measured by sampling a well with a well screen at the same location. For purposes of calculation of groundwater concentration at the compliance location, a uniform well screen interval of approximately 5 m is assumed.

3.2 NATURE AND EXTENT OF CONTAMINATION

The VZ within IDF is a relatively pristine region. A tritium plume and an I-129 plume do exist within the unconfined aquifer beneath the IDF from out-of-model-domain sources. For the types of source release for IDF PA, as illustrated by the example test case calculations (Appendix D), at the 100 m downgradient of IDF permit boundary, the first arrival of I-129 occurs at ~ 6000 years and the simulated peak concentration for I-129 is ~4.48 pCi/L.

This page intentionally left blank.

4.0 MODEL IMPLEMENTATION

4.1 SOFTWARE

The basis for selection of numerical software used to implement the vadose zone and saturated zone flow and transport model is included in Section 5. Software features incorporating FEPs are mapped in Appendix A. FEPs that are specific to combined VZ/SZ modeling are identified in Appendix A; potential limitations are discussed in Section 7.

STOMP will be used to implement the integrated vadose zone and saturated zone flow and transport model. Section 5 includes details on compliance with PRC-PRO-IRM-309, *Controlled Software Management*, and CH2M HILL Plateau Remediation Company (CHPRC) software control documents (e.g., Functional Requirements Document, Software Management Plan, Software Test Plan, Requirements Traceability Matrix, and Acceptance Test Report), user authorization and training, and Software Checkout and Installation record.

4.2 DISCRETIZATION

The MPR for the geologic framework, RPP-RPT-59343, serves as the predecessor for development of the 3-D combined VZ/GW model domain for STOMP. The model domain for the GFM is represented in three-dimensional space with a rectangular horizontal profile. Land surface introduced in the form of LiDAR topography[5] represents the vertical upper boundary and an interpreted topography of the basalt surface (SGW-48478, *Interpretation and Integration of Seismic Data in the Gable Gap*) represents the lower vertical surface.

Figure 4-1 shows the lateral extent of the STOMP model domain, whereas Figure 4-2 shows the entire 3-D combined VZ/SZ model domain. Following are the criteria used for the discretization process.

- Use GFM hydrostratigraphy (RPP-RPT-59343)
- Allow for the horizontal directions a minimum discretized grid cell size of 10 m by 10 m in and under IDF to capture the resolution of specific waste-stream source release
- Allow for a vertical discretization of 2 m
- For the RCRA surface barrier, allow for a small cell width to calculated edge of cap where drains will focus recharge
- Align edge of one row exactly 100 m east of edge of excavation
- Relax grid resolution outward by the harmonic rule (<1.5 times the discretization increment)
- Allow 500 m beyond cap (i.e., RCRA surface barrier) in all directions so that the boundary effects are not felt

[5] AeroMetric, Inc., Sheboygan, Wisconsin

Figure 4-1. Lateral (X-Y) Model Domain for the Three-Dimensional STOMP Grid.

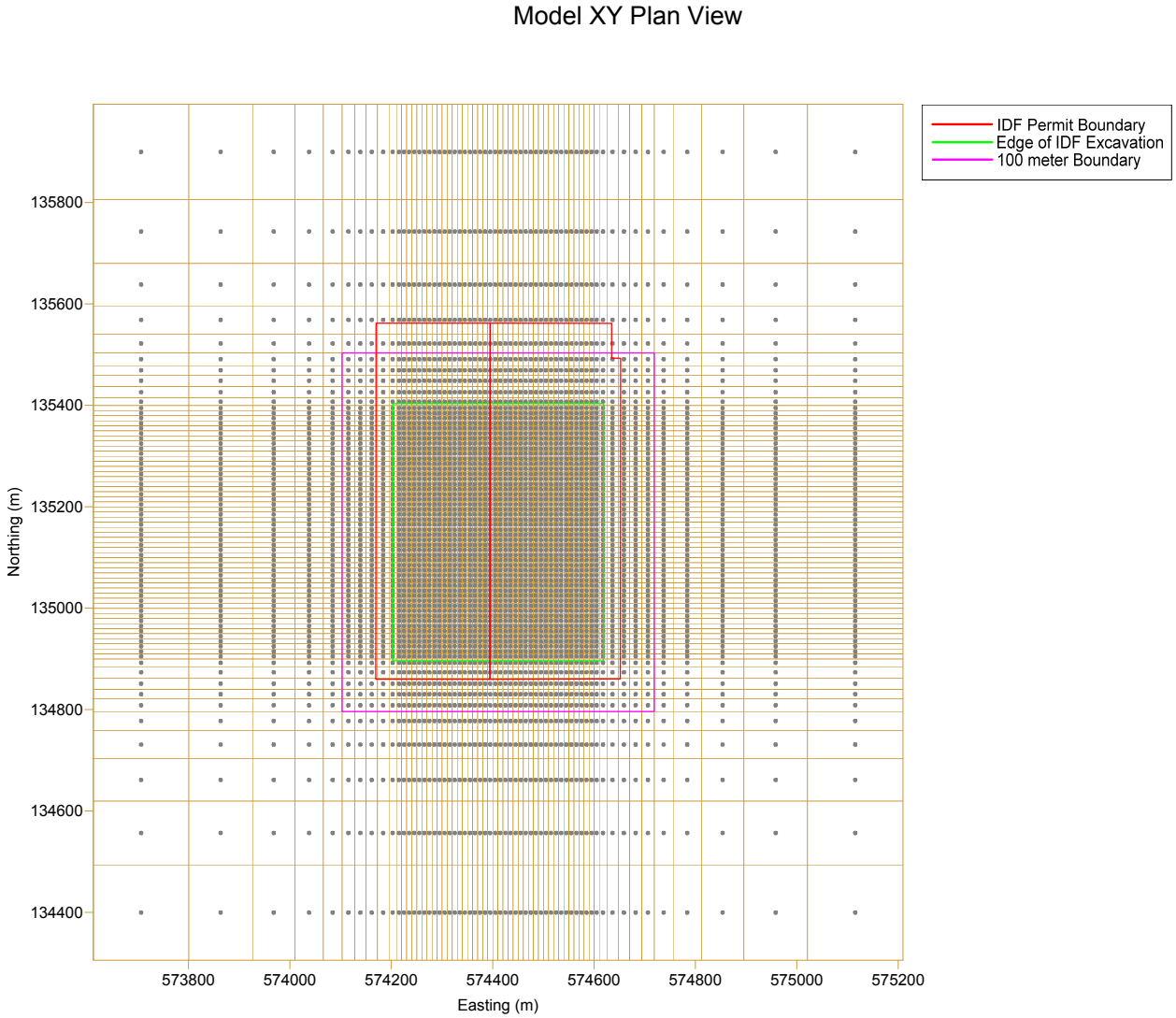

Figure 4-2. Hydrostratigraphic Units for the Three-Dimensional STOMP Grid.

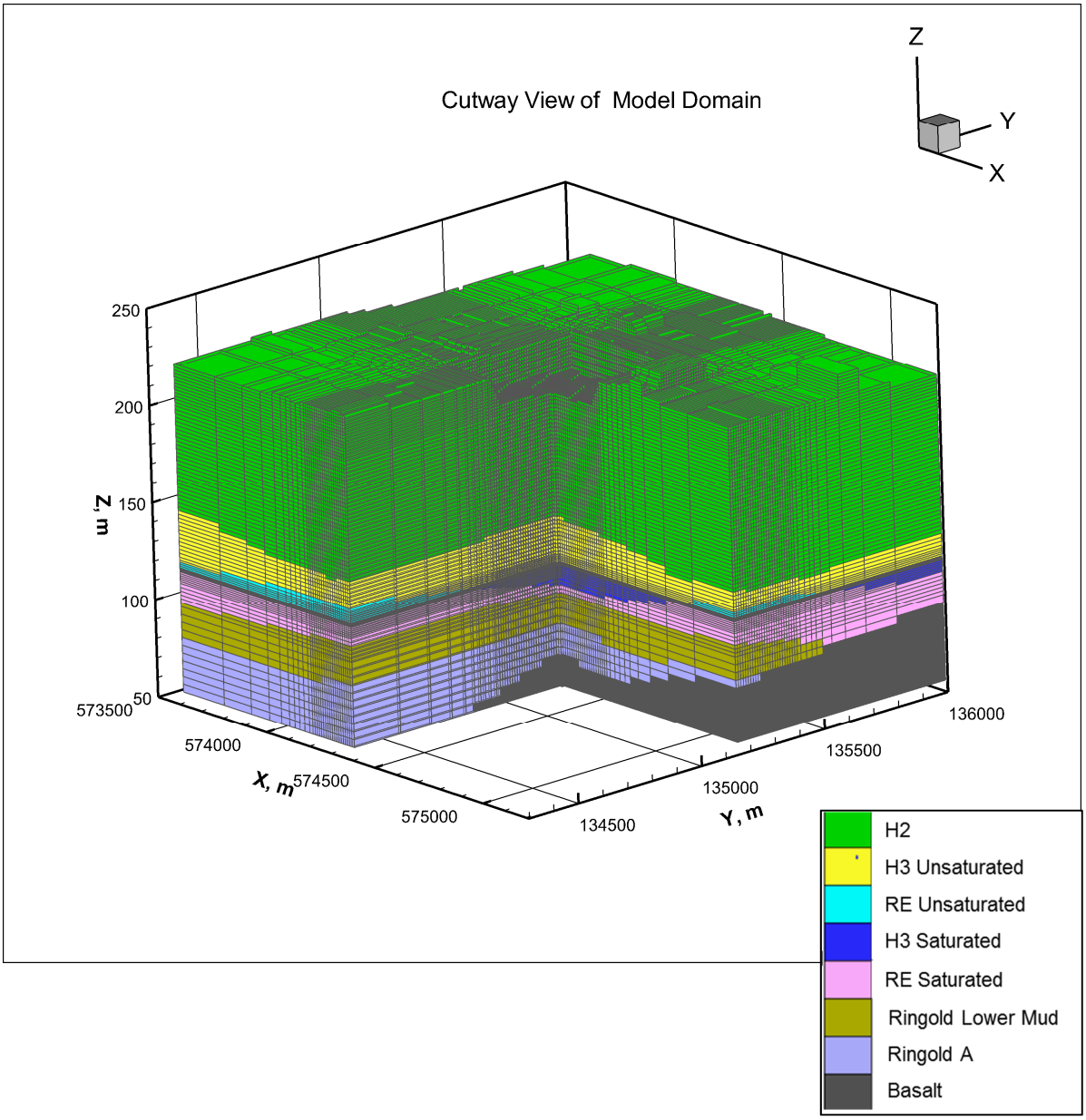

- The impacts of clastic dikes and the presence of paleosols (fine-textured thin lenses) within the IDF will be considered as part of 2-D STOMP models and are not explicitly included in the 3-D model
- A long term steady state head of 119.5 m (NAVD88) was used to set up the boundary condition in the saturated model domain and assigning hydraulic properties in the model grid cells. The 119.5 m steady state head is predicted near IDF by Central Plateau Groundwater Model (CPGWM) (CP-47631)
- Allow for extension of the 3-D model to the top of the basalt. However, for the example test case implementation (Appendix D), only the top 5 m of the SZ is included in the 3-D model, i.e., the region from the top of the basalt to the bottom of the 5 m screen beneath the top of the water table was kept inactive in STOMP.

Figure 4-3 shows the north-south as well as the west-east cross-sections through IDF excavation for the 3-D STOMP grid. Additional west-east and north-south cross-sections are shown in Figures 4-4 and 4-5, respectively. Figures 4-6 (a) and 4-6(b) illustrate the distribution of hydrostratigraphic units at the 119.5 m elevation and 114.5 m elevation, respectively.

4.2.1 Numerical Model Stability Considerations.

A complicating factor in numerical modeling of contaminant transport in porous media is that both finite-difference and finite-element solutions are affected by "numerical dispersion," which refers to artificial dispersion caused by errors associated with discretization of the flow domain. To minimize such errors, the grid should be designed so that the Peclet number (P_e = discretized distance/dispersivity) is less than or equal to one, although acceptable solutions can be obtained with P_e as high as 10 (Huyakorn and Pinder 1983, *Computational Methods in Subsurface Flow*). With low macrodispersivities within the vadose zone, the Peclet number criterion results in grid spacings that are not very practical to implement. This is why numerical modelers often resort to higher values of macrodispersivity. An alternative is to consider use of "upwinding" option (Huyakorn and Pinder, 1983) to control numerical dispersion.

Another consideration is discretization of simulation time so that the Courant number (C_r = pore velocity*time interval/grid spacing) is less than or equal to one. That is, the time step should be selected so that the chosen time interval is less than the value obtained by the ratio of grid spacing to pore velocity. Thus, the time step should be selected so that it is less than the time it takes for the solute to move one grid spacing. Note that, for a 3-D problem, the P_e and C_r criteria are applicable to transport in all three directions.

The automatic Courant control of STOMP was used in selection of the maximum time step (i.e., restricting the time step such that the Courant number always remain less than 1). For the 3-D STOMP modeling for the example test case (Appendix D), the Peclet number was restricted below 1 within the vadose zone and allowed to be as high as 10 in the saturated zone.

Figure 4-3. West-East and North-South Cross-Sections through IDF Excavation for the Three-Dimensional STOMP Grid.

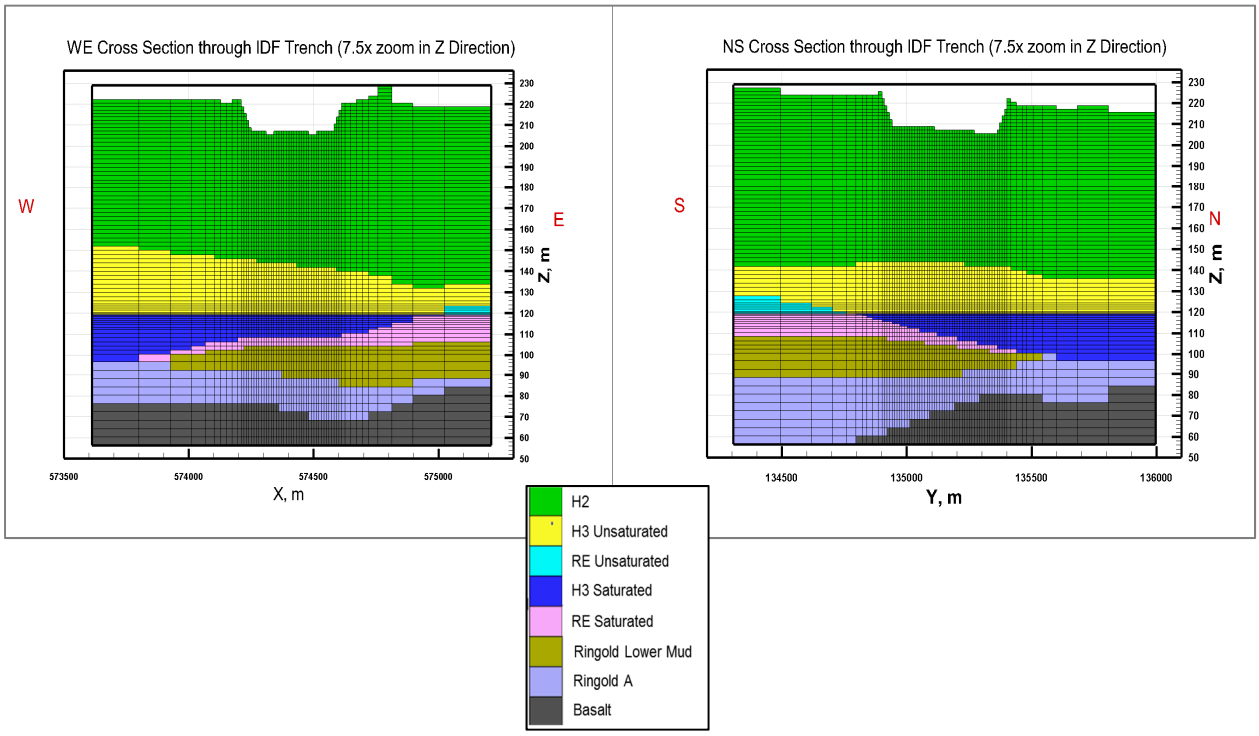

Figure 4-4. West-East Cross-Sections for the Three-Dimensional STOMP Grid.

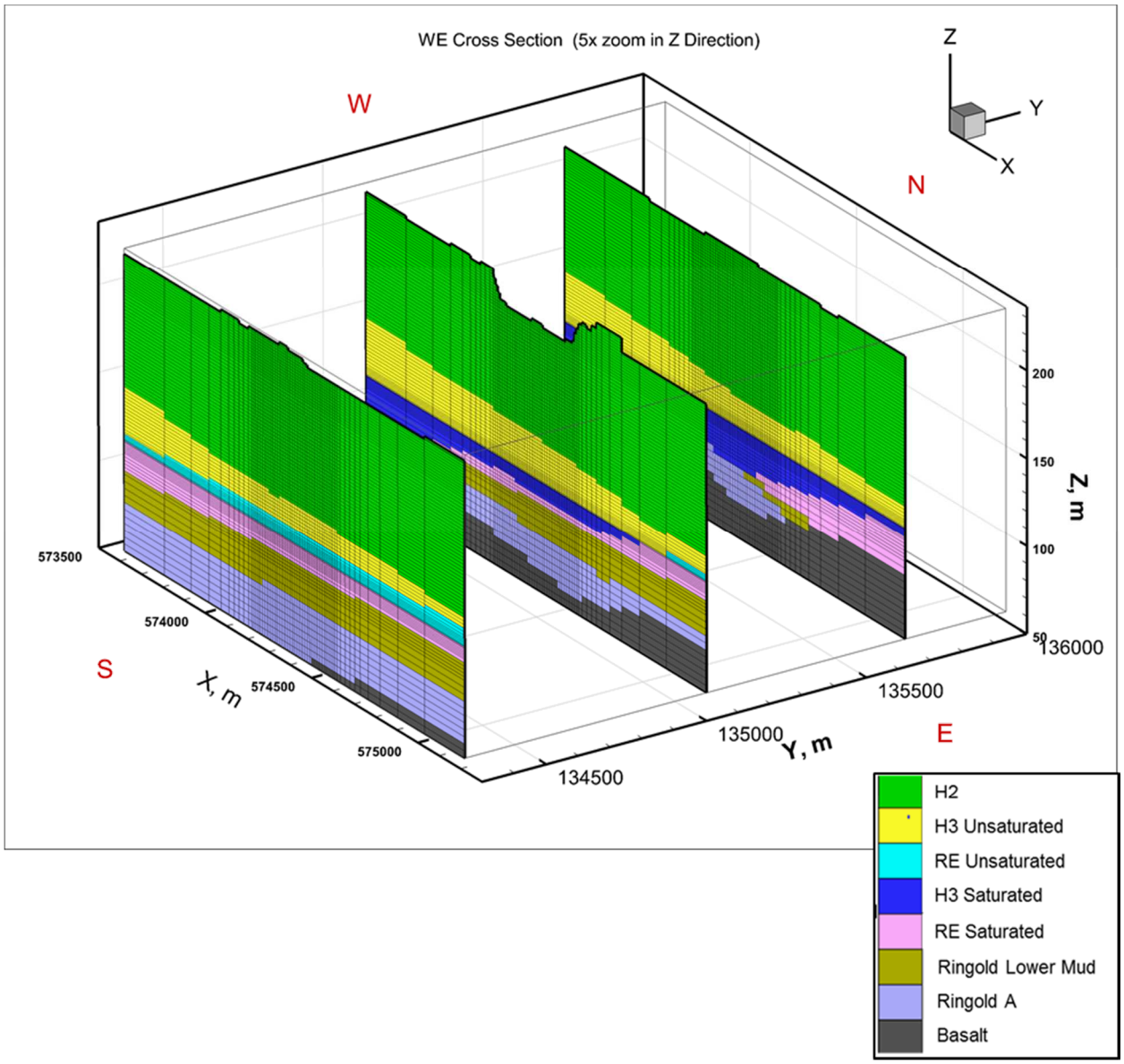

Figure 4-5. North-South Cross-Sections for the Three-Dimensional STOMP Grid.

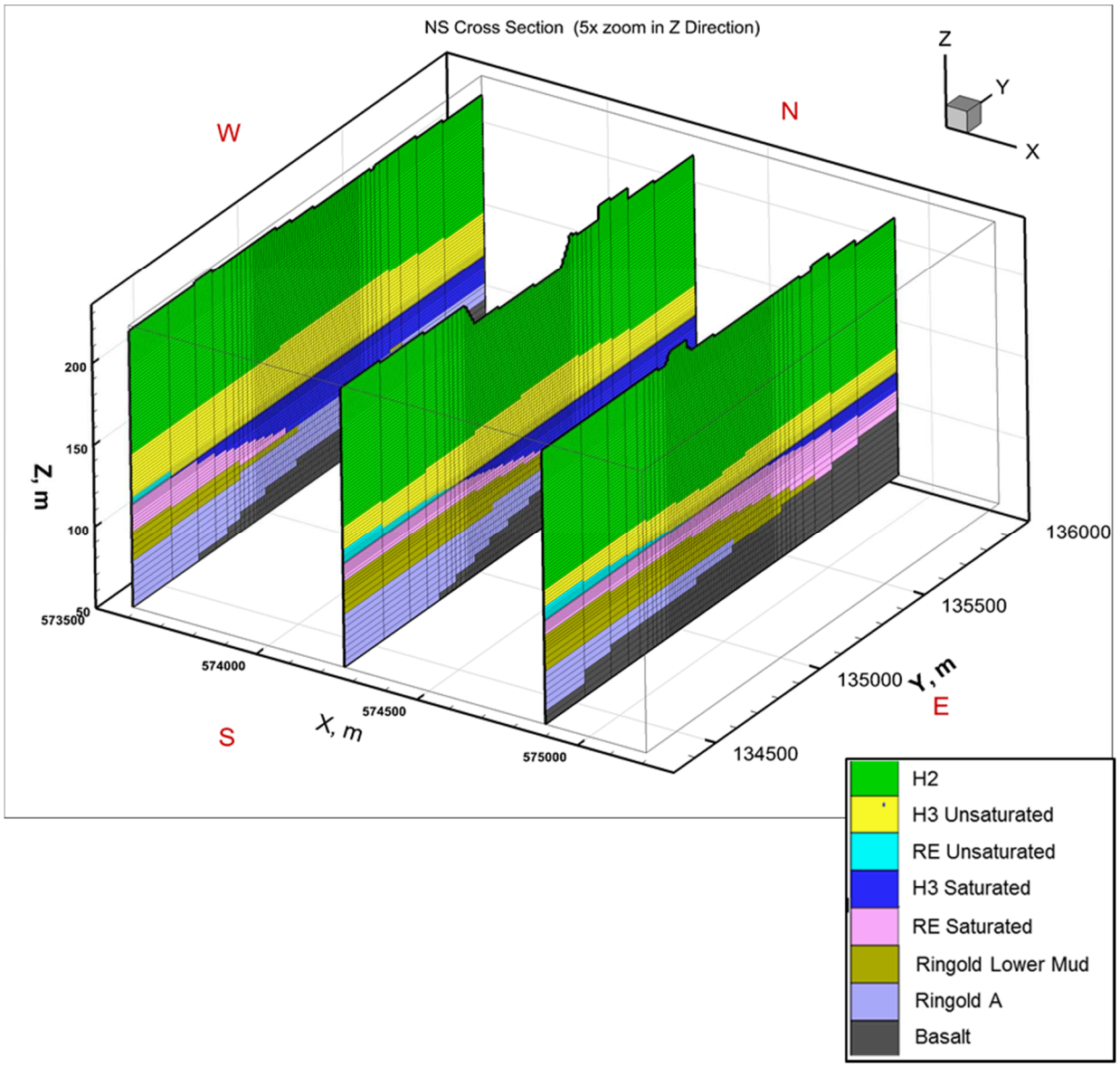

Figure 4-6a. Distribution of H3 and RE Formation at (a) 119.5 m Elevation (b) 114.5 m Elevation (1 of 2 sheets).

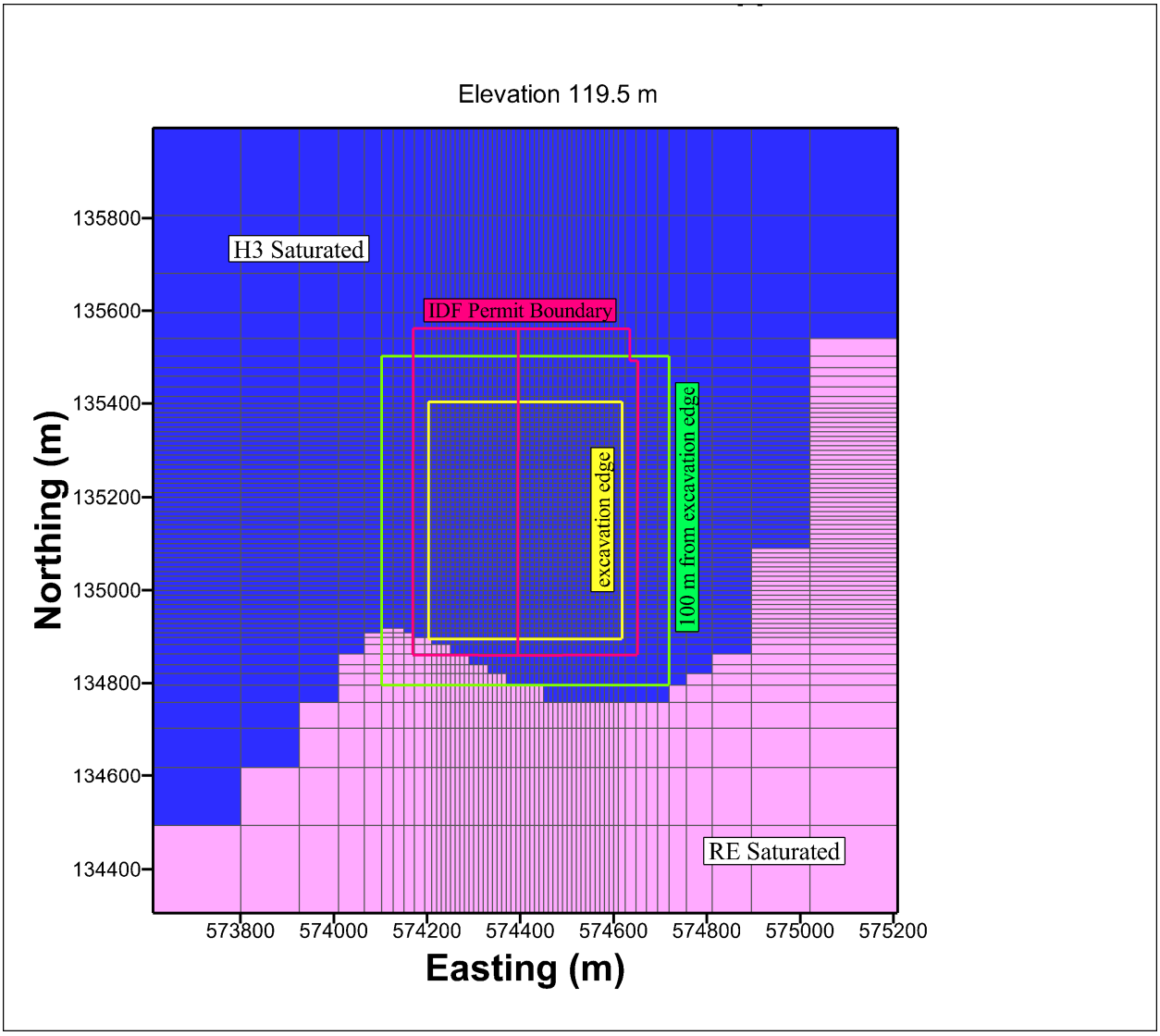

(a)

Figure 4-6b. Distribution of H3 and RE Formation at (a) 119.5 m Elevation (b) 114.5 m Elevation (2 of 2 sheets).

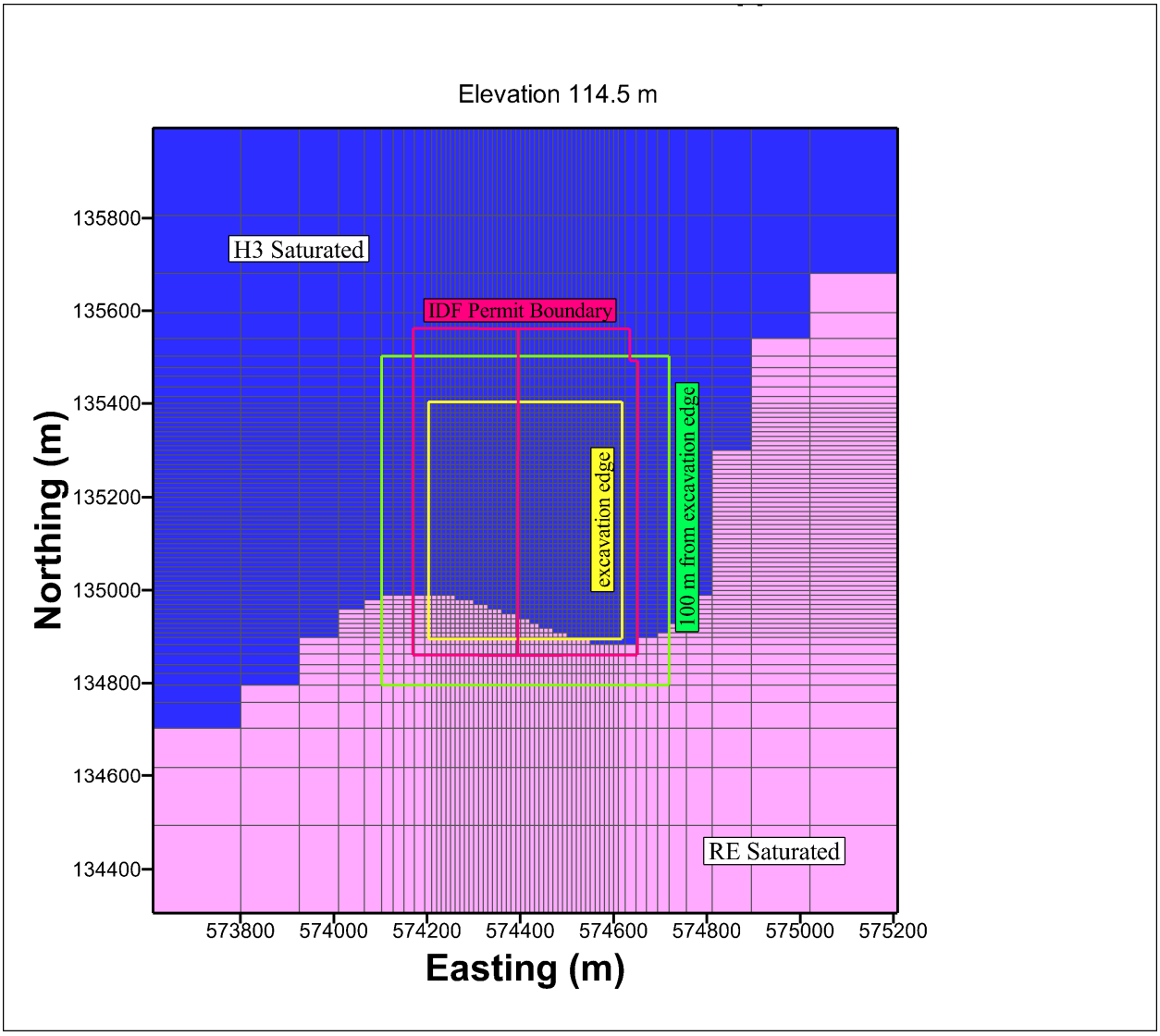

(b)

4.3 PARAMETERIZATION

Table 4-1 presents a summary of the model parameters and values assigned, including boundary and initial conditions, and identifies the section where the data sources and data quality are discussed.

Table 4-1. Summary of Key Elements and Representative Parameters Associated with Site-Specific Model Components for IDF PA

Model Domain and Boundary Conditions	The model domain for the 3-D combined VZ/SZ model is illustrated via Figures 4-1 through 4-6. The boundary conditions specified for the upper (ground) surface of the model domain were specified time- and space-dependent rate of infiltration with no flow of constituents. For each source, the variation in the timing of the background (non-anthropogenic) infiltration rate was represented as a time series of specified values. The external vertical sides of the model domain were defined as no flow of water and constituent boundaries. The horizontal extents of the model grid were wide enough to prevent adverse effects from the no-flow boundary conditions. The vertical sides of the STOMP domain are no-flow boundaries, which do not have to be explicitly called out in the Boundary Conditions Card. Prescribed flux across the top (Recharge); no-flow along vertical side boundaries in the vadose zone; prescribed head along the up-gradient and down-gradient vertical side boundaries in the aquifer, respectively; no-flow along the vertical-side boundaries in the aquifer opposite to direction of flow; and no-flow along the bottom of the model (aquifer). The prescribed volumetric water flux boundary condition is calculated to maintain mass conservation in the aquifer independent of recharge.
Geologic Setting	The entire Hanford formation is ~93 to 124 m thick within the IDF model domain (see Leapfrog MPR Section 3.1.1); the distance between the base of IDF and the fiscal year 2014 water table is ~87 m. The IDF lies within the sand-dominated H2 unit in the vadose zone. The stratigraphic units of the combined VZ/SZ IDF model domain include, from top to bottom: • Recent (Holocene) backfill material • Hanford formation unit H2 – Sand-dominated sequence • Hanford formation unit H3 – gravel-dominated sequence • Ringold formation unit E (undifferentiated) – partially consolidated to consolidated silts, sands and gravels • Ringold formation Lower Mud unit – Silt and clay dominated unit • Ringold formation unit A – gravel-dominated sequence

Table 4-1. Summary of Key Elements and Representative Parameters Associated with Site-Specific Model Components for IDF PA

Vadose Zone Hydraulic Properties

Source: Physical, Hydraulic, and Transport Properties of Sediments and Engineered Materials Associated with Hanford Immobilized Low-Activity Waste (PNNL-23711)

Parameters		Sand Sequence	Gravel Sequence
θ_s^e ($cm^3\ cm^{-3}$)		0.384	0.174
θ_r^e ($cm^3\ cm^{-3}$)		0.029	0.00380
α^e (cm^{-1})		0.06419	0.08859
n^e (-)		1.698	1.271
K_s^e ($cm\ s^{-1}$)	p = 1	6.196×10^{-3}	4.671×10^{-2}
	p = $^1/_3$	6.157×10^{-3}	7.714×10^{-3}
	p = 0	6.575×10^{-3}	3.790×10^{-3}
	p = -1	7.741×10^{-3}	1.959×10^{-4}
L^e (-)	p = 1	-0.683	0.637
	p = $^1/_3$	0.375	-0.225
	p = 0	0.916	-0.111
	p = -1	2.386	1.471

For each HSU, vadose zone hydraulic conductivity and anisotropy allowed to vary as a function of the moisture content (or matric potential) in accordance with the TCT model (Zhang et al. 2003). Because of its gravelly nature, the unsaturated hydraulic properties as well as anisotropy for Ringold E are assigned same as those for H3 gravelly media.

Degree of Anisotropy in Hydraulic Conductivity (Zhang and Khaleel 2010; PNNL-23711)

Anisotropy Level	*p* value for the horizontal direction (*i* = 1, 2)	*p* value for the vertical direction (*i* = 3)
Low Anisotropy	1	$^1/_3$
Intermediate Anisotropy	1	0
High Anisotropy	1	-1

Recharge/ Infiltration

Infiltration (Recharge) Estimates for Pre-Construction Period, Pre-Closure Period, and Following Emplacement of the IDF Closure Barrier.

Period	IDF Region and Vicinity	Recharge Rate (mm/yr)
Pre-construction	Undisturbed region (Rupert sand with vegetation)	1.7
Pre-closure period	Undisturbed region (Rupert sand with vegetation)	1.7
	Disturbed region (Rupert Sand without vegetation)	55.4
	Region under construction (IDF cells)	0
Early post-closure (1st 500 years)	Undisturbed region (Rupert sand with vegetation)	1.7
	Side slopes (compacted silt)	2.0
	Functioning barrier	0.5
Late post-closure	Undisturbed region (Rupert sand with vegetation)	1.7

Table 4-1. Summary of Key Elements and Representative Parameters Associated with Site-Specific Model Components for IDF PA

	(500 years and beyond) Degraded side slopes with vegetation 2.0 Degraded top portion of the barrier 1
K_d Sorption Coefficients	IDF PA COPCs are nitrate, chromium, iodine, neptunium, selenium, technetium, and uranium (PNNL-13037) for transport in the vadose zone and groundwater. One simulation run for generic contaminants having a range of K_ds (i.e., 0, 0.02, 0.04, 0.1, 0.2, 0.25, 0.5, 1 mL/g) will characterize the sensitivity and screen out COPCs. As described below, a corrected K_d (gc) (PNNL-13037, Equation 2.6) is used to correct for the "empirical" Kd values for the IDF gravel dominated sequence K_d (gc) =(1-g)*K_d(<2-mm) (4-1) Where: K_d (gc) is the gravel corrected K_d (gc =gravel correction), *g* is the gravel weight fraction of sediment, and K_d (<2mm [<0.78 in.]) is the traditional Kd value measured for the less than 2-mm [<0.78 in.] size fraction.
Diffusion Coefficients	The effective, large-scale diffusion coefficients for all strata in the vadose zone at the IDF site are a function of volumetric moisture content, θ, and are expressed using the Millington/Quirk 1961 empirical relation: $D_e(\theta) = D_0 \frac{\theta^{10/3}}{\theta_s^2}$(4-1) (4-2) where: $D_e(\theta)$ = the effective diffusion coefficient of an ionic species D_0 = the effective diffusion coefficient for the same species in free water θ = the localized volumetric moisture content θ_s = the localized volumetric moisture content at saturation. The tortuosity formulation in the Millington-Quirk 1961 model is based on theoretical considerations absent from other empirical models, and accounts for the moisture content variability. The molecular diffusion coefficient for all species in pore water is assumed to be 2.5×10^5 cm^2/s (WHC-SD-WM-EE-004, 1995), which is consistent with, and representative of, values used in other Hanford PAs (WHC-EP-0645, 1995; BHI-00169, WHC-SD-WM-TI-730, and DOE/ORP-2000-24).
Effective Bulk Density and Particle Density	Effective bulk density (ρ_b) estimates are needed to calculate retardation factors for different species. The average ρ_b, estimates and ranges for various strata at IDF are presented in table below. These estimates are derived from bulk density sample values listed in Appendix B. For all material types, sediment particle density=2.65 g/cm^3 HSU — Bulk Density (g/cm^3): Average — Range Sand-dominated sequence: 1. 71 — 1.58-1.98 Gravel-dominated sequence: 2.20 — 2.06-2.38

Table 4-1. Summary of Key Elements and Representative Parameters Associated with Site-Specific Model Components for IDF PA

Vadose Zone Macro-Dispersivity	See Appendix D. Recommended longitudinal macrodispersivity estimates are shown below. Transverse estimates are 1/10th of the longitudinal estimates. **Vadose Zone Longitudinal Macrodispersivity Estimates (cm)** Hydrostratigraphic Unit / Numerical Simulation / Stochastic Theory (#Russo and ##Mantoglou Equations) H2 Sand-Dominated Unit: 25 / ~32[a] – 360[a] H3 Gravelly Units: NA / ~20[b] – 100[b] [a]Evaluated at a mean tension of 2 m. [b]Evaluated at a mean tension of 4 m. [c]Extrapolated experimental data (RPP-20621).
Saturated Media Flow and Transport Properties	Water Table Elevation (m, NAVD88): ~119.5 H3 Horizontal Saturated Hydraulic Conductivity (m/day): 17,000 H3 Vertical Saturated Hydraulic Conductivity (m/day): 1,200 Ringold E Horizontal Saturated Hydraulic Conductivity (m/day): 5 Hydraulic Gradient (m/m): ~2.0×10^{-5} Depth to Water Table (m): ~84-88 Aquifer Thickness (m): ~12-16 Longitudinal Macrodispersivity (m): ~10.5 Transverse Macrodispersivity (m): ~ 0.1-1.05* Vertical Macrodispersivity (m): ~0.0004* Prescribed head along southeast cross-section boundary: 119.5 m Groundwater thickness is ~12 m in the aquifer; Groundwater concentrations evaluated for upper 5 of the aquifer (rationale for aquifer depth presented in section on Point of Calculation, Protectiven Metric, and Timeframe Considerations). Aquifer Hydraulic Conductivity Horizontal to Vertical Ratio 10:1 unless noted otherwise. Aquifer Macrodispersivity Horizontal to Vertical Ratio 10:1 unless noted otherwise. No macrodispersivity enhancement is considered for retarded COPCs (i.e., enhancement factor was se in STOMP input file).
Saturated Media Flow and Transport Properties	The saturated media longitudinal and transverse macrodispersivity estimates are based on a review of three general relationships (Neuman 1990; Schulze-Makuch 2005; and Xu and Eckstein 1995) that quantify the dependence of this parameter on measurement scale (Ls). For 100 m, which is the travel distance to the compliance well within the saturated zone, the calculated values fall within the range of 1 m to 20 m (see following table). Thus, a value of 10.5 m is considered representative of the range of values, and is within the range of values for the Gelhar et al., 1992 (see following figure). No macrodispersivity enhancement was considered for the retarded COPCs (i.e., the enhancement factor was set to 1 in the STOMP input file).

Table 4-1. Summary of Key Elements and Representative Parameters Associated with Site-Specific Model Components for IDF PA

Longitudinal Macrodispersivity in Saturated Media as a Function of Overall Problem Scale with Data Classified by Reliability (after Gelhar et al. 1992)

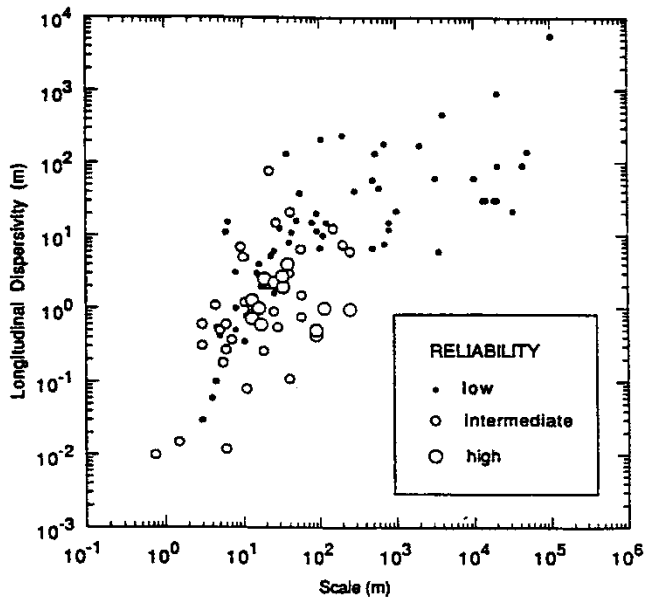

Relationship Between Saturated Longitudinal Macrodispersivity (αL) and Scale of Measurement (Ls).

Reference	Relationship	Origin	Saturated Longitudinal Macrodispersivity Estimate (m) for 100 m (328 ft) Scale
Neuman (1990)	$\alpha_L \approx 0.017 L_s^{1.5}$	"Universal relationship" established considering both field and laboratory data (excluding modeling results)	17.0
Schulze-Makuch (2005)	$\alpha_L \approx 0.085 L_s^{0.81}$	Established considering field and modeling results (all reliabilities) and excluding laboratory data	3.5
Xu and Eckstein (1995)	$\alpha_L \approx 0.94(\log_{10} L_s)^2$	Established considering the same data set as Neuman (1990) including numerical model results	6.0

The ratio of longitudinal to transverse macrodispersivity is chosen to be 10 based on PNNL-23711. The vertical macrodispersivity is based on van der Kamp et al. 1994.

Table 4-1. Summary of Key Elements and Representative Parameters Associated with Site-Specific Model Components for IDF PA

TABLE 4-1 NOTES and REFERENCES:

*Applies to all subfacies of this unit (van der Kamp et al. 1994, "Field Study of a Long and Very Narrow Contaminant Plume"

NAVD88 = *North American Vertical Datum of 1988*, National Geodetic Survey, U. S. Department of Commerce.

NA = not available.

NP = not present.

TCT = tensorial connectivity-tortuosity.

References:

Mantoglou 1984, "Large-Scale Models of Transient Unsaturated Flow and Contaminant Transport Using Stochastic Methods"

Russo 1991, "Stochastic Analysis of Simulated Vadose Zone Solute Transport in a Vertical Cross Section of Heterogeneous Soil During Nonsteady Water Flow"

*van der Kamp et al. 1994, "Field Study of a Long and Very Narrow Contaminant Plume"

BHI-00169, *Environmental Restoration Disposal Facility Performance Assessment*, Rev. 00, Bechtel Hanford, Inc., Richland, Washington

DOE/ORP-2000-24, *Hanford Immobilized Low Activity Waste Performance Assessment: 2001 Version*, Rev. 0,

Gelhar et al., 1992, A Critical Review of Data on Field-Scale Dispersion in Aquifers"

Millington and Quirk 1961, "Permeability of Porous Solids"

Neuman 1990, "Universal Scaling of Hydraulic Conductivities and Dispersivities in Geologic Media"

PNNL-13037, 2004, *Geochemical Data Package for the 2005 Hanford Integrated Disposal Facility Performance Assessment,* Rev 2

PNNL-23711, *Physical, Hydraulic, and Transport Properties of Sediments and Engineered Materials Associated with Hanford Immobilized Low-Activity Waste*

RPP-20621, *Far-Field Hydrology Data Package for the Integrated Disposal Facility Performance Assessment*, Appendix E, "Hanford Low-Activity Tank Waste Performance Assessment Activity: Determination of In Situ Hydraulic Parameters of the Upper Hanford Formation"

Schulze-Makuch 2005, "Longitudinal Dispersivity Data and Implications for Scaling Behavior"]

WHC-EP-0645, 1995, *Performance Assessment for the Disposal of Low-Level Waste in the 200 West Area Burial Ground*

WHC-SD-WM-EE-004, *Volume 1: Performance Assessment of Grouted Double-Shell Tank Waste Disposal at Hanford*

WHC-SD-WM-TI-730, *Performance Assessment for the Disposal of Low-Level Waste in the 200 East Area Burial Grounds*, Rev. 0

Xu and Eckstein 1995, "Use of Weighted Least-Squares Method in Evaluation of the Relationship Between Dispersivity and Field Scale"

Zhang and Khaleel 2010, "Simulating field-scale moisture flow using a combined power-averaging and tensorial connectivity-tortuosity approach"

Zhang et al. 2003, Describing the unsaturated hydraulic properties of anisotropic soils using a tensorial connectivity-tortuosity (TCT) concept

4.4 MODEL VALIDATION AND MODEL CALIBRATION

A substantial body of literature exists indicating the manner in which scientific validation of models is pursued (e.g., Bredehoeft and Konikow 1993, "Ground-Water Models: Validate or Invalidate"; Neuman 1992, "Validation of safety assessment models as a process of scientific and public confidence building"; Tsang 1991, "The Modeling Process and Model Validation"). Because PA models cannot be tested over the spatial scales of interest and the long time periods for which the models make predictions, the customary definition of model validation (i.e., comparison of model estimates with actual data at the space-time scales of interest) is precluded (NUREG-1573, *A Performance Assessment Methodology for Low-Level Radioactive Waste Disposal Facilities: Recommendations of NRC's Performance Assessment Working Group*; NUREG-1636, *Regulatory Perspectives on Model Validation in High-Level Radioactive Waste Management Programs: A Joint NRC/SKI White Paper*). Therefore, this section on model validation is viewed as a summary of the documented theoretical or scientific basis for each of the PA model components that have been developed and their suitability for supporting the PA decision-making. Below is presented a variety of topical discussions which serve as the basis of confidence building and model validation of IDF PA groundwater pathway models and results.

- Basis for recharge estimates
- Basis for vadose zone model development and its evaluation
- Basis for saturated media model development and its calibration

4.4.1 Basis for Recharge Estimates

Recharge rates have been estimated from studies conducted at the Hanford Site over the last 30 years. Recharge rates are available for natural and disturbed soils, for soils with and without vegetation, and for various plant communities. In addition, recharge has been estimated for surface covers with varying plant communities. These estimates are based on lysimeter records, tracer tests (chloride mass balance), and computer simulations to match field data. PNNL-14744, PNNL-16688; and PNNL-14702, *Vadose Zone Hydrogeology Data Package for Hanford Assessments*, provide primary sources of information on recharge estimates for the Hanford Site that are relevant to IDF. The estimates used in the PA will consider estimates of recharge made for the 200 Areas and for conditions at IDF inferred from measurements made at the IDF site (Section 3.1.1).

An extensive set of data exists for estimates of recharge for engineered barriers. For example, almost two decades of field-scale recharge studies have been conducted on an engineered Prototype Hanford Barrier (a 5 m thick multilayered capillary barrier with 2 m of silt loam) that was constructed in the 200 East Area (north of IDF in 200 East Area) in August 1994. The barrier performance was monitored almost continuously for 15 years to document structural stability, erosion, and components of the water balance including precipitation, surface runoff, water storage, percolation out of the root zone, and evapotranspiration. The barrier recharge estimates used in the PA are supported by the Prototype Hanford Barrier data (PNNL-18845, *200-BP-1 Prototype Hanford Barrier – 15 Years of Performance Monitoring*).

4.4.2 Basis for Vadose Zone Model Development and Its Evaluation

The spatial extent of various HSUs within the WMA C model domain are based on an extensive borehole dataset discussed in Section 3.2.1. The geologic framework model for WMA C is derived

from the information provided in Section 3.2.1 of RPP-RPT-56356, "Development of Alternative Digital Geologic Models of Waste Management Area C". It should be noted that at the Hanford Site more than 3,000 boreholes have been logged (PNNL-13653, "A Catalog of Geologic Data for the Hanford Site") and primary HSU designations and extents are well established.

The vadose zone hydraulic properties for IDF PA are derived from a set of laboratory (core-scale) experiments conducted on samples representative of Hanford H2, and H3 units. The methodology is discussed in detail in PNNL-23711. For IDF PA vadose zone modeling, each heterogeneous geologic unit is replaced by an EHM with macroscopic flow properties. With each heterogeneous unit assigned its upscaled or effective hydraulic properties, the simulated flow fields predict the bulk or mean flow behavior at the field scale. Details are presented in PNNL-23711. Two evaluations conducted in support of IDF VZ modeling follow:

- EHM approximation
- Variable Anisotropy Model

4.4.2.1. Equivalent Homogeneous Model Approximation. An evaluation of the vadose zone conceptual model and the EHM approximation was performed using the nearby Sisson and Lu injection test site (Figure 4-7) moisture content database. The database at the nearby Sisson and Lu site therefore serves as a proxy for IDF, and is an important resource in understanding large-scale moisture movement in imperfectly stratified heterogeneous media and a relatively dry moisture regime such as those existing at IDF. Details of the Sisson and Lu site, field injections and the spatio-temporal distribution of observed moisture plume are described elsewhere (Ye et al. 2005, "Stochastic Analysis of Moisture Plume Dynamics of a Field Injection Experiment"; Zhang and Khaleel 2010, "Simulating field-scale moisture flow using a combined power-averaging and tensorial connectivity-tortuosity approach").

Two variations of EHM model for the heterogeneous Hanford sediments are explored based on the Sisson and Lu experiments. In the first method, the small-scale core measurements for hydraulic properties were used to predict the large-scale flow behavior at the Sisson and Lu site (Zhang and Khaleel 2010). The second method is based on an inverse approach that inverts the large-scale unsaturated properties using the temporal evolution of the moisture content distribution (Yeh et al. 2005, "Estimation of Effective Unsaturated Hydraulic Conductivity Tensor Using Spatial Moments of Observed Moisture Plume). For both approaches, a moment analysis (Ye et al. 2005) was used to quantify the center of mass and the spread of the injected water for the observed and simulated moisture plumes. The first moments represent the mass center of the plume in different directions at a given time. The second moments measure the spread of the plume about its mass centers. For the forward as well as the inverse EHM-based methods, spatial moments (first and second) of the simulated plume based on the effective hydraulic conductivities were in good agreement with those for the observed plume (Zhang and Khaleel 2010; Yeh et al. 2005). Details are included in the preceding two references.

Figure 4-7. Location of the Sisson and Lu Injection Test Site and the Integrated Disposal Facility in 200 East Area.

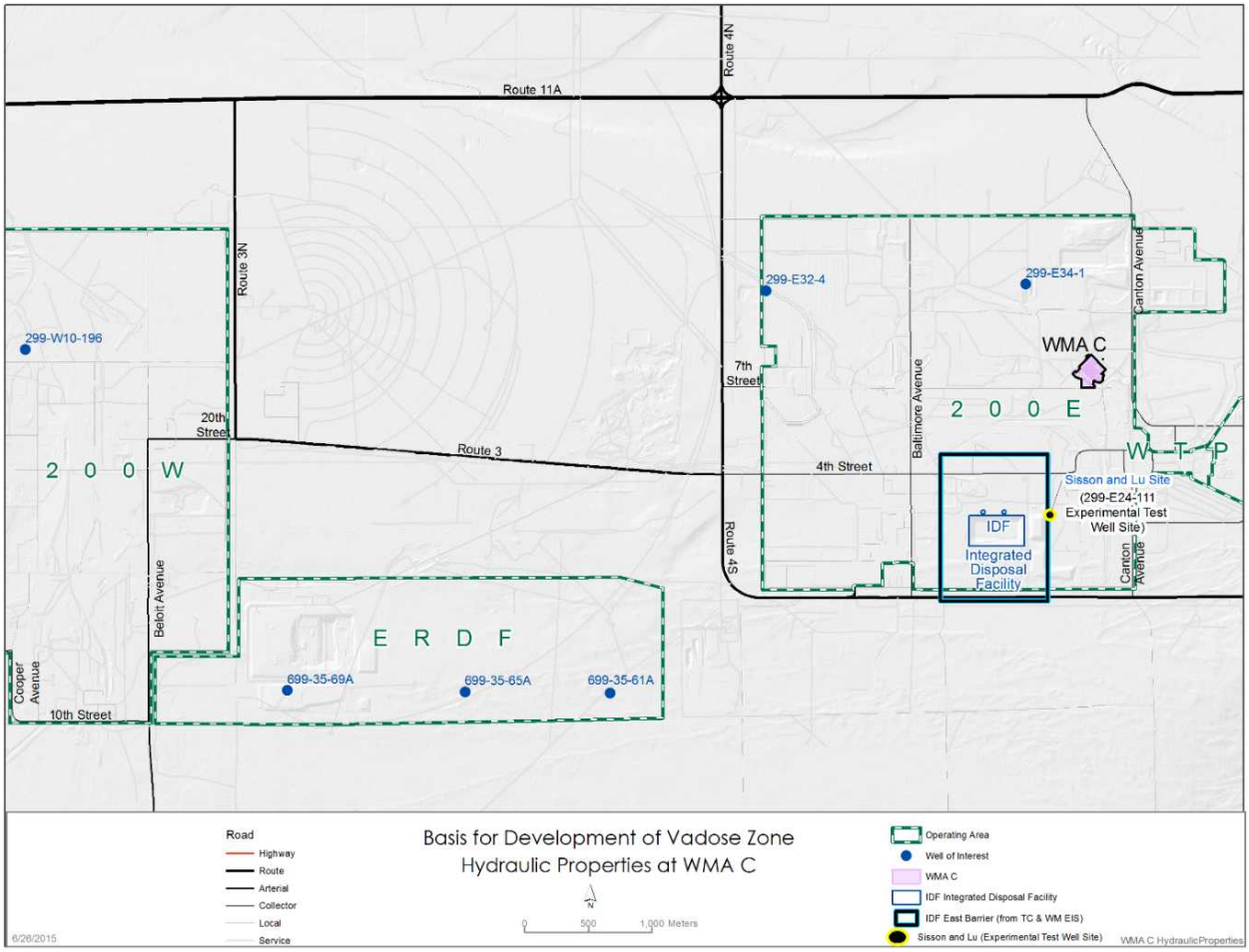

The Sisson and Lu site database also provided a framework for testing two heterogeneous modeling approaches based on combining soft (initial moisture content, bulk density and particle-size distribution) and hard (soil hydraulic properties) data (Ye et al. 2007 " Simulation of field injection experiments in heterogeneous unsaturated media using cokriging and artificial neural network"; Ye and Khaleel 2008 "An Evaluation of Three Methods for Characterizing Media Heterogeneity"). The heterogeneous models do not invoke the EHM approximation. The use of both soft and hard data was valuable in reproducing the detailed moisture plume for the two heterogeneous models (i.e., the splitting of the moisture plume sandwiched within the coarse media between two fine layers). The observed and simulated spatial moments (first and second), however, were not significantly different from those using the EHM-based methods. Hence, models using both hard and soft data, in addition to honoring the observed first and second moments, were able to reproduce the splitting of the observed plume. On the other hand, the EHM-based modeling does not capture the detailed plume behavior but honors the first and second moments of the observed moisture plume. With the IDF PA groundwater pathway simulations being conducted over a large flow domain and over a long time frame, the fact that the calculated

moments for both the EHM and heterogeneous models are of similar magnitude is an important finding, and provides justification for use of EHM approximation for vadose zone modeling.

4.4.2.2. Variable Anisotropy Model. As discussed earlier (Section 3.0), a TCT model (Zhang et al. 2003) is used to evaluate and apply variable, tension dependent anisotropy for the hydrostratigraphic units at IDF. Details about the development of the tension-dependent anisotropy model and its application to the hydrostratigraphic units at IDF are presented in PNNL-23711.

An evaluation of the TCT model was performed. Zhang and Khaleel (2010) estimated the 3D effective unsaturated hydraulic conductivity of the Sisson and Lu site via a combined Power Averaging-Tensorial Connectivity Tortuosity (PA-TCT) model. The heterogeneous media at the Sisson and Lu site were conceptualized as five geologic units, each of which was represented by an anisotropic EHM. The directional effective hydraulic conductivity for each anisotropic EHM was determined by upscaling the laboratory-measured hydraulic properties at the Sisson and Lu site with the combined PA-TCT approach. Based on the degree of soil stratification, four anisotropy levels, i.e., zero (isotropy), low, intermediate, and high anisotropy, were categorized. A high anisotropy corresponds to the perfectly layered structure and a low anisotropy means weak stratification. Because there were no data to determine the degree of soil stratification and no prior knowledge of the anisotropy level, Zhang and Khaleel (2010) quantified the levels of anisotropy in unsaturated conductivity (K) based on the use of typical power law values (p) to estimate the upscaled unsaturated K in the horizontal (Kh) and vertical (Kv) directions for different anisotropy categories. The definitions apply to the entire range of saturation and are described as follows:

- isotropic (ISO): p = 0, for both Kh and Kv
- low anisotropy (LA): p = 1 for Kh and p = 1/3 for Kv
- intermediate anisotropy (IA): p = 1 for Kh and p = 0 for Kv
- high anisotropy (HA): p = 1 for Kh and p = -1 for Kv

Note that the above calculation is equivalent to the arithmetic mean when p = 1, the geometric mean when p = 0, and the harmonic mean when p = -1. Larger differences between the p values in the horizontal and vertical directions mean a higher degree of anisotropy in unsaturated hydraulic conductivity. Hence, the EHMs were isotropic (zero anisotropy) for the ISO case, and were equivalent to perfectly layered media with the maximum anisotropy case HA.

Figure 4-8 shows the observed and simulated centers of the injected fluid plume within the monitored region in the *z* direction. The LA simulations gave the best prediction, while ISO overestimated, and intermediate anisotropy (IA) and high anisotropy (HA) underestimated the movement in the vertical direction (Figure 4-8). Unlike other cases, the trend in the movement of mass center in the *z* direction for the LA and the observed plumes is similar; the comparison between the two is reasonably good. As both the low anisotropy case and the observed plumes indicate, the mass centers moved most rapidly during the early part of the injection experiment. In the *z* direction, the mass center for the observed plume traveled downward ~1 m for the first 15 days but ~1.1 m in the following 45 days (Ye et al. 2005).

Figure 4-8. The Observed and Simulated Center of Mass in the Vertical (z) Direction.

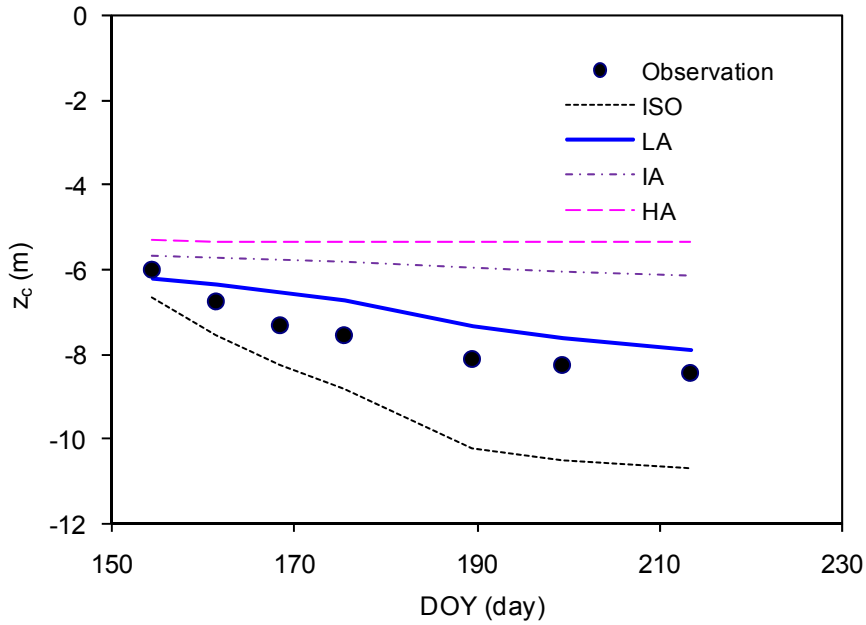

Source: Zhang, Z. F. and R. Khaleel, "Simulating field-scale moisture flow using a combined power-averaging and tensorial connectivity-tortuosity approach,"

DOY = day of year

Figure 4-9 illustrates the temporal evolution of components of the spatial variance tensor as an indication of the spreading of the injected water. The observed spatial variances (σ_{xx}^2, σ_{yy}^2 and σ_{zz}^2) of the plume increased with time, indicative of the continuous spreading of the plume around its mass center in the *x*-, *y*-, and *z*-directions during the injection experiment. The larger spatial variances in the *x*- and *y*-directions than in the *z*-direction suggest a greater spreading in the horizontal plane than in the vertical. The cross-covariances (σ_{xy}^2, σ_{xz}^2, and σ_{yz}^2) are non-zero because the principal directions of the moisture plume were not aligned with the *x*- *y*- *z* coordinate system. Among all cases, the simulation of LA predicted the spreading the best. The ISO overestimated, whereas IA and HA underestimated the vertical spreading. The opposite is true for the lateral spreading. Note the considerable deviation of HA and IA based spatial variances, in comparison to observed spatial variances.

Figure 4-9. The Observed and Simulated Center of Mass in the Vertical (z) Direction.

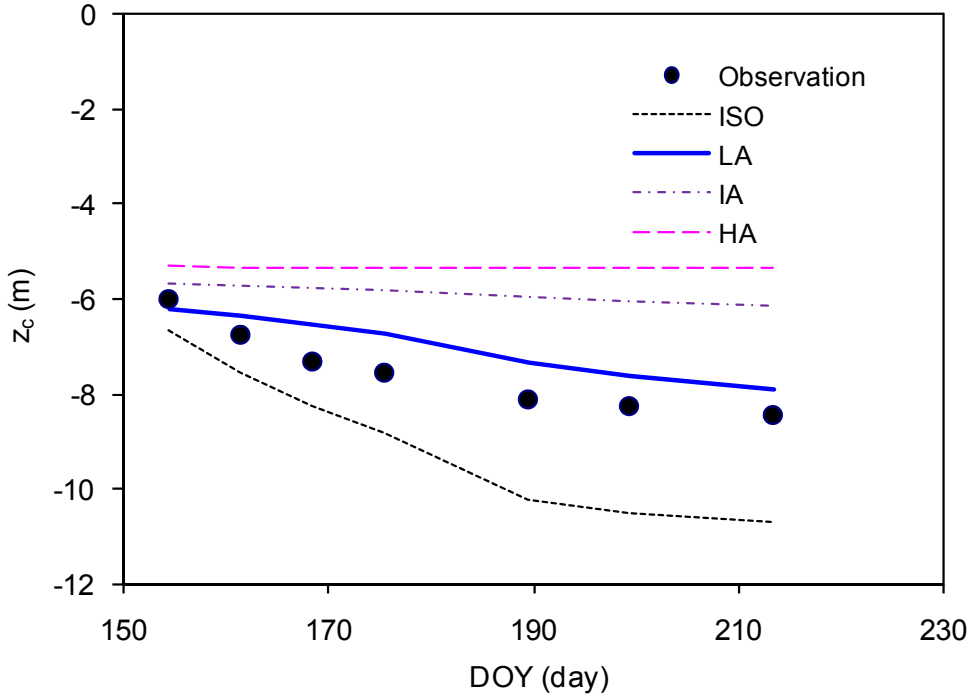

Source: Zhang, Z. F. and R. Khaleel, "Simulating field-scale moisture flow using a combined power-averaging and tensorial connectivity-tortuosity approach,"

DOY = day of year

Thus, the preceding numerical simulations showed that, if the Sisson and Lu site flow domain was treated as being isotropic, the vertical migration was significantly overestimated while the lateral movement was underestimated. To the contrary, if the media were treated as layered, the lateral moisture movement was considerably overestimated while the vertical movement was underestimated. However, when the flow domain was modeled as being mildly anisotropic with the PA-TCT based parameters, the model could successfully predict the moisture flow and the simulated plume matched best the center of mass and the spread of the injected water of the observed moisture plume. In summary, an application of the EHM approximation and the PA-TCT model suggests that the model provides a reasonable framework for upscaling core-scale measurements as well as an accurate simulation of moisture flow in a heterogeneous vadose zone.

4.4.3 Basis for Saturated Media Model Development and its Calibration

For the IDF PA modeling, each hydrostratigraphic unit within the unconfined aquifer is treated as an anisotropic EHM. Effective parameters and appropriate boundary conditions derived from a regional scale groundwater flow model are used in the PA. A calibrated CPGWM (CP-47631) serves as the basis for developing macro-scale parameters for the unconfined aquifer at IDF. The development of CPGWM incorporates over 30 years of experience on development and application of groundwater models for the Central Plateau (PNL-10886, *Development of a Three-Dimensional Ground-Water Model of the Hanford Site Unconfined Aquifer System: FY 1995 Status Report*; PNNL-13641, *Uncertainty Analysis Framework – Hanford Site-Wide*

Groundwater Flow and Transport Model; PNNL-14398, *Transient Inverse Calibration of the Site-Wide Groundwater Flow Model (ACM2): FY 2003 Progress Report*; PNNL-14753, *Groundwater Data Package for the 2004 Composite Analysis*; PNNL-12261, *Revised Hydrogeology for the Suprabasald Aquifer System, 200-East Area and Vicinity, Hanford Site, Washington*).

The CPGWM incorporates the large-scale geologic and hydrogeologic features and provides estimates of water levels, hydraulic gradients, and groundwater flows throughout the 200 West and 200 East Areas, for current and expected future groundwater conditions. A key aspect of unconfined aquifer modeling is the presence of the Old Columbia River channel (Figure 4-10) beneath IDF and the vicinity; its presence is manifested in exceedingly low hydraulic gradient measurements. The ancestral river deposits are characterized by open-framework gravel formations (Figure 4-11); these have exceptionally high permeability due to the lack of sediment in the pore spaces between the gravel particles. Digital photo logs (Figure 4-11) illustrate the nature of open-framework gravel deposits in the vicinity of WMA C which is located northeast of IDF; such logs are, however, not available for boreholes near IDF. Large-scale features such as ancient Columbia River deposits also left a footprint on groundwater plume migration; tritium and I-129 plume extents essentially follow the highly conductive paleochannel flow path (Figure 4-10).

Figure 4-10. The Observed and Simulated Center of Mass in the Vertical (z) Direction.

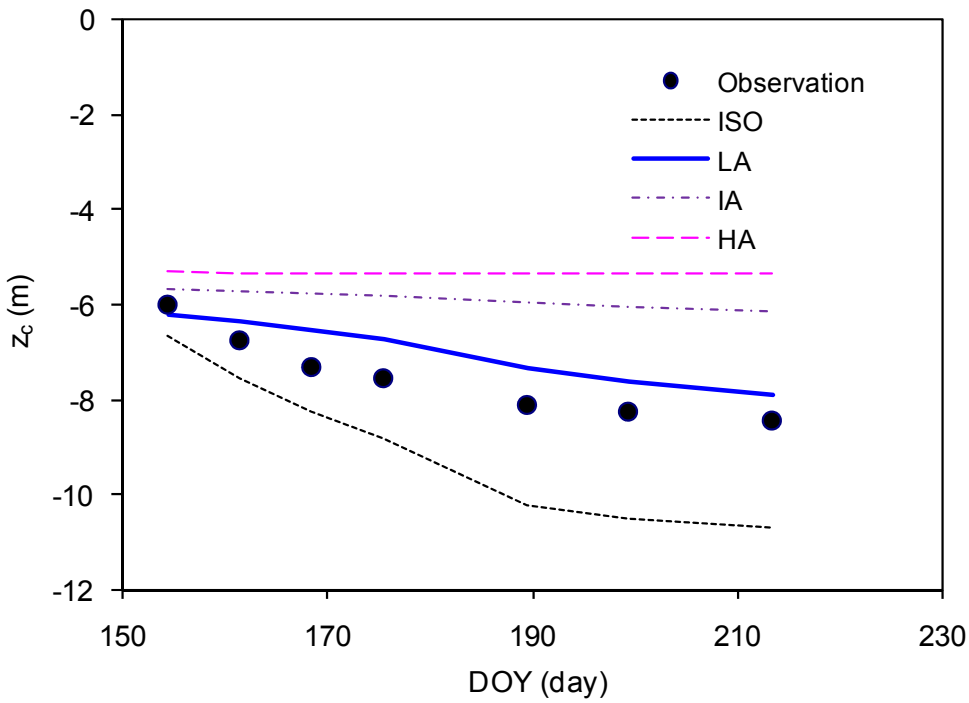

Source: Zhang, Z. F. and R. Khaleel, "Simulating field-scale moisture flow using a combined power-averaging and tensorial connectivity-tortuosity approach,"

DOY = day of year

Figure 4-11. Spreading of the Moisture Plume in (a) x (Easting), (b) y (Northing), and (c) z (Vertical) Directions Based on the Diagonal Components of the Second Moments.

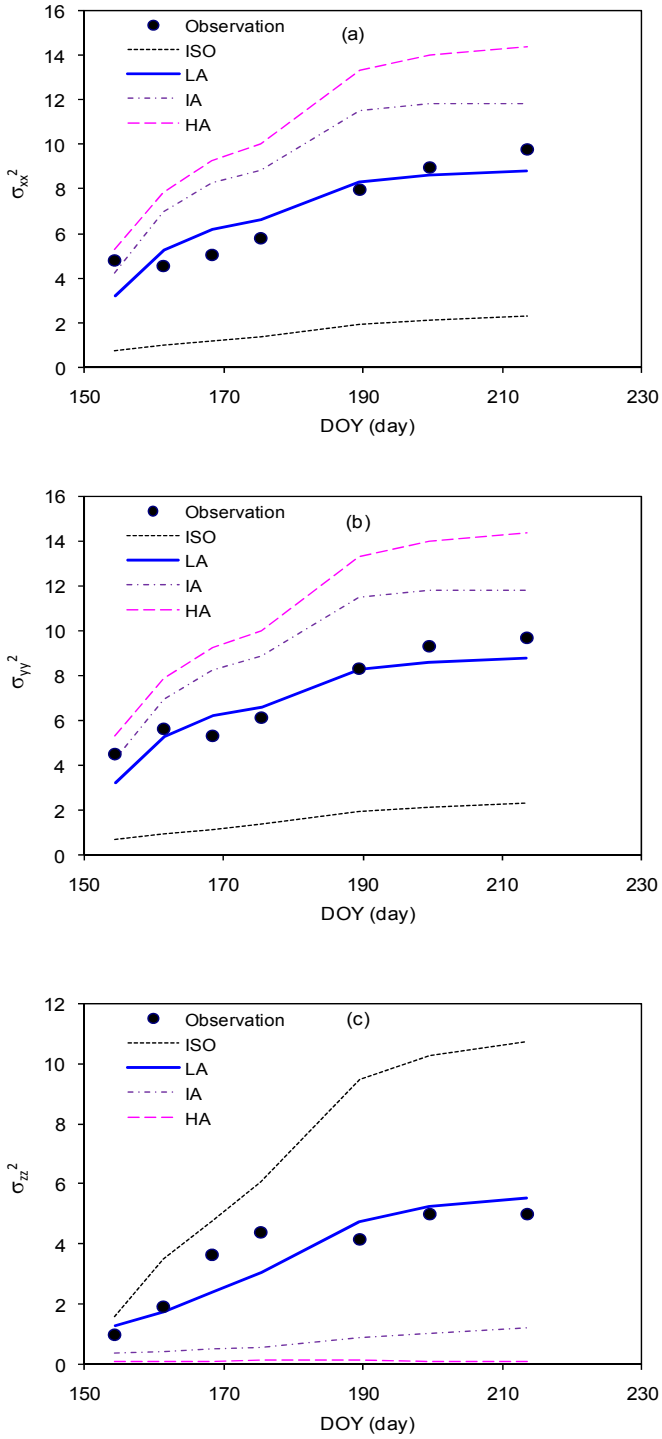

Source: Zhang, Z. F. and R. Khaleel, "Simulating field-scale moisture flow using a combined power-averaging and tensorial connectivity-tortuosity approach,"

DOY = day of year

The CPGWM-calibrated saturated hydraulic conductivity for Hanford gravels in the vicinity of IDF is exceedingly high (~17,000 m/day) (Figure 4-12). The tritium and I-129 plumes essentially track the high conductivity path (i.e., dark blue) in Figure 4-12. The CPGWM-simulated water levels are compared to observed values for the large number of wells within the Central Plateau (Figure 4-13) as well as to wells located upgradient and downgradient of IDF (Figures 4-14 and 4-15). The observed heads and CPGWM-simulated heads, representing a time span of over 20 years, compare well providing confidence in the predictive capabilities of the CPGWM as well as how the IDF site saturated media properties are parameterized and groundwater fluxes apportioned in the PA.

The presence of exceedingly high saturated conductivity and low hydraulic gradients for IDF unconfined aquifer is supported by another line of evidence. Figure 4-16 illustrates a comparison of 200 West Area versus 200 East Area groundwater mounding effects on water table elevation from discharges within the Central Plateau. The B Pond facility, located within 305 m east of IDF, started operating in 1945 and received a total discharge in excess of 1.0E+12 liters. The B-Pond operation ceased in August 1997; the discharge volumes were at a maximum during 1988. As illustrated by Figure 4-16, the groundwater mounding impacts are remarkably distinct for the two Areas as reflected in the considerable separation in water table elevations between the 200 West and 200 East Areas. Furthermore, following cessation of discharges, the 200 East Area water table elevations equilibrated to near-equilibrium levels by 2010, whereas the 200 West Area water table conditions are still far from equilibrium by 2010, thus further supporting the presence of low hydraulic gradient condition in the vicinity of IDF.

4.5 MODEL SENSITIVITY, UNCERTAINTY, AND SCREENING ANALYSES

The 2017 IDF PA will evaluate the effects of conceptual and parameter uncertainties on natural system flow and transport. The effects of uncertainties in transport parameters will be assessed in sensitivity analyses and uncertainty analyses. The objective of the sensitivity analyses will be to quantify the effects of parameter variations on the results of numerical simulations using STOMP/eSTOMP. The objective of the uncertainty analyses will be to assess the effects of parameter uncertainties on uncertainties in the numerical results.

A preliminary list of sensitivity and uncertainty cases is included in Section 4.5.1 and Section 4.5.2, respectively. The list is compiled by considering the FEPs that could possibly affect releases flow and transport in the natural system. When considering what FEPs may be important to the performance of the natural system, consideration is given to the input parameters applied to the soil types that could result in retardation of COPCs in the vadose and saturated zones, parameters that could affect the subsurface saturation, and previous modeling experience. In addition, sensitivity and uncertainty runs that address comments received during development meetings with stakeholders and subject matter experts are also considered. These considerations are used to develop a preliminary list of runs to be performed. When analyzing the results of the initial sensitivity runs, additional sensitivity and uncertainty runs may be identified and previously identified runs may be eliminated from further consideration. Ultimately the purpose of the sensitivity and uncertainty analyses is to build confidence that the IDF will adequately retain COPCs (or identify where additional mitigation measures are needed) to develop a reasonable assurance that the facility will be protective of human health and the environment after it is closed.

4.5.1 Sensitivity Analysis

This model package focuses on the 3-D saturated-unsaturated numerical flow and transport model itself and its applicability. The use of the model to perform sensitivity calculations is documented in separate EMCFs. Sensitivity results are not included in this MPR, with the exception of those evaluations that are necessary to demonstrate the soundness of the model (Section 4.8). As discussed earlier, 2-D VZ/SZ models will be run to evaluate the presence of clastic dikes on BTCs at the 100 m boundary. In addition, 2-D VZ/SZ models will be developed and run to evaluate the presence of thin-layered, discontinuous paleosols on contaminant breakthrough curves (BTC) at the 100 m boundary.

Figure 4-12. Location of the Paleochannel Associated with the Ancestral Columbia River near the IDF Site.

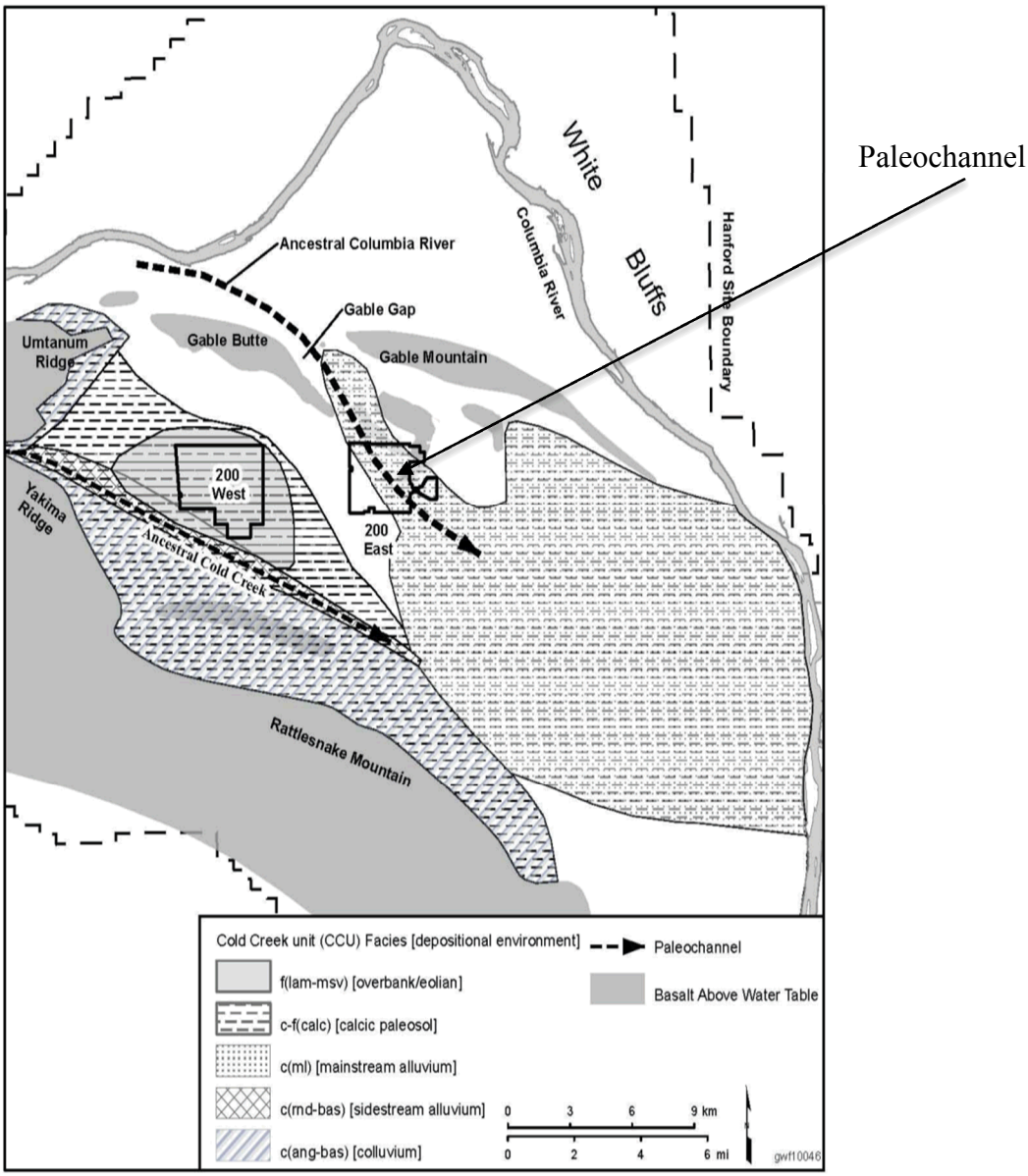

Figure 4-13. Digital Photo Log for Borehole 299-E27-4 with an Expansion Showing the Open-Framework Gravel above and below the Water Table.

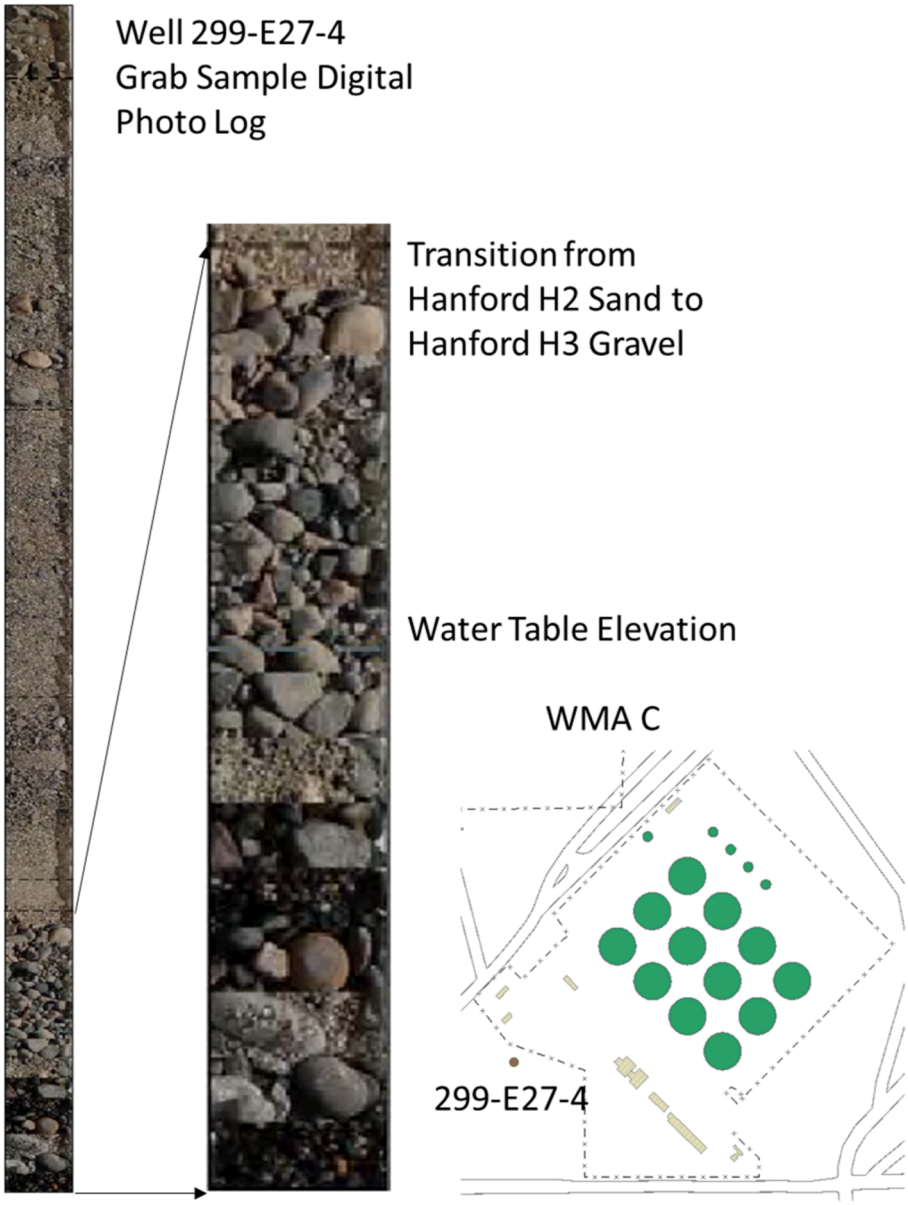

Source: PNNL-14656, *Borehole Data Package for Four CY 2003 RCRA Wells 299-E27-4, 299-E27-21, 299-E27-22, and 299-E27-23 at Single-Shell Tank, Waste Management Area C, Hanford Site, Washington*.

WMA = Waste Management Area

Figure 4-14. Model-Calibrated Saturated Hydraulic Conductivity Values using the Central Plateau Groundwater Model Version 6.3.3.

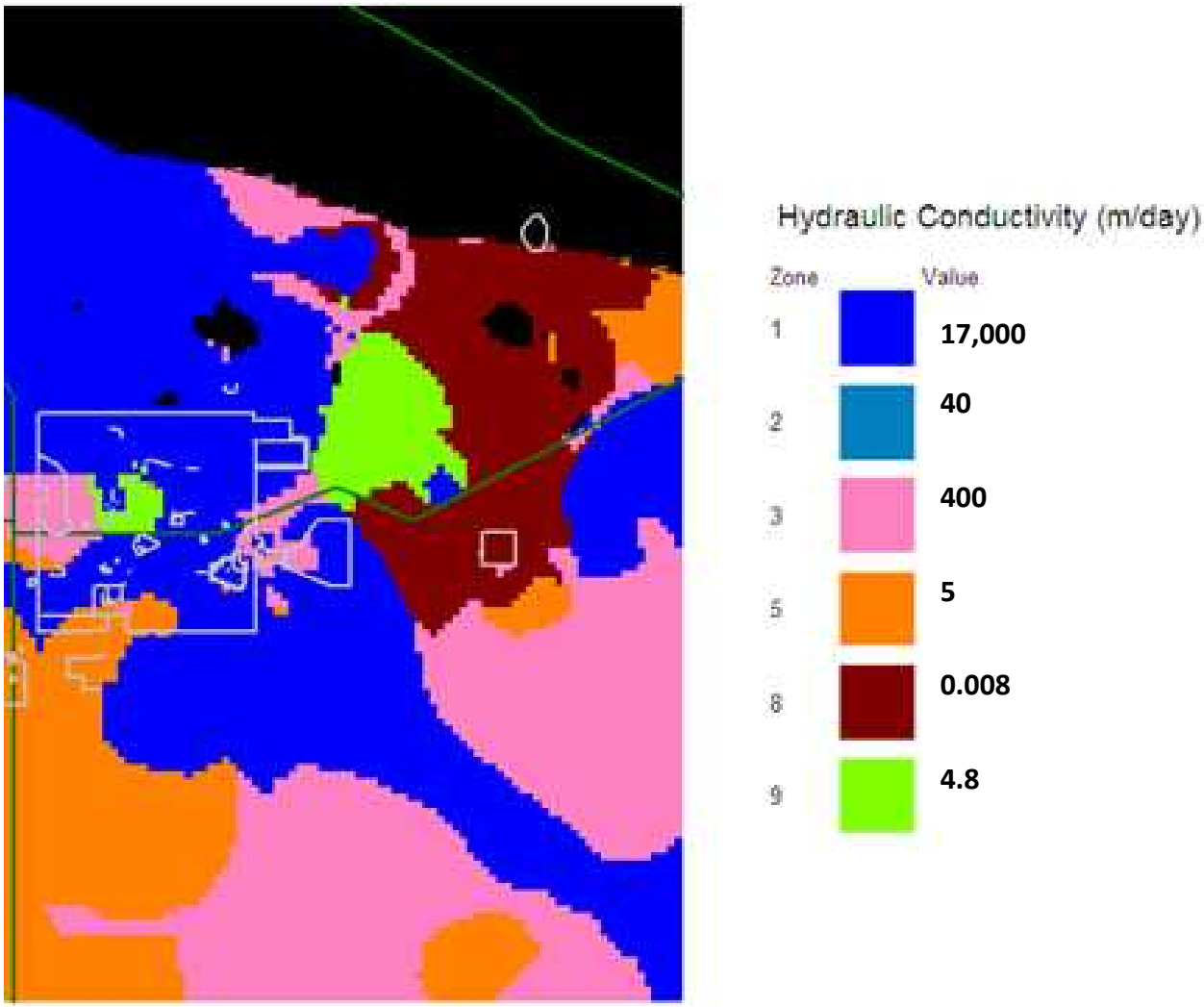

Source: CP-47631, *Model Package Report: Central Plateau Groundwater Model Version 6.3.3*

Figure 4-15. Comparison of (a) Measured versus Simulated Water Levels, and (b) Probability Density of Water Elevation Misfits for the Central Plateau Groundwater Model.

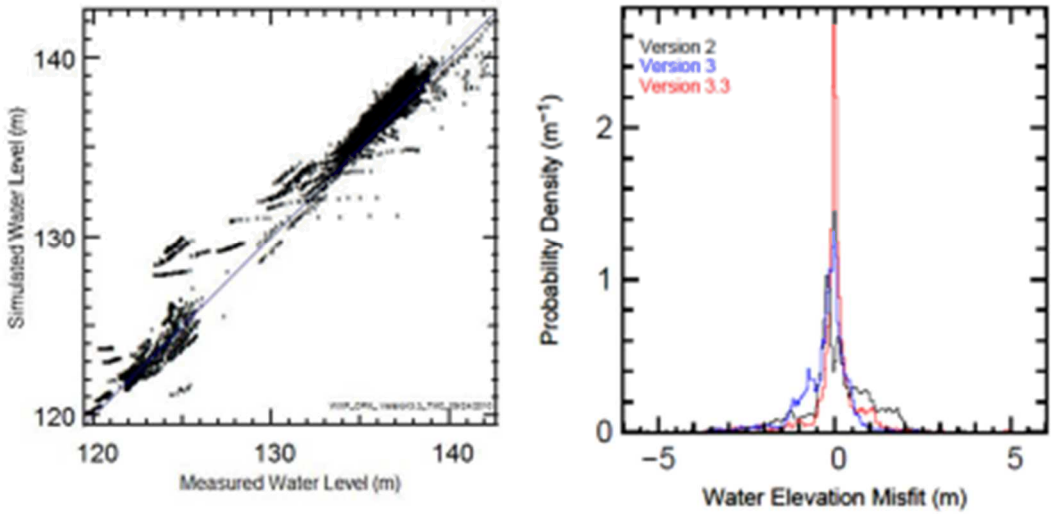

Source: CP-47631, *Model Package Report: Central Plateau Groundwater Model Version 6.3.3*

Figure 4-16. Location of Wells near IDF site for Comparison of Measured versus Simulated Water Levels.

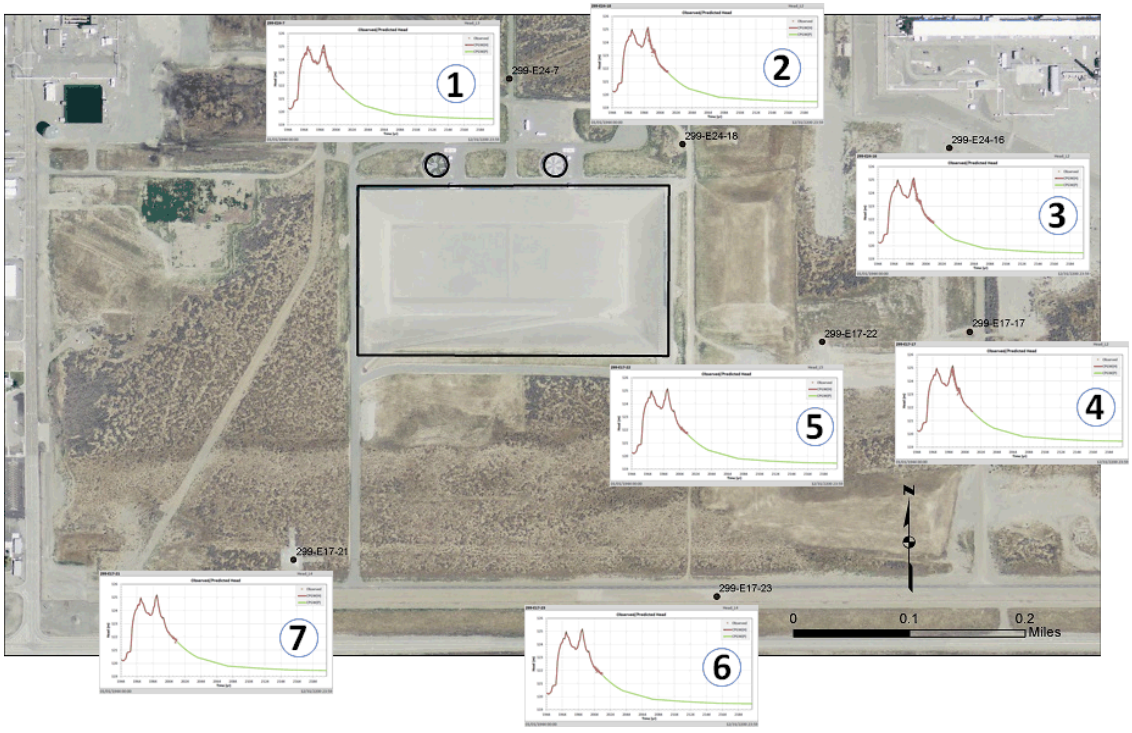

Source: CP-47631, *Model Package Report: Central Plateau Groundwater Model Version 6.3.3*

Figure 4-17. Comparison of Measured versus Simulated Water Levels for Wells near the IDF Site.

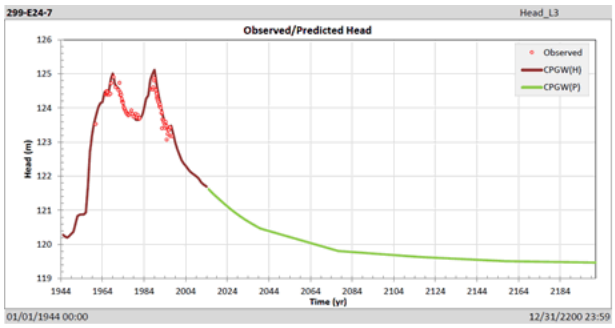

Plot 1

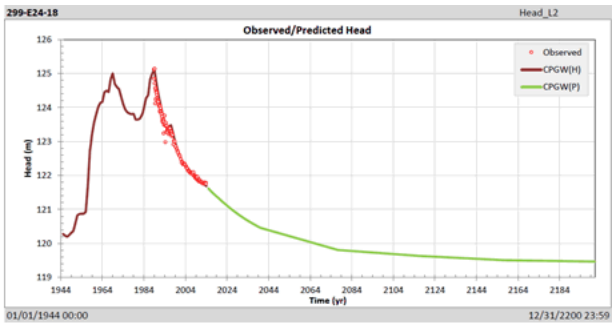

Plot 2

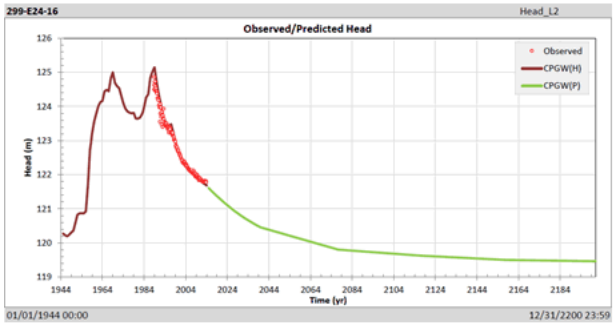

Plot 3

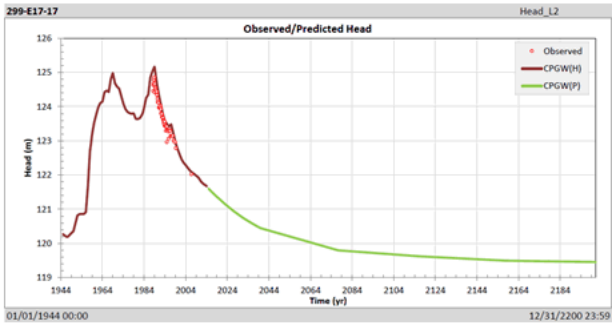

Plot 4

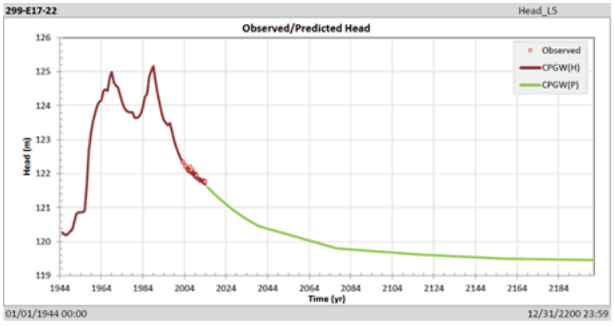

Plot 5

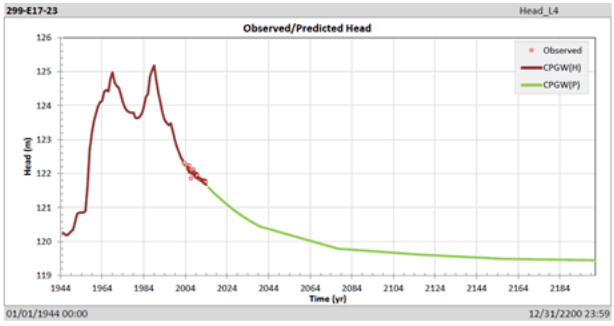

Plot 6

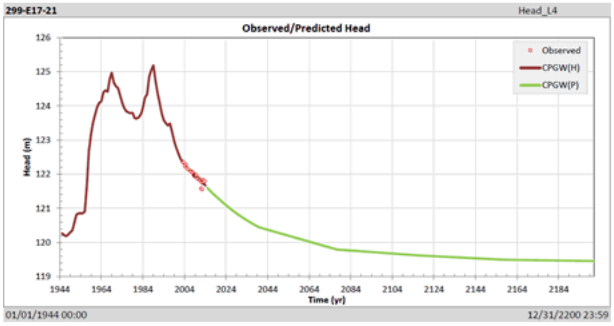

Plot 7

Figure 4-18. Comparison of Groundwater Mounding Effects from Discharges in the 200 West Area and 200 East Area.

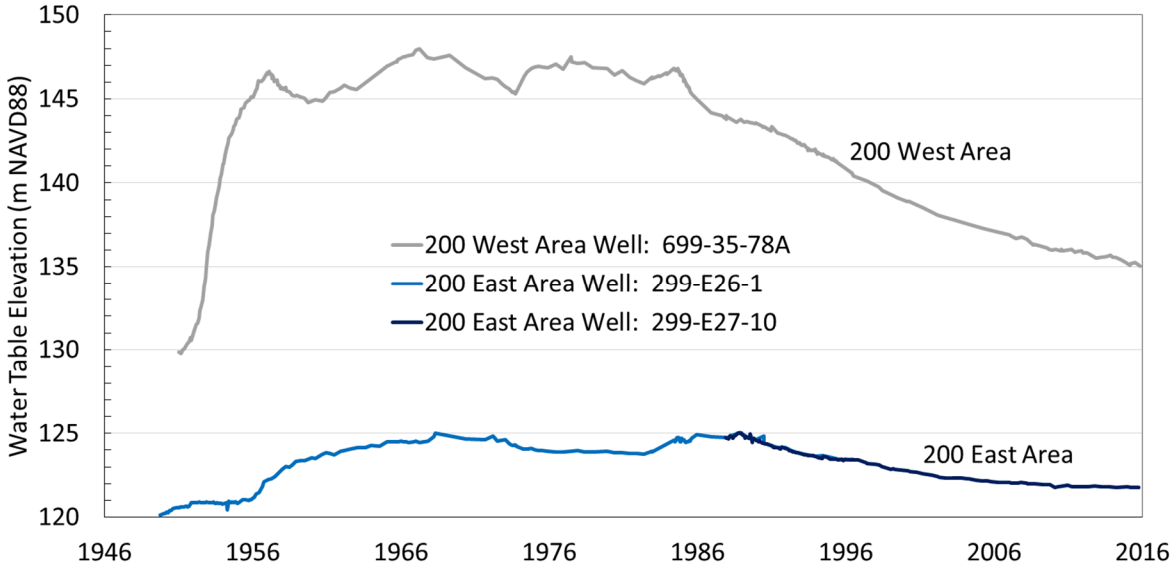

Source: CP-47631, *Model Package Report: Central Plateau Groundwater Model Version 6.3.3*

4.5.2 Uncertainty Analysis

This model package focuses on the 3-D saturated-unsaturated numerical flow and transport model itself and its applicability. The use of the model to perform uncertainty calculations is documented in separate EMCFs. Uncertainty results are not included in this MPR, with the exception of those evaluations that are necessary to demonstrate the soundness of the model (Section 4.8).

4.5.3 Screening Analysis

Screening calculations are necessary to demonstrate the soundness of the model. Such calculations provide a check that the model domain is sufficiently sized to prevent the boundary conditions from inappropriately affecting the solution in the region of interest. The screening calculations presented below used varying cap drainage rates, and varying degrees of vadose zone anisotropy to ensure that the model domain is sufficiently robust over a range of expected scenarios.

An enhanced recharge occurs for the IDF cap (surface barrier) side slope edges (Table 4-1). Figures 4-17 and F-18 illustrate the simulated moisture difference, within the vadose zone model domain, between the cap drainage simulation and the background recharge simulation at 0.9 mm/yr with high vadose zone anisotropy for IDF west-east and north-south sections, respectively. Similarly, Figures 4-19 and 4-20 illustrate the simulated moisture difference between the cap drainage simulation and the background recharge simulation at 5 mm/yr with high vadose zone anisotropy for IDF west-east and north-south sections, respectively. A background recharge of 1.7 mm/yr was used for the example model implementation case (Appendix D); recharge scenarios of 0.9 and 5 mm/yr are used to bracket the range of expected values. Also, a low anisotropy best matched the simulated moisture plume at the controlled test site near IDF (Section 4.4.2). A high anisotropy scenario was used to test if the model domain boundaries are sufficiently robust. Simulation results demonstrate that the simulated moisture difference is close to zero for the varying cases of recharge and anisotropy for west-east as well as north-south directions (Figures 4-17 and 4-20).

Figure 4-19. Simulated Moisture Difference Between Cap Drainage Simulation and Background Recharge Simulation at 0.9 mm/y with High Anisotropy (West-East Section).

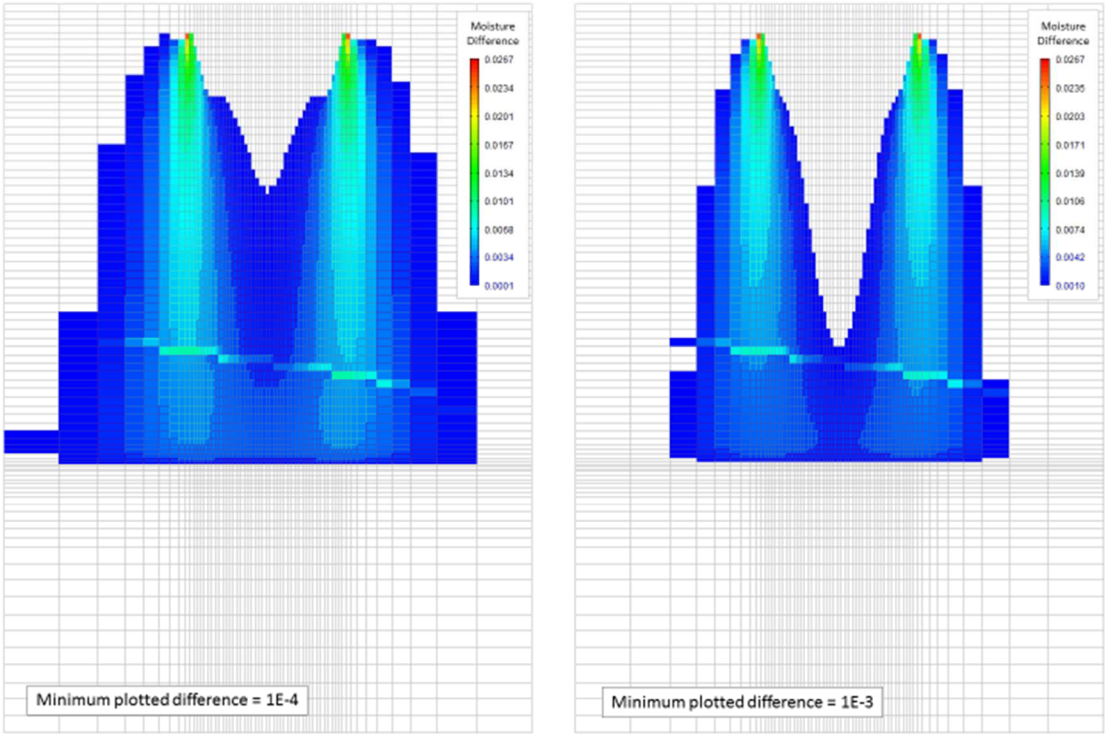

Figure 4-20. Simulated Moisture Difference Between Cap Drainage Simulation and Background Recharge Simulation at 0.9 mm/y with High Anisotropy (North-South Section).

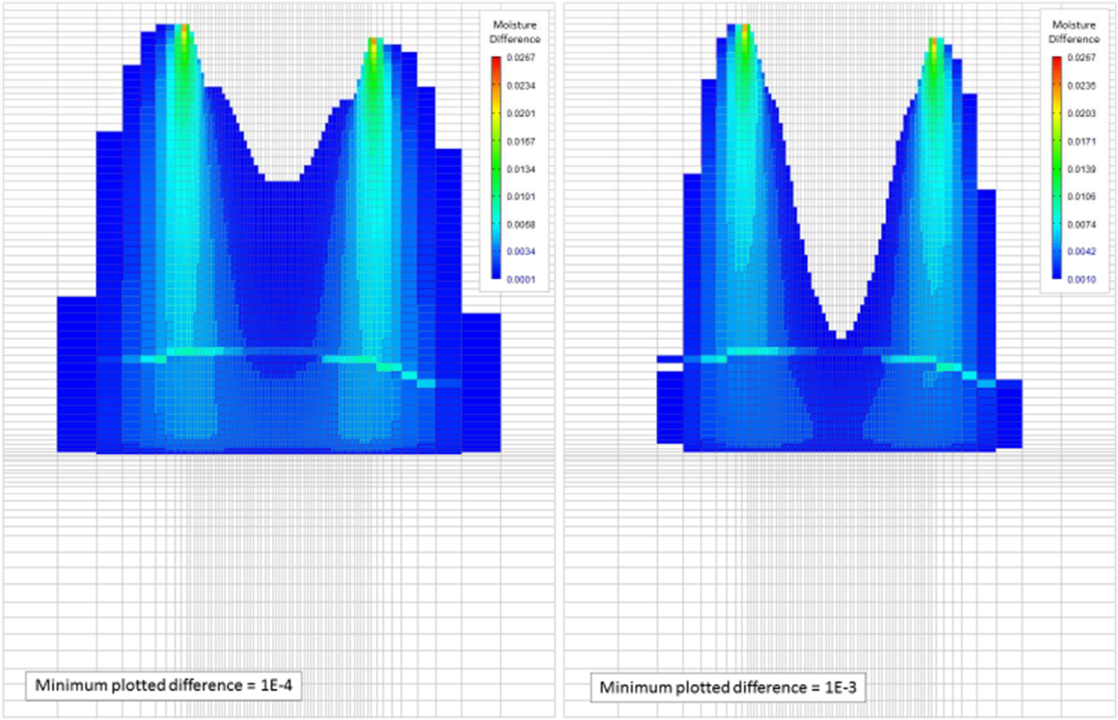

Figure 4-21. Simulated Moisture Difference Between Cap Drainage Simulation and Background Recharge Simulation at 5.0 mm/y with High Anisotropy (West-East Section).

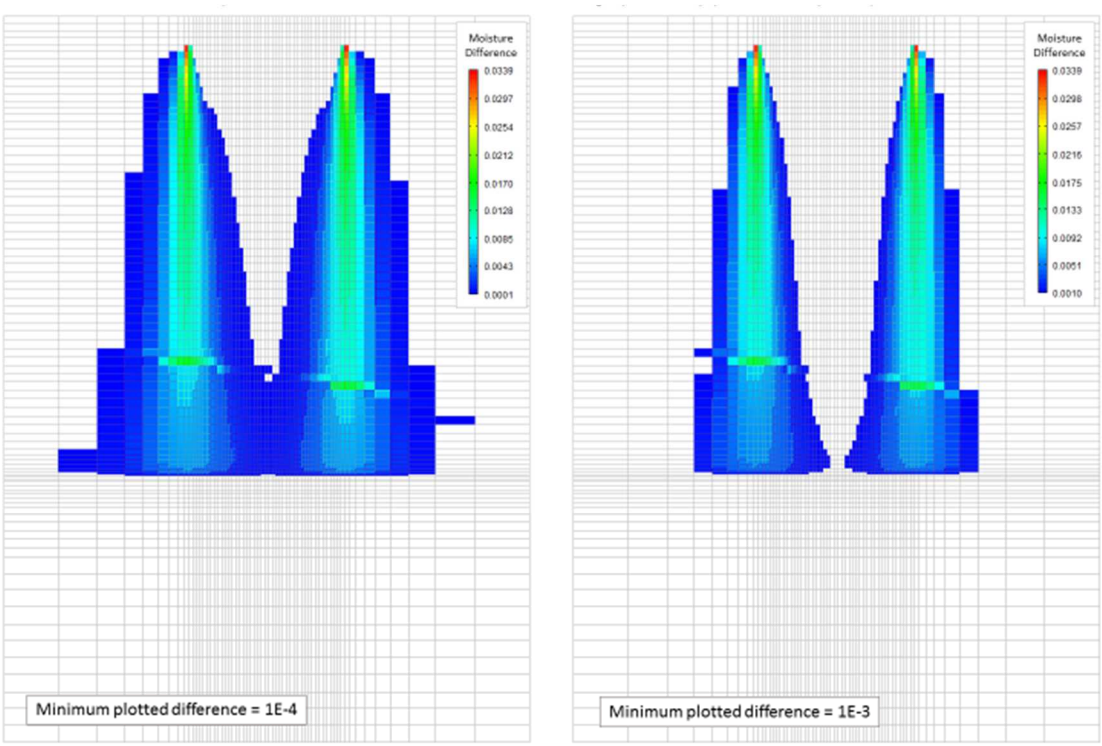

Figure 4-22. Simulated Moisture Difference Between Cap Drainage Simulation and Background Recharge Simulation at 5.0 mm/y with High Anisotropy (North-South Section).

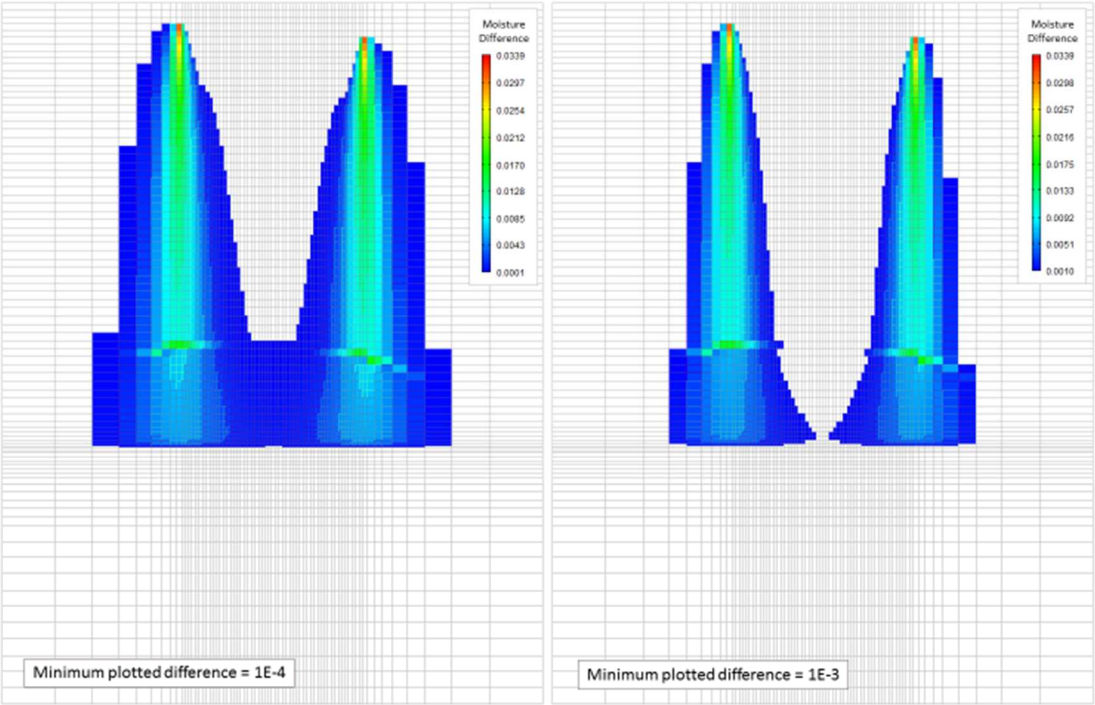

This page intentionally left blank.

5.0 STOMP SOFTWARE

The STOMP software is licensed by CHPRC for use under the terms of a limited government license from PNNL, which developed the code to meet Nuclear Quality Assurance (NQA)-1-2008 with 2009 addenda and DOE O 414.1D, *Quality Assurance*, software requirements. Specifically, PNNL manages STOMP under a Configuration Management Plan (PNNL-SA-92584, "Subsurface Transport Over Multiple Phases (STOMP) Software Configuration Management Plan") in conjunction with a Software Test Plan (PNNL-SA-92579, *STOMP Software Test Plan*), that detail the procedures used to test, document and archive modifications to the source code.

STOMP is used to solve the Richards' equation (the water mass conservation equation in PNNL-12030, *STOMP Subsurface Transport Over Multiple Phases Version 2.0 Theory Guide*) and the advection-dispersion equation (the solute mass conservation equation in PNNL-12030) that govern water flow and solute transport, respectively, under variably saturated conditions in the vadose zone and groundwater. Formal procedures for software problem reporting and corrective actions for software errors and updates are maintained and implemented (PNNL-24118). The STOMP software is also supported by a Software Requirement Specification (PNNL-24122, "Software Requirements Document for STOMP and eSTOMP") and a Software Design Document (PNNL-SA-92585). STOMP is supported by an online User Guide (http://stomp.pnnl.gov/user_guide/STOMP_guide.stm) and a Theory Guide (PNNL-12030). The User Guide is available in an online format that is frequently updated at http://stomp.pnnl.gov/user_guide/STOMP_guide.stm. The Theory Guide is updated periodically by addenda (e.g., PNNL-15482, "STOMP Subsurface Transport Over Multiple Phases Version 1.0 Addendum: ECKEChem Equilibrium-Conservation-Kinetic Equation Chemistry and Reactive Transport"). STOMP was selected to simulate the transport of contaminants in the vadose zone of the 200 Area in and around IDF because STOMP fulfills the following specifications.

- The STOMP simulator operational modes needed for implementation of this model is available free for government use under a limited government-use agreement.
- The STOMP simulator solves the necessary governing equations (i.e., Richards' equation and solute conservation of mass).
- It is capable of directly simulating the principal FEPs that are relevant (Appendix A and highlighted items).
- The STOMP simulator is well documented.
- The STOMP simulator development meets NQA-1 -2008 with 2009 addenda software requirements and is compliant with DOE O 414.1D requirements for Safety Software (PNNL-SA-92579; PNNL-SA-92584; PNNL-SA-54079, *Requirements for STOMP Subsurface Transport Over Multiple Phases*).
- The STOMP simulator is distributed with source code, enhancing transparency.
- The modeling team implementing this model has expertise in use of this simulator.
- There is an extensive history of application of STOMP at Hanford and elsewhere including verification, validation, and benchmarking (DOE/RL-2011-50, *Regulatory*

Basis and Implementation of a Graded Approach to Evaluation *of Groundwater Protection*).

Use of STOMP is in keeping with DOE direction for simulation of vadose zone flow and transport at the Hanford Site (06-AMCP-0133, *Hanford Groundwater Modeling Integration*).

5.1 STOMP SOFTWARE QUALITY ASSURANCE

The use of STOMP to implement the IDF PA model and perform calculations is performed in a manner that satisfies and complies with environmental quality assurance requirements indicated by 10 CFR 830, "Nuclear Safety Management," and Subpart A, "Quality Assurance"; DOE O 414.1D; and state and federal environmental regulations. EM-QA-001, Rev. 1, *EM Quality Assurance Program*, Attachment G "Software Quality Requirements" and Attachment H "Model Development, Use, and Validation," list DOE management expectations for compliance, including configuration control, evaluation, implementation, verification and validation, and operation and maintenance.

Quality assurance project planning for STOMP modeling follows the guidance in EPA/240/R-02/007, *Guide for Quality Assurance Project Plans for Modeling*. Model project planning includes documenting specific model development efforts and applications. It addresses as relevant and important all nine "Group A" elements presented in EPA/240/B-01/003, *EPA Requirements for Quality Assurance Project Plans*. The nine elements include problem definition and background, quality objectives and criteria for measurements and data acquisition leading to model inputs and outputs, data validation and usability, references, documentation and records management, special training requirements and certifications for modelers, and assessments and reports to management.

5.2 STOMP CONTROLLED CALCULATION SOFTWARE

The following describes the STOMP controlled calculation software and its computational platform.

- Software Title: STOMP-W (a scientific tool for analyzing single- and multiple-phase subsurface flow and transport using the integrated finite volume discretization technique with Newton-Raphson iteration).
- Software Version: STOMP-W was provided by PNNL on January 30, 2013, and was tested and approved for use by CHPRC as "CHPRC Build 4."
- Hanford Information System Inventory Identification Number: 2471 (Safety Software S3, graded Level C).
- Computational Platform: Tellus Subsurface Modeling Platform (Tellus) hosted by Mission Support Alliance for CHPRC:
  - Server Chassis: Dell PowerEdge[6] M1000e Blade Enclosure
  - Compute Nodes: 16 Dell PowerEdge® M610 Blade Servers
- Intel Xeon[7] X5670 CPU (x2), 6 Cores/CPU, 2.93 GHz, 12MB Cache

[6] Dell and PowerEdge are registered trademarks of Dell Products, Inc.

[7] Intel and Xenon are registered trademark of Intel Corporation, Santa Clara, California.

- 96 GB RAM; DDR3; 1333 MHz
- 10Gbps Ethernet Mezzanine Card – Dual Port – X520DA2 x 2
- Storage: internal hard drives on management (frontend) server includes 4 SAMSUNG 830 Series MZ-7PC512D/AM 2.5" SATAIII MLC Internal Solid State Drives (SSDs)
- Operating System and Version
- Red Hat Enterprise Linux[8] 5 (Tikanga), Release 5.8

- Rocks Cluster/Ganglia open source software operating system
- Approved User: A. Wahi/ N. Hasan/A. Ali

5.3 SOFTWARE INSTALLATION AND CHECKOUT

After receipt of the STOMP source code from PNNL, CHPRC commits the code to the MKS Integrity[9] configuration management system that ensures traceability and precludes loss of information. Successful acceptance and installation includes confirming that the software is operating correctly by benchmarking results produced on the local computer system to those presented for selected problems described in CHPRC-00211 "STOMP Software Test Plan". The CHPRC software owner maintains the configuration-managed copies in MKS Integrity and grants access to the executable files to users upon request in accordance with the approved software installation and checkout forms.

Receipt of the current STOMP source code occurred in January 2013, and testing of CHPRC Build 4 on Tellus successfully concluded in April 2013. Approved users are registered in the Hanford Information System Inventory for safety software, which identifies users as authorized users of STOMP on the Tellus Platform as of May 6, 2013.

5.4 STATEMENT OF VALID SOFTWARE APPLICATION

The IDF PA requires calculations of the potential long-term impact on groundwater at the 100 m boundary. STOMP was developed for these type of applications, among others, and is used to solve the Richards' equation and the Advection-Dispersion equation that governs water flow and solute transport, respectively, under variably saturated conditions in the vadose zone and groundwater. The IDF PA implementation of STOMP to perform calculations satisfies and complies with environmental quality assurance requirements indicated by 10 CFR 830 Subpart A, DOE O 414.1D, and state and federal environmental regulations. Successful acceptance and installation of STOMP on Tellus concluded in April 2013, and the Hanford Information System Inventory for safety software lists A. Wahi, N. Hasan, and A. Ali, as authorized users of Build 4 of STOMP on the Tellus Platform.

The quality assurance project planning for STOMP modeling follows the guidance in EPA/240/R-02/007, and the conduct of implementation is shown to comply with DOE management expectations for compliance. Therefore, for this application STOMP is an appropriate software code to use, using it to implement the IDF PA model described in this report is consistent with STOMP's intended use, and its use is shown to comply with applicable quality assurance requirements.

---

[8] Linux is a registered trademark of Linus Torvolds in the U.S. and other countries.

[9] MKS Integrity is a trademark of the Parametric Technology Corporation, Needham, Massachusetts.

This page intentionally left blank.

6.0 MODEL CONFIGURATION MANAGEMENT

All inputs and outputs for the development of IDF PA models are required to be submitted to the CHPRC Environmental Model Management Archive (EMMA) to maintain and preserve configuration managed models. Inputs include the input files used in the STOMP simulations and the files called by the input files such as the zonation and boundary node list files. Basis information (the information collected to form the basis for model input parameterization) is also stored in the EMMA for traceability purposes. Use of the STOMP software for implementing the model described in this report is consistent with its intended use for CHPRC, as indicated in Section 5.4 “Statement of Valid Software Application.”

This page intentionally left blank.

7.0 MODEL LIMITATIONS

The IDF PA model limitations are largely centered on future land use of the Central Plateau, and the existence of Modified RCRA Subtitle C barrier for the closed facility. As discussed in Section 3.0, net infiltration and deep percolation are the major transport mechanisms for moving contaminants from the closed facility to the groundwater. In arid and semiarid regions with thick vadose zones, such as the Hanford Site, long-term factors like climate change, changes in the annual precipitation rates, and changes in vegetation structure and community are necessary to influence the deep moisture fluxes. For such arid/semiarid regions, large seasonal fluctuations in soil-moisture matric potential are essentially contained within the upper few meters of sediments, and the spatially and temporally varying moisture fluxes even out within the deep subsurface above the water table.

With expected changes to the land cover over time due to growth of vegetation, several time periods have been conceptualized (Section 3.1.1) to represent the changes in recharge rates and hydrologic conditions at the IDF site. Each of these time periods is characterized by a different recharge rate. Following is a discussion of two assumptions that pertain to recharge.

- Net infiltration through the thick, heterogeneous vadose zone in the 200 Areas dampens the effect of discrete events and, therefore, episodic precipitation events can be replaced by an average annual recharge rate.
- Impacts resulting from plausible climate change that may occur during the evaluation period do not adversely impact the performance of the surface or vadose zone as a barrier.

Multi-year evaluations of soil moisture content data collected from vegetated desert soils throughout the United States indicate that matric potentials remain highly negative (i.e., reflective of a dry moisture regime) and relatively invariant below depths of 2 to 5 m (Seyfried et al. 2005, “Ecohydrological Control of Deep Drainage in Arid and Semiarid Regions”). In response to intermittent years of elevated precipitation such as those caused by El Nino in the southwestern United States, the biomass usage of water by deep-rooted xeric vegetation increases, depleting the excess water, and no net increase in groundwater recharge occurs (Scanlon et al. 2006, “Global synthesis of groundwater recharge in semiarid and arid regions”; Leary 1990, “Analysis of Techniques for Estimating Potential Recharge and Shallow Unsaturated Zone Water Balance near Yucca Mountain, Nevada”). Simulation results representing the impact of a 20-year period of temporally varying precipitation on a surface barrier and a clean, graveled surface indicate that the temporal variation in drainage can effectively be ignored, and that an average value can be used with little loss of accuracy (WHC-EP-0332, *Simulations of Infiltration of Meteoric Water and Contaminant Plume Movement in the Vadose Zone at Single-Shell Tank 241-T-106 at the Hanford Site*, pp. 18-21).

The sensitivity-uncertainty period of analysis extends to 10,000 years. Therefore, impacts to the performance of the vadose zone as a barrier caused by climate change during the evaluation period are plausible. However, climate change is not likely to affect the performance of the vadose zone as a barrier appreciably. Recharge rates applied to the design and post-design periods of the modeling are likely to remain unchanged, even if the precipitation increases as a consequence of climate change (Section 3.1.2). Long-term climate studies (Section 3.1.2.6, Climate Change) indicate that for the last 10,000 years, precipitation ranged from 50 percent less

than current levels to as high as 128 percent of modern levels during the glacial period before the Holocene (PNNL-13033). As discussed in Section 3.1.2, the sagebrush community appears capable of exploiting any increases in soil moisture caused by increases in the annual precipitation consistent with or even in excess of the previous glacial period.

8.0 MODEL RECOMMENDATIONS

DOE/RL-2011-50 identifies a generalized model and limitations associated with the relevant FEPs for the 200 Areas vadose zone. Appendix A lists the FEPs relevant for the combined VZ/SZ modeling. Limitations specific to IDF PA were considered during FEPs process working sessions conducted earlier in 2015, and additional discussions and inputs were obtained from regulators and stakeholders. A document entitled *Summary Analysis for the 2017 Integrated Disposal Facility Performance Assessment* provides a quantitative assessment of the possible effects of the proposed modeling approach for IDF PA as well as a detailed comparison of the 2017 IDF PA modeling approach with the modeling approach adopted in the TC&WM EIS. The modeling approach embedded in this MPR (Sections 3 and 4) is a follow-up of the summary analysis report and its recommendations.

This page intentionally left blank.

9.0 REFERENCES

78 FR 75913, 2013, "Final Tank Closure and Waste Management Environmental Impact Statement for the Hanford Site, Richland, Washington: Record of Decision," *Federal Register*, Vol. 78, No. 240, pp. 75913-75919 (December 13).

Benson, J. E., R. T. Tveten, M. G. Asher, and P. W. Dunwiddie, 2011, *Shrub-Steppe and Grassland Restoration Manual for the Columbia River Basin.* Washington Department of Fish and Wildlife, Olympia, Washington.

BHI-00007, 1994, *Prototype Hanford Surface Barrier: Design Basis Document*, Rev. 0, Bechtel Hanford, Inc., Richland, Washington.

Butters, G. L., and W. A. Jury, 1989, "Field Scale Transport of Bromide in an Unsaturated Soil, 2. Dispersion Modeling," Water Resources Research, Vol. 25, No. 7, pp. 1583–1589.

Carvallo, H. O., D. K. Cassel, J. Hammond, and A. Bauer, 1976, "Spatial Variability of in Situ Unsaturated Hydraulic Conductivity of Maddock Sandy Loam," Soil Science, Vol. 121, pp. 1–8.

Cherrey, K. D., M. Flury, and J. B. Harsh, 2003, "Nitrate and colloid transport through coarse Hanford sediments under steady state, variably saturated flow," Water Resour. Res., 39(6), 1165, doi:10.1029/2002WR001944, 2003

CHPRC-00211, 2016, "STOMP Software Test Plan," Revision 3, CH2M HILL Plateau Remediation Company, Richland, Washington.

CP-47631, 2015, *Model Package Report: Central Plateau Groundwater Model Version 6.3.3*, Rev. 2, INTERA, Inc., Richland, Washington.

De Smedt, F. and P. J. Wierenga, 1984, "Solute Transfer through Columns of Glass Beads," *Water Resources Research*, Vol. 20, pp. 225232.

DOE M 435.1-1, 1999, *Radioactive Waste Management Manual*, U.S. Department of Energy, Washington, D.C.

DOE O 414.1D, 2011, *Quality Assurance*, U.S. Department of Energy, Washington, D.C.

DOE O 435.1, 1999, *Radioactive Waste Management*, U.S. Department of Energy, Washington, D.C.

DOE/EIS-0391, 2012, Final Tank Closure and Waste Management Environmental Impact Statement for the Hanford Site, Richland, Washington, U.S. Department of Energy, Washington, D.C.

DOE/ORP-2000-01, Maintenance Plan for the Hanford Immobilized Low-Activity Tank Waste Performance Assessment, Rev. 0, Fluor Federal Services, Richland, Washington.

DOE/ORP-2000-24, 2001, Hanford Immobilized Low Activity Waste Performance Assessment: 2001 Version, Rev. 0, U.S. Department of Energy, Office of River Protection, Richland, Washington.

DOE/RL-93-33, 1996, Focused Feasibility Study of Engineered Barriers for Waste Management Units in the 200 Areas, Rev. 1, U.S. Department of Energy, Richland Operations Office, Richland, Washington.

DOE/RL-94-47, 1994, *Proposed Plan for ERDF at Hanford Site*, Rev. 1, U.S. Department of Energy, Richland Operations Office, Richland, Washington.

DOE/RL-97-69, 1998, *Hanford Immobilized Low-Activity Tank Waste Performance Assessment*, Rev. 0, U.S. Department of Energy, Richland, Washington.

DOE/RL-2002-39, Rev. 0, 2002. *Standardized Stratigraphic Nomenclature for Post-Ringold Formation Sediments Within the Central Pasco Basin.* U.S. Department of Energy, Richland, Washington.

DOE/RL-2011-50, 2012, *Regulatory Basis and Implementation of a Graded Approach to* Evaluation *of Groundwater Protection*, Rev. 1, U.S. Department of Energy, Richland Operations Office, Richland, Washington.

DOE/RL-2012-57, 2012, Annual Summary of the Integrated Disposal Facility Performance Assessment 2012, U.S. Department of Energy, Richland, Washington.

EPA 402-R-94-012, 1994, *Technical Guide to Ground-Water Model Selection at Sites Contaminated with Radioactive Substances*, U.S. Environmental Protection Agency, Washington, D.C.

Fayer, M. J., G. W. Gee, M. L. Rockhold, M. D. Freshley, and T. B. Walters, 1996, "Estimating Recharge Rates for a Groundwater Model Using a GIS," *Journal of Environmental Quality*, Vol. 25, pp. 510518.

Gee, G. W., M. J. Fayer, M. L. Rockhold, and M. D. Campbell, 1992, "Variations in Recharge at the Hanford Site," *Northwest Science* 66:237250.

Gelhar, L. W. and C. L. Axness, 1983, "Three-Dimensional Stochastic Analysis of Macrodispersion in Aquifers," Water Resources Research, Vol. 19, No. 1, pp. 161–180.

Gelhar, L. W., 1993, Stochastic Subsurface Hydrology, Prentice Hall, New York, New York.

Gelhar, L. W., C. Welty, and K. R. Rehfeldt, 1992, "A Critical Review of Data on Field-Scale Dispersion in Aquifers," Water Resources Research, Vol. 28, No. 7, pp. 1955–1974.

Hills, R. G., P. J. Wierenga, D. B. Hudson, and M. R. Kirkland, 1991, "The Second Las Cruces Trench Experiment: Experimental Results and Two-Dimensional Flow Predictions," Water Resources Research, Vol. 27, No. 10, pp. 2707–2718.

HNF-5294, 1999, *Computer Code Selection Criteria for Flow and Transport Code(s) to Be Used in Vadose Zone Calculations for Environmental Analyses in the Hanford Site's Central Plateau*, Rev. 0, CH2M HILL Hanford Group, Inc., Richland, Washington.

Huyakorn, P. S. and G. F. Pinder, 1983, *Computational Methods in Subsurface Flow*, Academic Press, Salt Lake City, Utah.

International Atomic Energy Agency (IAEA), 2004, Safety Assessment Methodologies for Near Surface Disposal Facilities, Volumes 1 and 2, International Atomic Energy Agency, Vienna, Austria.

Khaleel, R. and J. F. Relyea, 2001, "Variability of Gardner's α for coarse-textured sediments," Water Resources Research, Vol. 37, No. 6, pp. 1567–1575.

Khaleel, R., T.-C. J. Yeh, and Z. Lu, 2002, "Upscaled Flow and Transport Properties for Heterogeneous Unsaturated Media," Water Resources Research, Vol. 38, No. 5, pp. 11.1–11.12.

06-AMCP-0133, 2006, *Hanford Groundwater Modeling Integration,* letter dated March 9, 2006 from K. A. Klein, DOE-RL, to P. L. Pettiette, Washington Closure Hanford, U.S. Department of Energy, Richland Operations Office, Richland, Washington.

PNNL-13037, 2004, *Geochemical Data Package for the 2005 Hanford Integrated Disposal Facility Performance Assessment,* Rev. 2., Pacific Northwest National Laboratory, Richland, Washington.

Leary 1990, "Analysis of Techniques for Estimating Potential Recharge and Shallow Unsaturated Zone Water Balance near Yucca Mountain, Nevada", University of Nevada, Reno.

Liu, Z., M. Flury, J. B. Harsh, J. B. Mathison, and C. Vogs (2013), *Colloid mobilization in an undisturbed sediment core under semiarid recharge rates*, Water Resour. Res., 49, 4985–4996, doi:10.1002/wrcr.20343

Luftig, S. D. and L. Weinstock, 1997, "Establishment of Cleanup Levels for CERCLA Sites with Radioactive Contamination" (memorandum to Addressees), OSWER No. 9200.418, Office of Emergency and Remedial Response and Office of Radiation and Indoor Air, U.S. Environmental Protection Agency, Washington, D.C., August 22.

Mantoglou, A. and L. W. Gelhar, 1987, "Stochastic Modeling of Large-Scale Transient Unsaturated Flow Systems," Water Resources Research, Vol. 23, No. 1, pp. 37–46.

Mantoglou, A., 1984, "Large-Scale Models of Transient Unsaturated Flow and Contaminant Transport Using Stochastic Methods," Ph.D. Thesis, Massachusetts Institute of Technology, Department of Civil Engineering, Cambridge, Massachusetts.

Millington, R. J. and J. P. Quirk, 1961, "Permeability of Porous Solids," Transactions of the Faraday Society, Vol. 57, pp. 1200–1207.

NAVD88, North American Vertical Datum of 1988, National Geodetic Survey, U.S. Department of Commerce, National Oceanic and Atmospheric Administration, Silver Spring, Maryland.

NEA, 02549, *Features, Events and Processes (FEPs) for Geologic Disposal of Radioactive Waste:* An International Database, Nuclear Energy Agency Organisation for Economic Co-Operation and Development, Paris, France.

Neuman, S. P., 1990, "Universal Scaling of Hydraulic Conductivities and Dispersivities in Geologic Media," *Water Resources Research*, Vol. 26, No. 8, p. 1749-1758.

Neuman S. P.,1992, Validation of safety assessment models as a process of scientific and public confidence building. In *Proceedings of HLWM Conference*, Vol. 2, Las Vegas.

Nielsen, D. R., J. M. Biggar, and K. T. Erh, 1973, "Spatial Variability of Field-Measured Soil-Water Properties," Hilgardia, Vol. 42, No. 7, pp. 215–260.

Nkedi-Kizza, P., J. W. Biggar, M. T. van Genuchten, P. J. Wierenga, H. M. Selim, J. M. Davidson, and D. R. Nielsen, 1983, "Modeling Tritium and Chloride 36 Transport Through an Aggregated Oxisol," *Water Resources Research*, Vol. 19, pp. 691700.

NUREG/CR-5965, 1994, Modeling Field Scale Unsaturated Flow and Transport Processes, Nuclear Regulatory Commission, Washington, D.C.

NUREG/CR-6114, 1994, Auxiliary Analyses in Support of Performance Assessment of a Hypothetical Low-Level Waste Facility: Groundwater Flow and Transport Simulation, Vol. 3, U.S. Nuclear Regulatory Commission, Washington, D.C.

NUREG-1573, 2000, A Performance Assessment Methodology for Low-Level Radioactive Waste Disposal Facilities: Recommendations of NRC's Performance Assessment Working Group, U.S. Nuclear Regulatory Commission, Washington, D.C.

NUREG-1636, 1999, Regulatory Perspectives on Model Validation in High-Level Radioactive Waste Management Programs: A Joint NRC/SKI White Paper. U.S. Nuclear Regulatory Commission .00 Office of Nuclear Material Safety and Safeguards Washington, DC.

Phillips, F. M., J. L. Mattick, T. A. Duval, D. Elmore, and P. W. Kubik, 1988, "Chlorine 36 and Tritium from Nuclear Weapons Fallout as Tracers for Long-Term Liquid and Vapor Movement in Desert Soils," Water Resources Research, Vol. 24, No. 11, pp. 1877-1891.

PNL-10788, 1995, *The Role of Plants and Animals in Isolation Barriers at Hanford, Washington*, Pacific Northwest National Laboratory, Richland, Washington.

PNL-10886, 1995, *Development of a Three-Dimensional Ground-Water Model of the Hanford Site Unconfined Aquifer System: FY 1995 Status Report,* Pacific Northwest National Laboratory, Richland, Washington.

PNNL-10285, 1995, *Estimated Recharge Rates at the Hanford Site,* Pacific Northwest National Laboratory, Richland, Washington.

PNNL-11367, 1996, *Hanford Prototype-Barrier Status Report: FY 1996,* Pacific Northwest National Laboratory, Richland, Washington.

PNNL-11463, 1997, A Comprehensive Analysis of Contaminant Transport in the Vadose Zone Beneath Tank SX-109, Pacific Northwest National Laboratory, Richland, Washington.

PNNL-12030, 2000, *STOMP Subsurface Transport Over Multiple Phases Version 2.0 Theory Guide*, Pacific Northwest National Laboratory, Richland, Washington.

PNNL-12261, 2000, *Revised Hydrogeology for the Suprabasald Aquifer System, 200-East Area and Vicinity, Hanford Site, Washington,* Pacific Northwest National Laboratory, Richland, Washington.

PNNL-13033, 1999, *Recharge Data Package for the Immobilized Low-Activity Waste 2001 Performance Assessment*, Pacific Northwest National Laboratory, Richland, Washington.

PNNL-13641, 2001, *Uncertainty Analysis Framework – Hanford Site-Wide Groundwater Flow and Transport Model,* Pacific Northwest National Laboratory, Richland, Washington.

PNNL-13653, 2005, *A Catalog of Geologic Data for the Hanford Site*, Rev. 2, Pacific Northwest National Laboratory, Richland, Washington.

PNNL-14398, 2003, *Transient Inverse Calibration of the Site-Wide Groundwater Flow Model (ACM2): FY 2003 Progress Report,* Pacific Northwest National Laboratory, Richland, Washington.

PNNL-14702, 2006, *Vadose Zone Hydrogeology Data Package for Hanford Assessments*, Rev. 1, Pacific Northwest National Laboratory, Richland, Washington.

PNNL-14725, 2004, *Geographic and Operational Site Parameters List (GOSPL) for the 2004 Composite Analysis*, Rev. 0, Pacific Northwest National Laboratory, Richland, Washington.

PNNL-14744, 2004, *Recharge Data Package for the 2005 Integrated Disposal Facility Performance Assessment,* Rev. 0, Pacific Northwest National Laboratory, Richland, Washington.

PNNL-14753, 2004, *Groundwater Data Package for the 2004 Composite Analysis,* Rev. 0, Pacific Northwest National Laboratory, Richland, Washington.

PNNL-15237, 2005, *Geology of the Integrated Disposal Facility Trench*, Pacific Northwest National Laboratory, Richland, Washington.

PNNL-15482, 2005, *STOMP Subsurface Transport Over Multiple Phases Version 1.0 Addendum: ECKEChem Equilibrium-Conservation-Kinetic Equation Chemistry and Reactive Transport*, Pacific Northwest National Laboratory, Richland, Washington.

PNNL-16688, 2007, *Recharge Data Package for Hanford Single-Shell Tank Waste Management Areas*, Pacific Northwest National Laboratory, Richland, Washington.

PNNL-17154, 2008, *Geochemical Characterization Data Package for the Vadose Zone in the Single-Shell Tank Waste Management Areas at the Hanford Site,* Pacific Northwest National Laboratory, Richland, Washington.

PNNL-18845, 2011, *200-BP-1 Prototype Hanford Barrier – 15 Years of Performance Monitoring*, Rev. 1, Pacific Northwest National Laboratory, Richland, Washington.

PNNL-22886, 2013, *System-Scale Model of Aquifer, Vadose Zone, and River Interactions for the Hanford 300 Area –Application to Uranium Reactive Transport*, RPT-DVZ-AFRI-019, Pacific Northwest National Laboratory, Richland, Washington.

PNNL-23711, 2015, *Physical, Hydraulic, and Transport Properties of Sediments and Engineered Materials Associated with Hanford Immobilized Low-Activity Waste*, Pacific Northwest National Laboratory, Richland, Washington.

PNNL-24122, 2016, "Software Requirements Document for STOMP and eSTOMP," Revision 3.2, Pacific Northwest National Laboratory, Richland, Washington.

PNNL-SA-92579, 2012, "STOMP Software Test Plan," Rev. 2.0, Pacific Northwest Laboratory, Richland, Washington.

PNNL-SA-92584, 2012, STOMP Software Configuration Management Plan, Rev. 1.5, Pacific Northwest Laboratory, Richland, Washington.

PNNL-SA-92585, 2012, "Software Design Description (SDD) for Subsurface Transport Over Multiple Phases (STOMP)", Revision 2.0, Pacific Northwest National Laboratory, Richland, Washington.

PNNL-SA-54079, *Requirements for STOMP Subsurface Transport Over Multiple Phases*, Rev. 1.1, Pacific Northwest National Laboratory, Richland, Washington.

Polmann, D. J., 1990, *Application of Stochastic Methods to Transient Flow and Transport in Heterogeneous Unsaturated Soils,* Ph.D. Thesis, Massachusetts Institute of Technology, Cambridge, Massachusetts.

PRC-PRO-IRM-309, 2014, *Controlled Software Management*, Revision 5, Change 0, Administrative Procedure, CH2M Hill Plateau Remediation Company, Richland, Washington.

RCRA, *Resource Conservation and Recovery Act of 1976*, 42 USC 6901, et seq.

RPP-17675, 2003. Risk Assessment Supporting the Decision on the Initial Selection of Supplemental ILAW Technologies, Rev. 0, CH2M HILL Hanford Group, Inc., Richland, Washington, September 29.

RPP-20691 Rev. 1, 2015, Facility Data for the Hanford Integrated Disposal Facility Performance Assessment, Washington River Protection Solutions, Richland, WA

RPP-RPT-56356, 2014, Development of Alternative Digital Geologic Models of Waste Management Area C, Washington River Protection Solutions, Richland, WA

RPP-RPT-59341, 2016, Integrated Disposal Facility Model Package Report: ILAW Glass Release, Washington River Protection Solutions, Richland, WA

RPP-RPT-59342, 2016, Integrated Disposal Facility Model Package Report: Non-Glass Release, Washington River Protection Solutions, Richland, WA

RPP-RPT-59343, 2016, Integrated Disposal Facility Model Package Report: Geologic Framework, Washington River Protection Solutions, Richland, WA

Russo, D., 1991, "Stochastic Analysis of Simulated Vadose Zone Solute Transport in a Vertical Cross Section of Heterogeneous Soil During Nonsteady Water Flow," Water Resources Research, Vol. 27, No. 3, pp. 267–283.

Russo, D., 1993, "Stochastic Modeling of Macrodispersion for Solute Transport in a Heterogeneous Unsaturated Porous Formation," Water Resources Research, Vol. 29, No. 2, pp. 383–397.

Scanlon, B. R., 1992, "Evaluation of Liquid and Vapor Water Flow in Desert Soils Based on Chlorine 36 and Tritium Tracers and Nonisothermal Flow Simulations," Water Resources Research, Vol. 28, No. 1, pp. 285–297.

Scanlon, B. R., Keese, K. E., Flint, A. L., Flint, L. E., Gaye, C. B., Edmunds, W. M. and Simmers, I. (2006), Global synthesis of groundwater recharge in semiarid and arid regions. Hydrol. Process., 20: 3335–3370. doi: 10.1002/hyp.6335

Schulze-Makuch, D., 2005, "Longitudinal Dispersivity Data and Implications for Scaling Behavior," *Ground Water*, Vol. 43, No. 3, p. 443–456.

Seyfried, M. S., Schwinning, S., Walvoord, M. A., Pockman, W. T., Newman, B. D., Jackson, R. B. and Phillips, F. M. (2005), Ecohydrological Control of Deep Drainage in Arid and Semiarid Regions. Ecology, 86: 277–287. doi:10.1890/03-0568

SGW-48478, 2011, *Interpretation and Integration of Seismic Data in the Gable Gap*, Rev. 0, CH2M HILL Plateau Remediation Company, Richland, Washington.

van der Kamp, G., L. D. Luba, J. A. Cherry, and H. Maathuis, 1994, "Field Study of a Long and Very Narrow Contaminant Plume," *Ground Water,* Vol. 32, No. 6, p. 1008–1016.

van Genuchten, M.Th., 1980, "A Closed-form Equation for Predicting the Hydraulic Conductivity of Unsaturated Soils" *Soil Science Society of America Journal*, vol. 44 pp 892-898.

Wan, J. M., and T. K. Tokunaga*, Film straining of colloids in unsaturated porous media: Conceptual model and experimental testing,* Environ. Sci. Technol., 31, 2413–2420, 1997.

Wang, J. S. and T. N. Narasimhan, 1985, "Hydrologic Mechanisms Governing Fluid Flow in Saturated, Fractured Porous Media," *Water Resources Research*, Vol. 21, pp. 1861-74.

WCH-520, Performance Assessment for the Environmental Restoration Disposal Facility, Hanford Site, Washington, Rev 1, Washington Closure Hanford, Richland, Washington.

WHC-EP-0645, 1995, *Performance Assessment for the Disposal of Low-Level Waste in the 200 West Area Burial Grounds*, Westinghouse Hanford Company, Richland, Washington.

WHC-SD-WM-EE-004, 1995, *Volume 1: Performance Assessment of Grouted Double-Shell Tank Waste Disposal at Hanford*, Rev. 1, Westinghouse Hanford Company, Richland, Washington.

Wierenga, P. J., R. G. Hills, and D. B. Hudson, 1991, "The Las Cruces Trench Site: Characterization, Experimental Results, and One-Dimensional Flow Predictions," Water Resources Research, Vol. 27, No. 10, pp. 2695–2705.

Wing, N. R. and G. W. Gee, 1994, "Quest for the Perfect Cap," *Civil Engineering* 64(10):38-41.

Xu, M. and Y. Eckstein, 1995, "Use of Weighted Least-Squares Method in Evaluation of the Relationship Between Dispersivity and Filed Scale," *Ground Water*, Vol. 33, No. 6, p.905-908.

Yang, J., R. Zhang, J. Wu, and M. B. Allen, 1997, "Stochastic analysis of adsorbing solute transport in three-dimensional, heterogeneous, unsaturated soils," Water Resources Research, Vol. 33, No. 3, pp. 1947–1956.

Ye, M., R. Khaleel, and T.-C.J. Yeh, 2005. "Stochastic Analysis of Moisture Plume Dynamics of a Field Injection Experiment," *Water Resources Research*, Vol. 41, W03013, doi:10.1029/2004WR003735.

Ye, M., R. Khaleel, M. G. Schaap, and J. Zhu (2007), Simulation of field injection experiments in heterogeneous unsaturated media using cokriging and artificial neural network, Water Resour. Res., 43, W07413, doi:10.1029/2006WR005030.

Ye and Khaleel, 2008, "An Evaluation of Three Methods for Characterizing Media Heterogeneity," American Geophysical Union, Fall Meeting 2008.

Yeh, T.-C. J., L. W. Gelhar and A. L. Gutjahr, 1985, "Stochastic Analysis of Unsaturated Flow in Heterogeneous Soils, 2. Statistically Anisotropic Media with Variable α," Water Resources Research, Vol. 21, No. 4, pp. 457–464.

Yeh, T.-C.J., M. Ye, and R. Khaleel, 2005. "Estimation of Effective Unsaturated Hydraulic Conductivity Tensor Using Spatial Moments of Observed Moisture Plume," *Water Resources Research*, Vol. 41, W03014, doi:10.1029/2004WR003736.

Zhang, Z. F. and R. Khaleel, 2010, "Simulating field-scale moisture flow using a combined power-averaging and tensorial connectivity-tortuosity approach," Water Resources Research, Vol. 46, W09505, pp. 1–14.

Zhang, Z. F., A. L. Ward, and G. W. Gee, 2003, Describing the unsaturated hydraulic properties of anisotropic soils using a tensorial connectivity-tortuosity (TCT) concept, Vadose Zone J., 2(3), 313–321.

APPENDIX A

FEATURES, EVENTS, AND PROCESSES

This page intentionally left blank.

Table A-1. Features, Events and Processes.

Feature, Event, Process (FEP)	Included	Process Model
0 ASSESSMENT CONTEXT		
0.01 Assessment endpoints		
0.02 Timescales of concern		
0.03 Spatial domain of concern		
0.04 Repository assumptions		
0.05 Future human action assumptions		
0.06 Future human behavior (target group) assumptions		
0.07 Dose response assumptions		
0.08 Assessment purpose		
0.09 Regulatory requirements and exclusions		
0.10 Model and data issues		
1 EXTERNAL FACTORS		
1.1 REPOSITORY ISSUES		
1.1.01 Site investigation		
1.1.02 Design, repository		Near Field (NF) Hydrology
1.1.03 Construction, repository		NF Hydrology
1.1.04 Emplacement of wastes and backfilling		NF Hydrology Glass Release Non glass diffusive release Non glass advective-diffusive
1.1.05 Closure, repository		NF Hydrology
1.1.06 Records and markers, repository		
1.1.07 Waste allocation		
1.1.08 Quality control		
1.1.09 Schedule and planning		
1.1.10 Administrative control, repository site		
1.1.11 Monitoring of repository		
1.1.12 Accidents and unplanned events		
1.1.13 Retrievability		
1.2 GEOLOGICAL PROCESSES AND EFFECTS		
1.2.01 Orogeny and related tectonic processes at plate boundaries		
1.2.02 Anorogenic and within-plate tectonic processes (Deformation, elastic, plastic and brittle)		
1.2.03 Seismicity		
1.2.04 Volcanic and magmatic activity		
1.2.05 Metamorphism		
1.2.06 Hydrothermal activity		
1.2.07 Erosion and sedimentation		VZ/SZ Flow and Transport
1.2.08 Diagenesis and pedogenesis		
1.2.09 Salt diapirism and dissolution		
1.2.10 Hydrological/hydrogeological response to geological changes		
1.3 CLIMATIC PROCESSES AND EFFECTS		
1.3.01 Climate change, global		
1.3.02 Climate change, regional and local		

Table A-1. Features, Events and Processes.

Feature, Event, Process (FEP)	Included	Process Model
1.3.03 Sea level change		
1.3.04 Periglacial effects		
1.3.05 Glacial and ice sheet effects, local		
1.3.06 Warm climate effects (tropical and desert)		
1.3.07 Hydrological/hydrogeological response to climate changes		NF Hydrology VZ/SZ Flow and Transport
1.3.08 Ecological response to climate changes		NF Hydrology VZ/SZ Flow and Transport
1.3.09 Human response to climate changes		
1.3.10 Other geomorphological changes		
1.4 FUTURE HUMAN ACTIONS		
1.4.01 Human influences on climate		
1.4.02 Motivation and knowledge issues (inadvertent/deliberate human actions)		
1.4.03 Drilling activities (human intrusion)		Human intrusion scenario
1.4.04 Mining and other underground activities (human intrusion)		
1.4.05 Un-intrusive site investigation		
1.4.06 Surface excavations		
1.4.07 Pollution		
1.4.08 Site Development		
1.4.09 Archaeology		
1.4.10 Water management (wells, reservoirs, dams)		
1.4.11 Social and institutional developments		
1.4.12 Technological developments		
1.4.13 Remedial actions		
1.4.14 Explosions and crashes		
2 DISPOSAL SYSTEM DOMAIN: ENVIRONMENTAL FACTORS		
2.1 WASTES AND ENGINEERED FEATURES		
2.1.01 Inventory, radionuclide and other material		Glass release Non glass diffusive release Non glass advective diffusive
2.1.02 Waste form materials, characteristics and degradation processes		Glass release Non glass diffusive release Non glass advective diffusive Non glass degradation model
2.1.03 Container materials, characteristics and degradation processes		
2.1.04 Buffer/backfill materials, characteristics and degradation processes		Glass release Non glass diffusive release Non glass advective diffusive
2.1.05 Engineered barriers system, characteristics and degradation processes		Glass release Non glass diffusive release Non glass advective diffusive Non glass degradation model

Table A-1. Features, Events and Processes.

Feature, Event, Process (FEP)	Included	Process Model
2.1.06 Other engineered features materials, characteristics and degradation processes		
2.1.07 Mechanical processes and conditions (in wastes and EBS)		Glass release Non glass diffusive release Non glass advective diffusive Non glass degradation model
2.1.08 Hydraulic/hydrogeological processes and conditions (in wastes and EBS)		Glass release Non glass diffusive release Non glass advective diffusive
2.1.09 Chemical/geochemical processes and conditions (in wastes and EBS)		Glass release Non glass diffusive release Non glass advective diffusive Non glass degradation model
2.1.10 Biological/biochemical processes and conditions (in wastes and EBS)		
2.1.11 Thermal processes and conditions (in wastes and EBS)		
2.1.12 Gas sources and effects (in wastes and EBS)		
2.1.13 Radiation effects (in wastes and EBS)		
2.1.14 Nuclear criticality		
2.1.15 Extraneous materials		
2.2 GEOLOGICAL ENVIRONMENT		
2.2.01 Disturbed zone, host lithology		Vadose Zone (VZ)/Saturated Zone (SZ) Flow and Transport
2.2.02 Host lithology		VZ/SZ Flow and Transport
2.2.03 Lithological units, other		VZ/SZ Flow and Transport
2.2.04 Discontinuities, large scale (in geosphere)		VZ/SZ Flow and Transport
2.2.05 Contaminant transport path characteristics (in geosphere)		VZ/SZ Flow and Transport
2.2.06 Mechanical processes and conditions (in geosphere)		
2.2.07 Hydraulic/hydrogeological processes and conditions (in geosphere)		VZ/SZ Flow and Transport
2.2.08 Chemical/geochemical processes and conditions (in geosphere)		VZ/SZ Flow and Transport
2.2.09 Biological/biochemical processes and conditions (in geosphere)		
2.2.10 Thermal processes and conditions (in geosphere)		
2.2.11 Gas sources and effects (in geosphere)		
2.2.12 Undetected features (in geosphere)		
2.2.13 Geological resources		
2.3 SURFACE ENVIRONMENT		
2.3.01 Topography and morphology		VZ/SZ Flow and Transport
2.3.02 Soil and sediment		VZ/SZ Flow and Transport
2.3.03 Aquifers and water-bearing features, near surface		VZ/SZ Flow and Transport
2.3.04 Lakes, rivers, streams and springs		

Table A-1. Features, Events and Processes.

Feature, Event, Process (FEP)	Included	Process Model
2.3.05 Coastal features		
2.3.06 Marine features		
2.3.07 Atmosphere		
2.3.08 Vegetation		VZ/SZ Flow and Transport
2.3.09 Animal populations		
2.3.10 Meteorology		VZ/SZ Flow and Transport
2.3.11 Hydrological regime and water balance (near surface)		VZ/SZ Flow and Transport
2.3.12 Erosion and deposition		VZ/SZ Flow and Transport
2.3.13 Ecological/biological/microbial systems		
2.3.14 Animal/plant intrusion leading to vault/trench disruption		
2.4 HUMAN BEHAVIOR		
2.4.01 Human characteristics (physiology, metabolism)		Exposure models
2.4.02 Adults, children, infants and other variations		Exposure models
2.4.03 Diet and fluid intake		Exposure models
2.4.04 Habits (non-diet-related behavior)		Exposure models
2.4.05 Community characteristics		Exposure models
2.4.06 Food and water processing and preparation		Exposure models
2.4.07 Dwellings		Exposure models
2.4.08 Wild and natural land and water use		Exposure models
2.4.09 Rural and agricultural land and water use (incl. fisheries)		Exposure models
2.4.10 Urban and industrial land and water use		Exposure models
2.4.11 Leisure and other uses of environment		Exposure models
3 RADIONUCLIDE/CONTAMINANT FACTORS		
3.1 CONTAMINANT CHARACTERISTICS		
3.1.01 Radioactive decay and in-growth		VZ/SZ Flow and Transport
3.1.02 Chemical/organic toxin stability		
3.1.03 Inorganic solids/solutes		
3.1.04 Volatiles and potential for volatility		
3.1.05 Organics and potential for organic forms		
3.1.06 Noble gases		
3.2 CONTAMINANT RELEASE/MIGRATION FACTORS		
3.2.01 Dissolution, precipitation and crystallization, contaminant		
3.2.02 Speciation and solubility, contaminant		
3.2.03 Sorption/desorption processes, contaminant		VZ/SZ Flow and Transport
3.2.04 Colloids, contaminant interactions and transport		
3.2.05 Chemical/complexing agents, effects on contaminant speciation/transport		
3.2.06 Microbial/biological/plant-mediated processes, contaminant		
3.2.07 Water-mediated transport of contaminants		VZ/SZ Flow and Transport
3.2.08 Solid-mediated transport of contaminants		

Table A-1. Features, Events and Processes.

Feature, Event, Process (FEP)	Included	Process Model
3.2.09 Gas-mediated transport of contaminants		Atmospheric pathway
3.2.10 Atmospheric transport of contaminants		Atmospheric pathway
3.2.11 Animal, plant and microbe mediated transport of contaminants		
3.2.12 Human-action-mediated transport of contaminants		
3.2.13 Food chains, uptake of contaminants in		
3.3 EXPOSURE FACTORS		
3.3.01 Drinking water, foodstuffs and drugs, contaminant concentrations in		Exposure models
3.3.02 Environmental media, contaminant concentrations in		Exposure models
3.3.03 Non-food products, contaminant concentrations in		Exposure models
3.3.04 Exposure modes		Exposure models
3.3.05 Dosimetry		Exposure models
3.3.06 Radiological toxicity/effects		Exposure models
3.3.07 Non-radiological toxicity/effects		Exposure models

Note: The FEPs applicable to vadose zone and saturated zone flow and transport model are identified (highlighted yellow) in the table.

APPENDIX B

VADOSE ZONE HYDRAULIC PROPERTIES AND VARIABLE ANISOTROPY MODELING

This page intentionally left blank.

B.1 Vadose Zone Hydraulic Properties and Variable Anisotropy Modeling

This section is a summary of relevant sections in PNNL-23711, *Physical, Hydraulic, and Transport Properties of Sediments and Engineered Materials Associated with Hanford Immobilized Low-Activity Waste*. Description of samples and methods of measurement were summarized in RPP-20621, *Far-Field Hydrology Data Package for the Integrated Disposal Facility Performance Assessment* and PNNL-22886, *System-Scale Model of Aquifer, Vadose Zone, and River Interactions for the Hanford 300 Area—Application to Uranium Reactive Transport*. They are recaptured briefly below. The PA-TCT model (Zhang et al. 2003, "Describing the unsaturated hydraulic properties of anisotropic soils using a tensorial connectivity-tortuosity (TCT) concept, Vadose Zone J., 2(3)") was used to describe the variable, moisture-dependent anisotropy for the IDF sediments. Once again, key figures on the PA-TCT modeling results (PNNL-23711) are repeated here for completeness.

Sediment samples at the IDF site were obtained in fiscal years 1998, 2001, and 2002 in three boreholes. Details on sampling, laboratory procedures, and analysis of samples from these boreholes are included as Appendices A, B, and C of RPP-20621. The Hanford formation sand sequence is about 200 ft thick and is the dominant facies at the site. The lower gravel sequence is about 70 ft thick. Multistep outflow and steady state flux control methods were used to obtain moisture retention and unsaturated conductivity data for the sand samples. Both methods were performed on the same core using the same sensor locations. These data were used in conjunction with a numerical inversion procedure to determine the optimal set of van Genuchten model (van Genuchten 1980, "A Closed-form Equation for Predicting the Hydraulic Conductivity of Unsaturated Soils") parameters. The hydraulic parameters for 44 samples of the sand sequence were from these boreholes and are summarized in Table B-1.

There were no site-specific hydraulic data available for the gravel sequence. Digital photo logs (Figure 4-13) illustrate the nature of open-framework gravel deposits in the vicinity of the IDF. Borehole samples with high gravel contents from the 100 and 300 Areas were used as surrogate to represent the H3 gravel sequence. The 15 samples from the 100 Area (RPP-20621) contain a gravel fraction from 43% to 75% with an average of 62%. The moisture retention data for the fine fraction (<2 mm) were measured using the Tempe pressure cells or the pressure plate extraction method. The hydraulic conductivity was measured using a constant-head permeameter or a variation of the unit gradient method. All five unknown parameters, θr, θs, α, n, and Ks, with $m = 1-1/n$ (van Genuchten 1980), were fitted to the data and the tortuosity-connectivity coefficient l was set as a constant 0.5. The hydraulic parameters for the 15 samples of the gravel sequence were summarized in Table 4 of RPP-20621 and are repeated in Table B-1.

The 10 samples from the 300 Area (PNNL-22886) contain a gravel fraction from 45% to 89% with an average of 71%. The hydraulic properties of the intact cores were measured using the multistep methods (see appendices of RPP-20621). Measured pressure data from two locations in each core and measured cumulative outflow data were used to calculate average capillary pressures and water contents. These data were used to fit the retention parameters θr, α, and n. The parameters Ks and θs were measured independently. The tortuosity-connectivity coefficient L was set as a constant 0.5. These parameters were summarized in Table A-2 of PNNL-22886 and are repeated in Table B-1. The two data sets noted above, reported by RPP-20621 and PNNL-22886, were combined to estimate properties for representing the gravel-dominated sequence at the IDF site.

Table B-1. The van Genuchten Parameters (based on the multistep method) and Saturated Hydraulic Conductivity Data for 44 Borehole Samples from the Sandy Sequence (after RPP-20621 and PNNL-23711).

Sample	θ_s	θ_r	α (1/cm)	n	K_s (cm/s)
7A	0.377	0.0404	0.029	1.825	1.04E-03
10A	0.413	0.0279	0.1161	1.784	2.95E-03
12A	0.363	0.0309	0.065	1.755	2.15E-03
14A	0.416	0.0324	0.0445	1.728	1.99E-03
15A	0.38	0.0254	0.0487	1.844	2.09E-03
16A	0.42	0.0228	0.0682	1.71	9.57E-03
17A	0.423	0.0382	0.0689	1.899	1.99E-03
19A	0.444	0.0279	0.201	1.542	4.31E-03
20A	0.419	0.0321	0.0305	2.081	2.54E-03
21A	0.403	0.0276	0.0545	1.926	2.94E-03
22A	0.352	0.0252	0.1078	1.585	5.06E-03
23A	0.371	0.0411	0.0079	1.553	2.65E-04
24A	0.321	0.0413	0.013	1.684	5.69E-04
25A	0.345	0.0267	0.0842	2.158	5.40E-03
27A	0.377	0.0354	0.083	1.532	8.14E-03
29A	0.359	0.0317	0.0784	1.732	3.75E-03
31A	0.418	0.0444	0.0058	2.012	8.21E-04
32A	0.359	0.0401	0.0931	1.703	6.71E-03
34A	0.316	0.0324	0.0819	2.398	1.32E-02
35A	0.299	0.0428	0.0897	2.16	1.06E-02
45L	0.385	0.008	0.1039	1.737	3.24E-02
45U	0.385	0.005	0.088	1.664	3.24E-02
50L	0.42	0.025	0.073	1.71	1.75E-03
50U	0.42	0.013	0.045	1.667	1.75E-03
80L	0.359	0.031	0.0403	2.368	1.05E-03
80U	0.359	0.033	0.0313	2.572	1.05E-03
85L	0.406	0.023	0.1074	1.697	3.84E-02
85U	0.406	0.027	0.0847	1.595	3.84E-02
110L	0.412	0.039	0.0362	2.328	5.16E-04
110U	0.412	0.046	0.0268	3.182	5.16E-04
130L	0.358	0.032	0.094	2.003	1.97E-02
130U	0.358	0.036	0.0674	1.934	1.97E-02
150L	0.431	0.015	0.0992	1.547	7.48E-03
150U	0.431	0.024	0.0703	1.514	7.48E-03
200L	0.41	0.002	0.0995	2.162	4.93E-02
215L	0.37	0.028	0.0448	1.918	2.24E-03
215U	0.37	0.023	0.0333	1.815	2.24E-03
230L	0.309	0.04	0.0472	1.658	3.56E-03
230U	0.309	0.038	0.04	1.658	3.56E-03
251L	0.427	0.032	0.084	1.845	1.43E-02
261L	0.39	0.045	0.0191	2.485	5.54E-04
C3826-171	0.382	0.0226	0.039	1.84	7.96E-03
C3827-63.5	0.444	0	0.0914	1.5	2.23E-02
C3827-221	0.361	0.022	0.066	1.77	7.30E-03

Table B-2. The van Genuchten Parameters (based on the multistep method) and Saturated Hydraulic Conductivity Data for 25 Borehole Samples Used to Represent the Gravel Sequence (after RPP-20621 and PNNL-23711).

Sample Locations	Sample	θ_s	θ_r	α (1/cm)	n	K_s (cm/s)
100 Area[(a)]	2-1307	0.236	0.0089	0.013	1.447	1.29E-04
	2-1308	0.12	0.0208	0.0126	1.628	6.97E-05
	2-1318	0.124	0.0108	0.0081	1.496	1.67E-04
	278713	0.135	0.0179	0.0067	1.527	6.73E-05
	279078	0.125	0.0136	0.0152	1.516	1.12E-04
	279809	0.138	0	0.0087	1.284	1.02E-04
	280174	0.094	0	0.0104	1.296	1.40E-04
	3-0570	0.141	0	0.0869	1.195	2.06E-02
	3-0577	0.107	0	0.0166	1.359	2.49E-04
	3-0686	0.184	0	0.0123	1.6	5.93E-04
	3-1702	0.103	0	0.0491	1.26	1.30E-03
	4-1086	0.137	0	0.1513	1.189	5.83E-02
	4-1090	0.152	0.0159	0.0159	1.619	4.05E-04
	4-1118	0.163	0	0.2481	1.183	3.89E-02
	4-1120	0.131	0.007	0.0138	1.501	2.85E-04
300 Area[(b)]	C6186,18.4-19.4	0.152	0	0.0388	1.378	2.83E-04
	C6197,27-28	0.176	0	0.115	1.324	4.33E-04
	C6197,42-43	0.178	0	0.0929	1.366	2.61E-02
	C6197,51-52	0.214	0	0.0435	1.272	5.43E-05
	C6200,21-22	0.219	0	0.0626	1.383	2.85E-01
	C6203,16-17	0.213	0	0.358	1.195	1.06E-01
	C6203,20-21	0.285	0	0.2286	1.269	3.72E-03
	C6203,35.8-36.8	0.302	0	2.4189	1.299	3.26E-02
	C6203,40-41	0.266	0	0.2733	1.509	1.30E-02
	C6208,23-24	0.246	0	0.1479	1.201	2.13E-02

(a) After Table 4 of RPP-2021

(b) After Table A-2 of PNNL-22886.

As described earlier, the stratigraphy at the IDF site was conceptualized as two EHMs, i.e., the sandy sequence over the gravelly sequence. The unsaturated hydraulic conductivity of each of the EHMs is assumed to be anisotropic and moisture- or tension-dependent. The upscaling process is described in detail in PNNL-23711. Figure B-1 and Figure B-2 illustrate the upscaled (effective) moisture retention and upscaled (effective) unsaturated hydraulic conductivity relations, respectively, for the sandy and gravelly sequences at the IDF site. Figure B-3 shows the PA-TCT based variable moisture-dependent anisotropy relations for the sandy and gravelly sequences at the IDF site.

Figure B-1. Effective Moisture Retention Curves for the (a) Sand Sequence and (b) Gravel Sequence (after PNNL-23711).

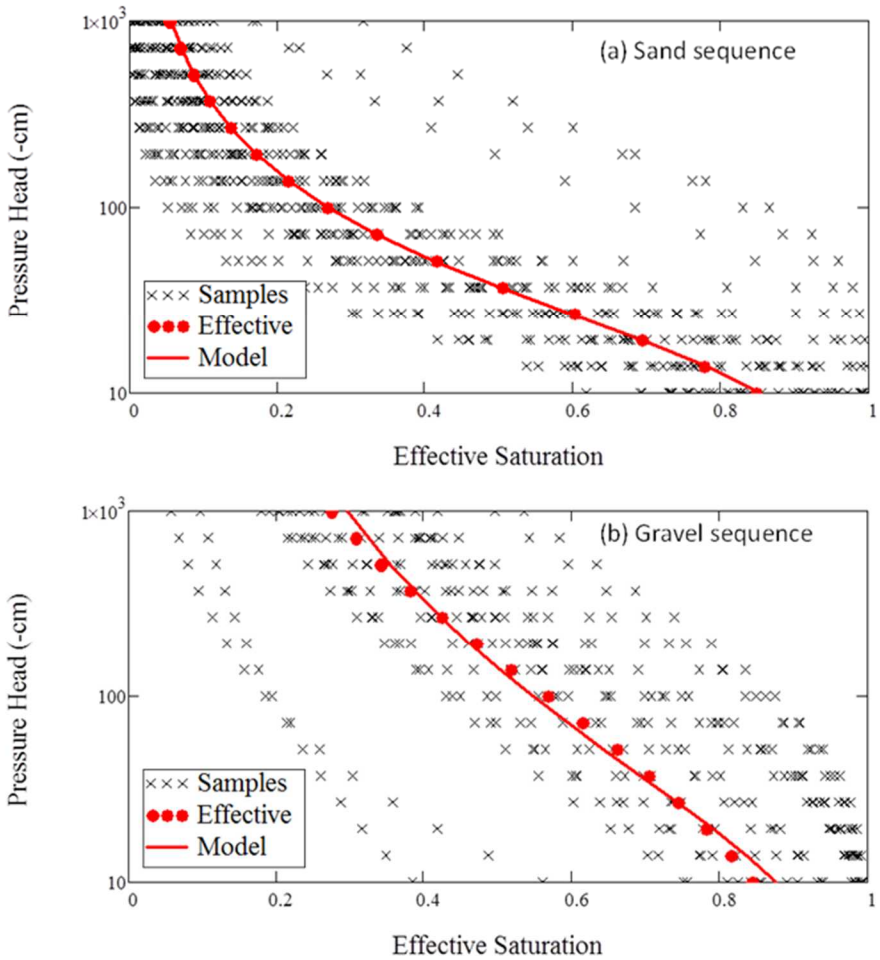

Figure B-2. Effective Unsaturated Hydraulic Conductivities for the (a) Sand Sequence and (b) Gravel Sequence (after PNNL-23711).

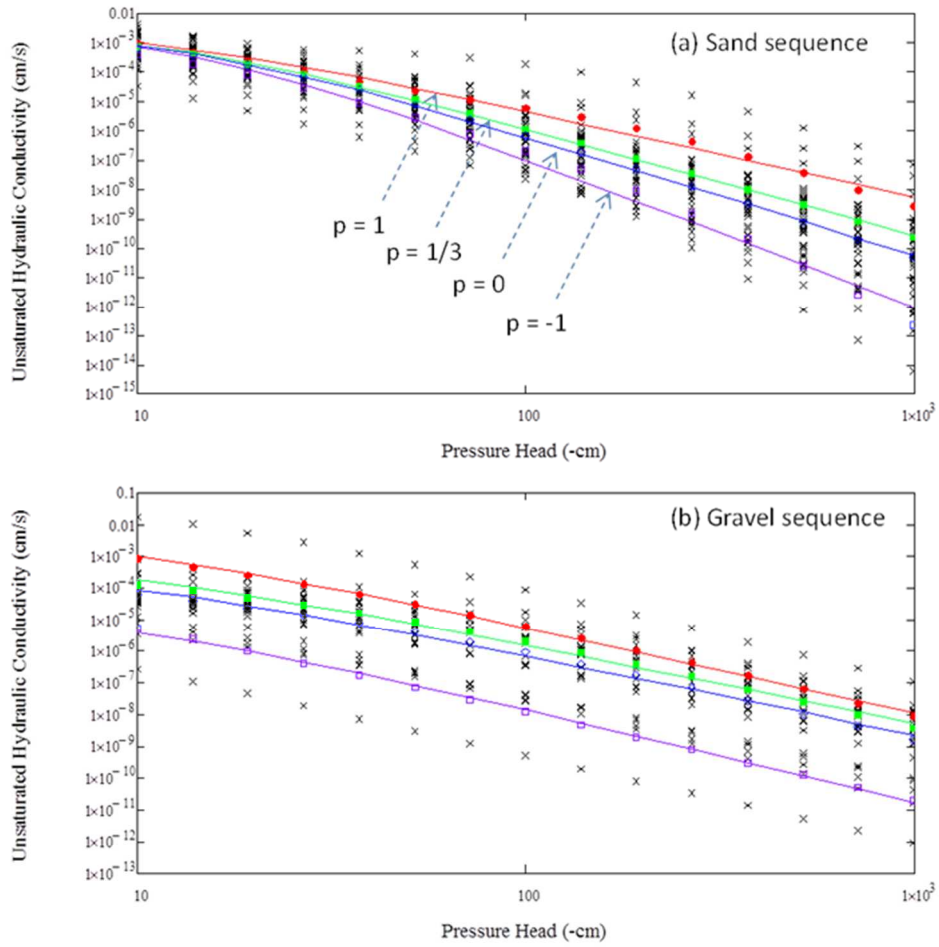

Figure B-2. Variable Tension-Dependent Anisotropy for the (a) Sand Sequence and (b) Gravel Sequence (after PNNL-23711).

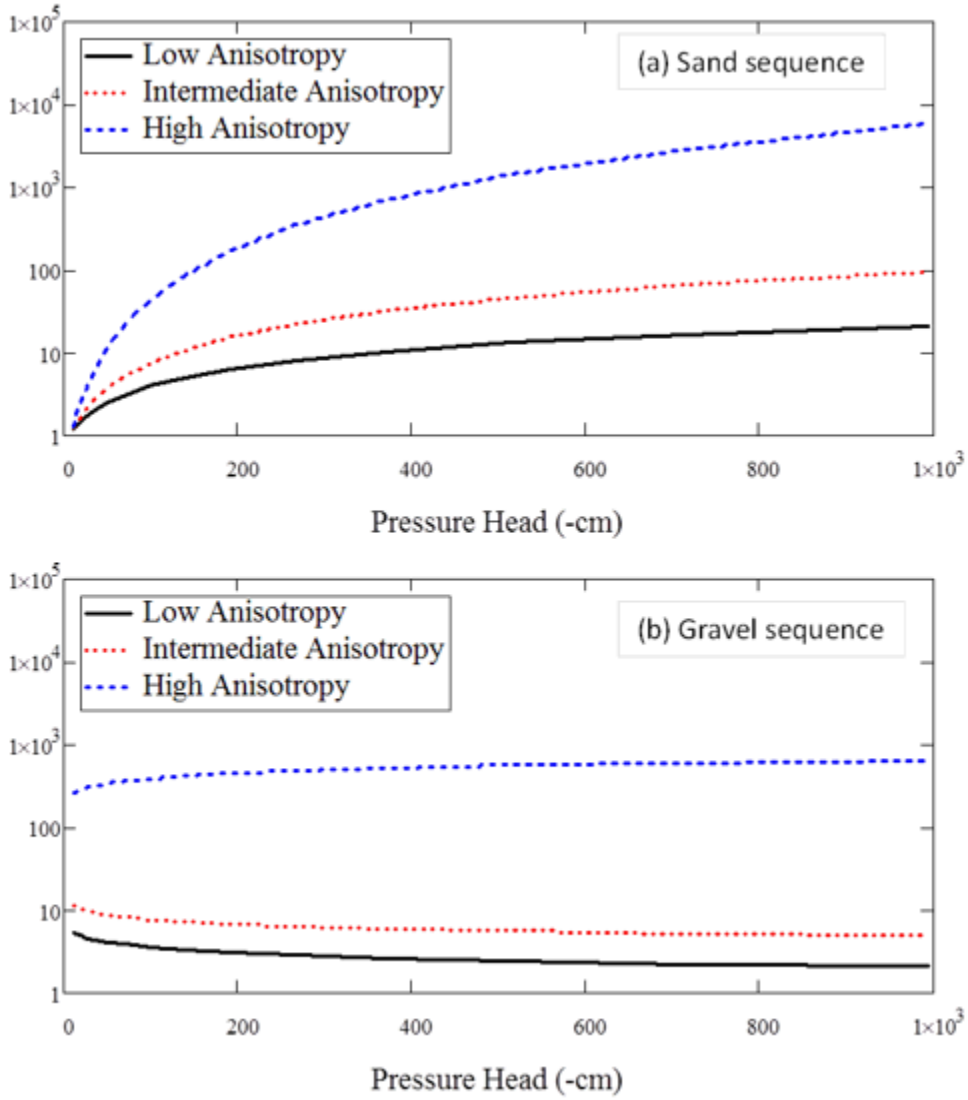

APPENDIX C

VADOSE ZONE MACRODISPERSIVITY ESTIMATES

This page intentionally left blank.

C. 1 Vadose Zone Macrodispersivity

Field-scale dispersivities are referred to as macrodispersivities. The terms macrodispersivity and dispersivity are used interchangeably in this section. Readers can go directly to Section C.1.4 for the macrodispersivity values recommended for IDF PA calculations. Details on how the selections are made using different methods are provided section C.1.1 (numerical simulations), Section C.1.2 (stochastic theory) and (Section C.1.3) experimental observations.

Field observations indicate that the dispersion coefficients required to describe the large-scale transport processes, at field scales of tens or hundreds of meters, are much different from those observed in small-scale laboratory experiments (Gelhar 1993, *Stochastic Subsurface Hydrology*). In fact, field-scale dispersivities may often be orders of magnitude larger than those observed in the laboratory. Consequently, laboratory-scale dispersivities, which are typically ~1 cm (0.39 in.) or less, are of little use in estimating field-scale dispersivities.

There is general agreement in hydrology literature that hydraulic conductivity variations induced by field-scale heterogeneities play an important role in field-scale transport processes. However, there does not appear to be a clear consensus about how best to describe such processes quantitatively (Gelhar 1993). While well-designed, large-scale tracer experiments would provide useful information, limited field data are available at this time to quantify macrodispersivities in unsaturated media.

Dispersivities are a function of matric potential (or soil moisture content) in unsaturated media (Mantoglou and Gelhar 1987, "Stochastic Modeling of Large-Scale Transient Unsaturated Flow Systems"). As with saturated media, heterogeneities that exist at various length scales result also in a scale dependence of macrodispersivities in unsaturated media (Gelhar et al. 1992, "A Critical Review of Data on Field-Scale Dispersion in Aquifers"). Dispersivities increase with time, or equivalently with distance, until they tend to converge on their unique asymptotic (large time) values. However, it can take a long time (e.g., years or decades) for the asymptotic Fickian approximation to take hold. This well-known behavior is usually attributed to heterogeneity-induced spreading and mixing until the point at which all of the heterogeneity has effectively been "sampled" by the contaminant plume such that dispersion becomes constant. The second moment evolution and the time-dependent, pre-asymptotic dispersivities (i.e., non-Fickian behavior) are therefore of marginal interest in simulations involving long times or large mean travel distances such as those involved in IDF PA modeling. The use of a constant (asymptotic) macrodispersivity is thus considered appropriate in PA simulations (NUREG/CR-6114, *Auxiliary Analyses in Support of Performance Assessment of a Hypothetical Low-Level Waste Facility: Groundwater Flow and Transport Simulation,* Vol. 3; NUREG/CR-5965, *Modeling Field Scale Unsaturated Flow and Transport Processes*).

Note that, because of the relatively dry moisture regime, unsaturated media macrodispersivity estimates are expected to be smaller, compared to saturated media estimates. Below, a range of estimates on the basis of numerical simulations (Section C.1.1), stochastic theory (Section C.1.2) and experimental observations (Section C.1.3) is provided. To obtain macrodispersivity, the local pore-scale dispersivities, which are typically small (<1 cm), are not included either in numerical simulations or stochastic solutions. This is consistent with the approach used by other investigators (Yang et al. 1997, "Stochastic analysis of adsorbing solute transport in three-dimensional, heterogeneous, unsaturated soils"; Gelhar 1993; Gelhar and Axness 1983, "Three-Dimensional Stochastic Analysis of Macrodispersion in Aquifers"]).

C.1.1 . Numerical Simulations. Details of the numerical simulation approach are described in Khaleel et al., 2002, "Upscaled Flow and Transport Properties for Heterogeneous Unsaturated Media"). Briefly, Monte Carlo (MC) simulations are used to obtain upscaled (effective) properties. The simulations mimic steady state, gravity infiltration for 50 realizations in two-dimensional (65.6 ft × 65.6 ft) heterogeneous flow regions. Constitutive relations for unsaturated media at the mesh-size scale are based on the van Genuchten-Mualem relationships. A realization of the flow field is shown in Figure C-1. The sediment properties are based on laboratory measurements of moisture retention and unsaturated *K* for coarse-textured sandy samples from the upper Hanford formation at the IDF site (HNF-4769, "Far-Field Hydrology Data Package for Immobilized Low-Activity Tank Waste Performance Assessment"). A unit mean-gradient approach is used to derive upscaled- properties for flow perpendicular to bedding. For a specified infiltration rate, the simulated pressure head distributions for 50 realizations are averaged to yield a mean pressure head, H. Because the simulated flow field is under a unit mean gradient condition, the infiltration rate is equal to the effective conductivity at the calculated H.

Following flow simulations, macrodispersivities are calculated on the basis of spatial moments of the ensemble-mean plume (Khaleel et al. 2002). For a given steady flow and a prescribed flux, the migration and spread of a slug of simulated tracer is simulated. Snapshots are taken of the two-dimensional plume distribution at different times. The snapshot at each sampling time is then averaged over the length across the flow domain to obtain the solute concentration profiles as a function of depth. The concentration profiles for all realizations are averaged to obtain the ensemble mean profile; these profiles are then used to evaluate their spatial moments. The calculated second spatial moment of the plume about the center of mass (i.e., spatial variance) over time allows estimation of the longitudinal macrodispersivity.

Figures C-2a, C-2b, and C-2c are snapshots, for a mean pressure head of -1.0 m, of the simulated plume for a single realization and for flow perpendicular to bedding at 400, 700, and 1,000 days after simulating the release of a conservative tracer across the top boundary of a mildly heterogeneous media (Figure C-1). The averaged concentration profiles for the flow regime and for the corresponding sampling times are illustrated in Figure C-2d. Bedding perpendicular to flow direction enhances lateral mixing and prevents growth of irregular flow paths. Consequently, the averaged concentration profiles for flow perpendicular to bedding (Figure C-3d) exhibit the typical bell-shaped distribution as described by the classical Fickian advection-dispersion equation. The computed longitudinal macrodispersivity for a mean pressure head (H) of -2 m (6.5 ft) was ~25 cm (9.8 cm), ranging from ~15 cm to ~40 cm (5.9 to 15.7 in.) for the 50 realizations. On the other hand, for a mean H of -20 m (65.6 ft), the macrodispersivity was ~100 cm (39.3 in.), ranging from ~70 cm to ~130 cm (27.5 to 51 in.) for the 50 realizations. As the MC simulations indicate, considerable variability in longitudinal macrodispersivity estimates is expected depending on the mean matric potential. Nonetheless, results show a clear dependence of longitudinal macrodispersivity on the moisture regime; longitudinal macrodispersivity estimates are higher for the drier moisture regime.

To evaluate directional dependence, simulations were also run for flow parallel to geologic bedding for the same flow domain. Figures C-3a, C-3b, and C-3c are snapshots of the plume at identical times for flow parallel to bedding for the same realization and for H=-1 m; Figure C-4d shows the averaged profile. A comparison of Figures C-2 and C-3 shows that the two-dimensional concentration distribution is more irregular in case of flow parallel to bedding than for flow perpendicular to bedding (Figures C-3a, C-3b, and C-3c versus Figures C-2a, C-2b,

and C-2c). Compared with flow perpendicular to bedding, the concentration profiles for flow parallel to bedding are highly skewed and characterized by multiple peaks, and spread out over greater distances, characteristics of a non-Fickian behavior. Thus, while the averaged concentration profiles for flow perpendicular to bedding show "textbook like" Fickian behavior, the averaged profiles for flow parallel to bedding are highly skewed and non-Fickian. At H=-2 m, the computed longitudinal macrodispersivity for flow parallel to bedding is considerably higher (~120 cm) than for flow perpendicular to bedding (~25 cm). For a mean H of -20 m, the macrodispersivity is ~180 cm (70.8 in.) for flow parallel to bedding versus ~100 cm (39.3 in.) for flow perpendicular to bedding.

In summary, the numerical results for Hanford H2 sands having mild heterogeneity (HNF-4769) show that the longitudinal dispersivities for flow parallel to bedding are higher than those for flow perpendicular to bedding (Khaleel et al. 2002). For both perpendicular and parallel to bedding, macrodispersivities increase as the mean matric potential becomes more negative. However, the Fickian regime is reached much earlier for cases with flow perpendicular to bedding than parallel to bedding (Khaleel et al. 2002). For IDF PA modeling, the flow is mostly perpendicular to geologic bedding; nonetheless, the preceding analysis provides estimates in situations where the flow is not necessarily perpendicular to bedding.

C.1.2 . Stochastic Models. For unsaturated media, in addition to the size of flow domain and media heterogeneities, macrodispersivities are expected to be a function of soil moisture content (or matric potential). Furthermore, as demonstrated via preceding MC simulations, macrodispersivities are larger for flow parallel to bedding than for flow perpendicular to bedding. The following describes two stochastic models to estimate IDF longitudinal macrodispersivities for flow perpendicular to the geologic bedding.

C.1.2.1. Mantoglou Model. Using spectral perturbation techniques (Gelhar and Axness 1983; Gelhar 1993), an approximate equation was derived for macrodispersivities in unsaturated media for flow perpendicular to bedding ("Large-Scale Models of Transient Unsaturated Flow and Contaminant Transport Using Stochastic Methods" [Mantoglou 1984]). Mantoglou showed that the asymptotic value of tension-dependent longitudinal macrodispersivity, $A_{\perp}$ under unit mean gradient condition, for flow perpendicular to bedding, is

$$\mathrm{A}_{\perp}(H) = \frac{\sigma^2_{\mathrm{LnK_u}}\lambda_{\mathrm{u}}}{\gamma^2} \qquad \text{(C-1)}$$

where $A_{\perp}$ depends on the mean pressure head H, σ^2_{LnKu} is the variance in log unsaturated K, λ_u is the correlation length scale for unsaturated hydraulic conductivity, and γ is a flow factor that depends on the direction of mean flow and the orientation of heterogeneity (Gelhar and Axness 1983).

Equation C-5 represents the asymptotic macrodispersivity estimate for steady-state uniform flow with uniform mean tension. Because macrodispersivity modeled by Equation C-5 is an asymptotic parameter, it applies only when the concentration plume has traveled a large distance in a geologic unit and has encountered numerous heterogeneities in the formation. Furthermore, it is important to note that similar to other stochastic perturbation approaches (Gelhar 1993), the

validity of Equation C-5 relies on the variance of hydraulic properties being relatively small (i.e., $\sigma^2_{LnKu} < 1$).

Mantoglou (1984; Figure 5-9) presents longitudinal macrodispersivity estimates, based on Equation C-5, for Maddock sandy loam ("Spatial Variability of in Situ Unsaturated Hydraulic Conductivity of Maddock Sandy Loam" [Carvallo et al. 1976]) and Panoche silty clay loam ("Spatial Variability of Field-Measured Soil-Water Properties" [Nielsen et al. 1973, "Spatial Variability of Field-Measured Soil-Water Properties"]) soil types. Mantoglou results show considerable variability even for mild tensions. Based on Mantoglou model [Equation C-5], f or Maddock soil type, the asymptotic longitudinal macrodispersivity was 2.4 m (7.8 ft) at a mean tension of 50 cm (19.6 in.). For Panoche soil type, the estimate was 0.8 m (2.6 ft) at a mean tension of 300 cm (118 in.).

C.1.2.2. Russo Model. Using the Lagrangian framework in conjunction with the Yeh et al (1985, "Stochastic Analysis of Unsaturated Flow in Heterogeneous Soils, 2. Statistically Anisotropic Media with Variable α") velocity covariance, theoretical expressions were developed for evolution of contaminant plume spatial moments in unsaturated heterogeneous media under steady-state conditions ("Stochastic Analysis of Simulated Vadose Zone Solute Transport in a Vertical Cross Section of Heterogeneous Soil During Nonsteady Water Flow" [Russo 1991]). The spatial moments were then used to assess the pre-asymptotic evolution of macrodispersivity.

$$A_{zz}(t) = \sigma^2_{LnK_u} \lambda_u \left\{ 1 - 3(2\tau)^{-1} - 3(\tau)^{-2} \exp(-\tau) + 3(\tau)^{-3}[1 - \exp(-\tau)] \right\} \qquad \text{(C-2)}$$

where A_{zz} is the longitudinal macrodispersivity (i.e., similar to $A_{\perp}$), z denotes vertical direction, t is time, λ_u is vertical correlation length, and $\tau = z_c(t)/\lambda_u$. The unsaturated conductivity variance σ^2_{LnKu} was derived by Russo (1991) using the Gardner (1958) exponential model for unsaturated conductivity. At large times, $\tau \rightarrow \infty$; the longitudinal asymptotic macrodispersivity is therefore

$$A_{zz}(\infty) = \sigma^2_{LnK_u} \lambda_u \,. \qquad \text{(C-3)}$$

Note that this is the same as Mantoglou Equation C-5 without the flow factor γ in the denominator. For hypothetical vadose zone flow domains having $\sigma^2_{LnK_u}$ = 0.29 and extending 15 m and 10 m (49.2 ft and 32.8 ft) in the horizontal and vertical directions, respectively, and a correlation length of 0.12 m (0.39 ft) in the vertical direction, Russo (1991) computed an asymptotic longitudinal macrodispersivity (Equation C-7) of 3.48 cm (1.37 in.). As discussed later, the conductivity variance of 0.29 is, however, much smaller compared to variance for Hanford H2 unsaturated conductivity data.

C.1.2.3. Stochastic Theory Based Macrodispersivity Estimates. To apply stochastic Equations C-5 and C-7, an estimate of λ_u for unsaturated K is needed. A correlation length of the order of 50 cm (19.6 in.) was obtained for saturated conductivity samples at the Sisson and Lu site (RPP-20621). However, as saturation decreases, an increase in the variance of log unsaturated conductivity is accompanied by a decrease in the correlation scale of log unsaturated K ("Stochastic Modeling of Macrodispersion for Solute Transport in a Heterogeneous Unsaturated

Porous Formation" [Russo 1993, "Stochastic Modeling of Macrodispersion for Solute Transport in a Heterogeneous Unsaturated Porous Formation"]).

Also, the Equation C-5 flow factor γ (Mantoglou 1984) in a predominantly vertical unsaturated flow through a layered system would be less than 1; it is approximately the ratio of the harmonic and geometric means of unsaturated K (Gelhar 1993; Gelhar and Axness 1983). Assuming a correlation length of 10 cm (7.8 in.) (approximate measurement scale for small-scale unsaturated K measurements [RPP-20621]), and γ estimates based on the ratio of the harmonic and geometric means (Khaleel et al. 2002), for H2 sands, Mantoglou's model yields asymptotic macrodispersivity estimates, for flow perpendicular to bedding, that are ~360 cm (141.7 in.) at relatively low tensions of ~2 m (0.7 in.). For the Russo (1991) model (Equation C-7), at ~2 m (6.56 ft) tension, the asymptotic longitudinal macrodispersivity for H2 sands is ~32 cm (12.6 in). Note that the MC simulations (Khaleel et al. 2002) yielded a longitudinal macrodispersivity of ~25 cm (9.8 in.) for flow perpendicular to bedding and for H=-2 m (6.56 ft). However, the favorable comparison with Russo's model is coincidental since σ^2_{LnK} and mean tension values are different.

Reported values have a relatively low tension of 2 m (6.56 ft) because of the limitation of low perturbation for stochastic models. The variance, $\sigma^2_{LnK_u}$ in Equation C-5 becomes rather large for H2 sands; at a mean tension of 1 m, $\sigma^2_{LnK_u}$ is about 1.96, whereas at a tension of 2 m, $\sigma^2_{LnK_u}$ is about 4.73. Compared to H2 sands, $\sigma^2_{LnK_u}$ for the H3 gravelly units is significantly lower; at a mean tension of 150 cm, $\sigma^2_{LnK_u}$ is about 1.22, whereas at a mean tension of 400 cm, σ^2_{LnK} is about 2.02. Such variance estimates are consistent with the unsaturated *K* data for the Hanford formation sandy and gravelly samples. To explore the impact of gravelly (> 2 mm [0.78 in.] size fraction) sediments for the drier moisture regime, a separate study was conducted ("Variability of Gardner's α for coarse-textured sediments" [Khaleel and Relyea 2001, "Variability of Gardner's α for coarse-textured sediments"]); a total of 79 gravelly and sandy samples were analyzed in the laboratory. The gravel fraction for 41 samples ranged from 20 to 71% (by weight); the remaining 38 samples were sandy with very little gravel fraction (Figure C-4). A noteworthy feature of 54 is the fact that the variability in saturated conductivity is much greater than the variability in unsaturated conductivity near saturation. Furthermore, the measured *K* for the gravelly samples showed less variability for the drier moisture regime, fell within a narrower range, and were well within the range of measured unsaturated *K* 64). At a matric potential of -1 m, the unsaturated *K* for sandy samples ranges over 4 orders of magnitude, whereas the unsaturated *K* for gravelly samples ranges over 2 orders of magnitude 74).

C.1.3 Experimental Data from 200 Areas and Other Sites. Field experiments were conducted at a location in 200 East Area, using potassium chloride as a tracer (RPP-20621 Appendix E, "Hanford Low-Activity Tank Waste Performance Assessment Activity: Determination of in Situ Hydraulic Parameters of the Upper Hanford Formation"). Analysis of the data, using moment analysis, provided dispersivities that ranged from 1.3 cm to 7.8 cm (0.5 to 3.0 in.) for travel distances ranging from 25 cm to 125 cm (9.8 to 49.2 in.). Although these estimates are for the Hanford formation, the transport distance within the vadose zone is indeed of limited extent. Nonetheless, results based on the limited data are consistent with the concept of a scale-dependent dispersivity; it is expected that the asymptotic value will be larger than those based on the small-scale tracer experiment. In fact, extrapolation of the trend line for the

data (RPP-20621 Appendix E) suggests that an asymptotic dispersivity- estimate of ~1 m (3.28 ft) s not unlikely if the heterogeneity at the field site is similar to that of the sandy sediments underlying C Farm, and if the entire sandy sequence of the Hanford formation is treated as equivalent homogeneous media.

In addition to preceding data, results of artificial tracer experiments are available from several arid/semi-arid regions. Two massively instrumented solute transport experiments were performed in desert soils near Las Cruces, New Mexico ("The Las Cruces Trench Site: Characterization, Experimental Results, and One-Dimensional Flow Predictions" [Wierenga et al. 1991, "The Las Cruces Trench Site: Characterization, Experimental Results, and One-Dimensional Flow Predictions"]; "The Second Las Cruces Trench Experiment: Experimental Results and Two-Dimensional Flow Predictions" [Hills et al. 1991, "The Second Las Cruces Trench Experiment: Experimental Results and Two-Dimensional Flow Predictions"]). Drip emitters were used to irrigate a plot adjoining a deep trench in undisturbed heterogeneous sediments, with well in excess of one order of magnitude standard deviation in saturated hydraulic conductivity. Monitoring of the trench face showed a spatially uniform progression of the wetting front and did not reveal indications of preferential flow (Wierenga et al. 1991). Hills et al. (1991) found that a dispersivity of 5 cm (1.9 in.) provided reasonably realistic simulations of tritium and bromine tracer distributions for the trench site (26.4 m long x 4.8 m wide x 6 m deep [86.6 ft long x 15.7 ft wide x 19.6 ft deep))

One additional study ("Chlorine 36 and Tritium from Nuclear Weapons Fallout as Tracers for Long-Term Liquid and Vapor Movement in Desert Soils" [Phillips et al. 1988, "Chlorine 36 and Tritium from Nuclear Weapons Fallout as Tracers for Long-Term Liquid and Vapor Movement in Desert Soils,"]) assessed the degree of mixing in desert soils using the conventional advection-dispersion modeling, yielding a dispersion coefficient of 50 cm^2/yr. This compared with the calculated effective diffusion coefficient of 25 cm^2/yr. A similar study ("Evaluation of Liquid and Vapor Water Flow in Desert Soils Based on Chlorine 36 and Tritium Tracers and Nonisothermal Flow Simulations" [Scanlon 1992]) at another southwestern arid site obtained a dispersion coefficient of about 14 cm^2/yr. These, then, lead to effective dispersivities of about 7 cm (2.7 in.) and 4 cm (1.5 in.) at the two arid sites, and Peclet numbers (displacement divided by dispersivity) of 23 and 17. In summary, long-term environmental tracer studies at several arid southwestern sites indicate vadose zone dispersivities being less than 10 cm. (3.9 in.)

Based on a different survey of literature, Gelhar (1993) presented the longitudinal vadose zone dispersivities as a function of the scale of the experiment (Figure C-8). The figure shows sparse data for scales larger than 2 m (6.56 ft). Nonetheless, similar to saturated flow (Gelhar et al. 1992), Figure C-9 shows an increase of dispersivity with an increase in scale. Also, shown in Figure C-10 are results of the 200 East Area field tracer experiment (RPP-20621 Appendix E); the trend line dispersivity estimate at a field scale of ~10 m (32.8 ft) is in close agreement with "Field Scale Transport of Bromide in an Unsaturated Soil, 2. Dispersion Modeling" (Butters and Jury 1989) field data.

C.1.4 . Recommended Macrodispersivities for IDF Performance Assessment. Table C-1 summarizes the macrodispersivity estimates based on results of numerical simulation, stochastic theory, and 200 Areas experimental data. Table C-2 shows that, for H2 sands, estimates are available by all three methods. For the H2 sand unit, for the PA modeling, the recommendation is to use longitudinal macrodispersivity values ranging from 25 cm (9.8 in.) (based on numerical simulations) to 100 cm (39.3 in.) (based on field experiments). For H3 sediments, the

recommendation is to use, based on stochastic theory, longitudinal macrodispersivity values range from 20 cm (7.8 in.) to 100 cm (39.3 in.). The transverse macrodispersivity is typically much lower; in saturated media, it may range from 1 to 10 percent of the longitudinal macrodispersivity (Gelhar and Axness 1983). In the absence of unsaturated media experimental data, the recommendation is to use a transverse macrodispersivity 1/10th of the longitudinal macrodispersivity.

Figure C-1. a) Ks, (b) α, and (c) n Random Distribution for a Single Realization.

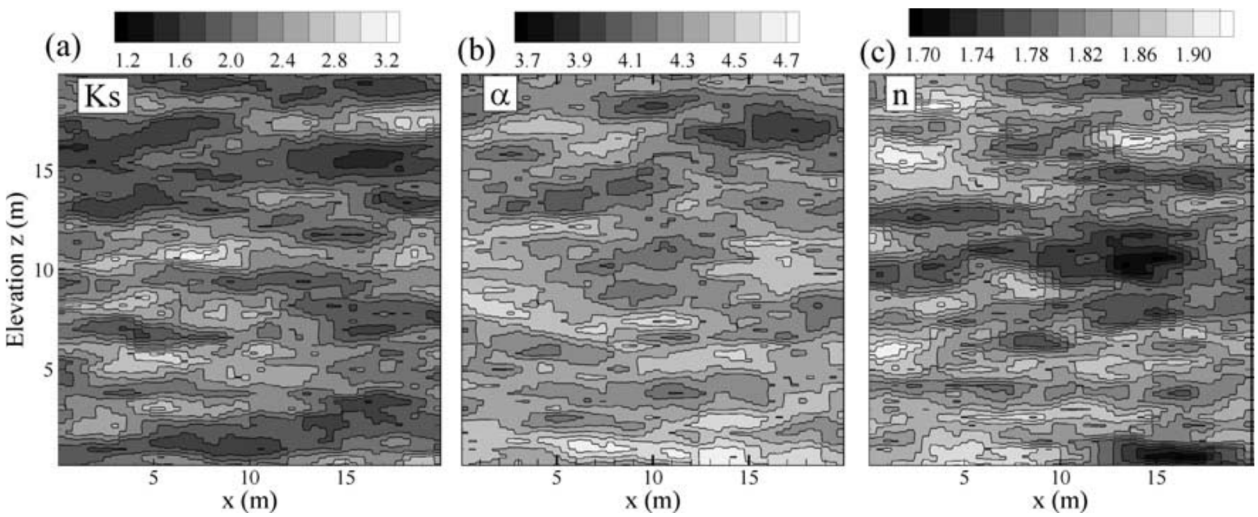

Source: Khaleel et al. 2002,"Upscaled Flow and Transport Properties for Heterogeneous Unsaturated Media"

Figure C-2. Simulated Concentration Distribution for a Single Realization at (a) 400 days, (b) 700 days, (c) 1,000 days, and (d) the Averaged Concentration Profile at Those Times for Flow Perpendicular to Bedding for a Mean Pressure Head (H) of -1 m (3.28 ft).

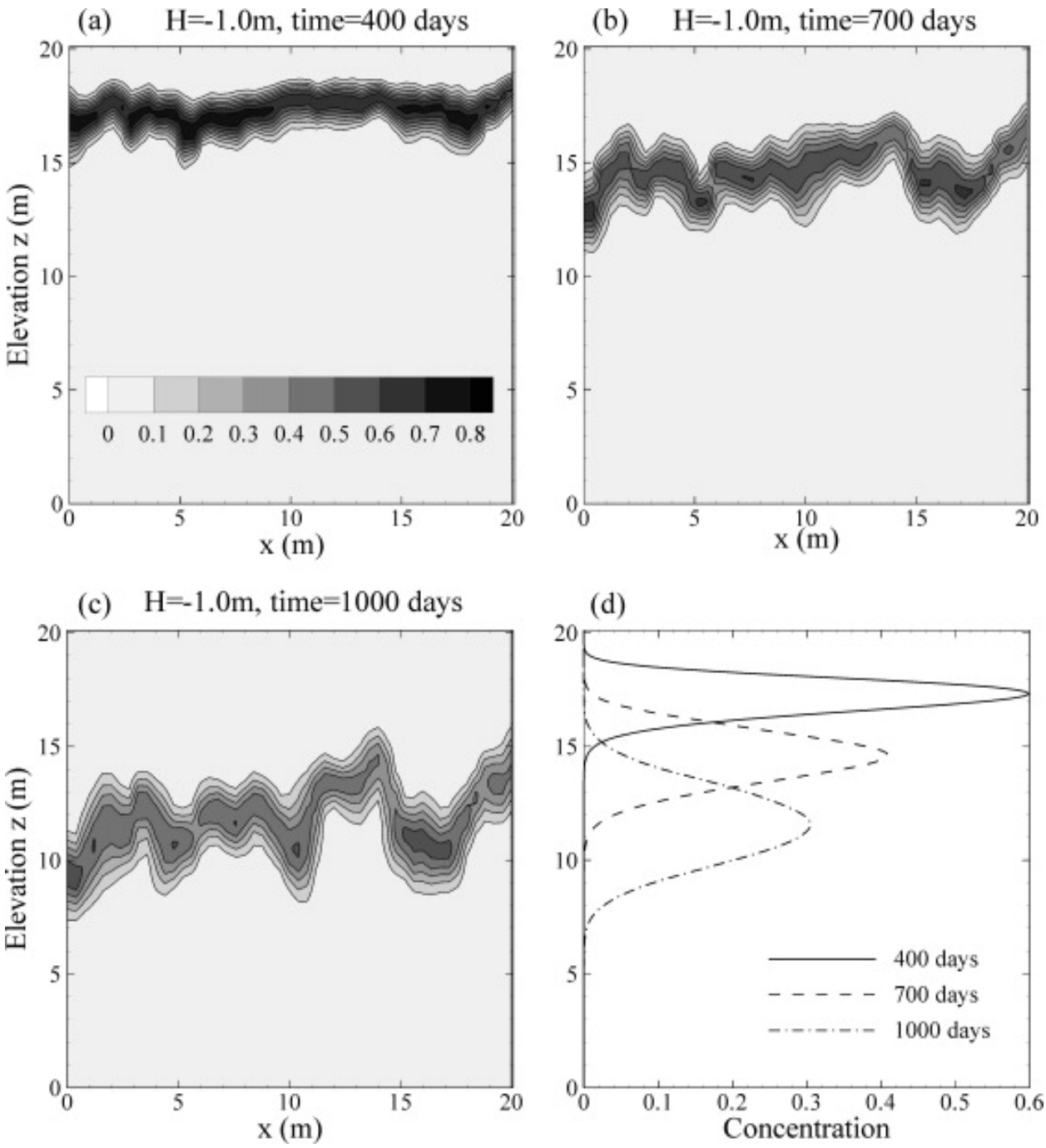

Source: Khaleel et al. 2002,"Upscaled Flow and Transport Properties for Heterogeneous Unsaturated Media"

Figure C-3. Simulated Concentration Distribution for a Single Realization at (a) 400 days, (b) 700 days, and (c) 1,000 days and (d) the Averaged Concentration Profile at Those Times for Flow Parallel to Bedding for a Mean Pressure Head (H) of -1 m (3.28 ft).

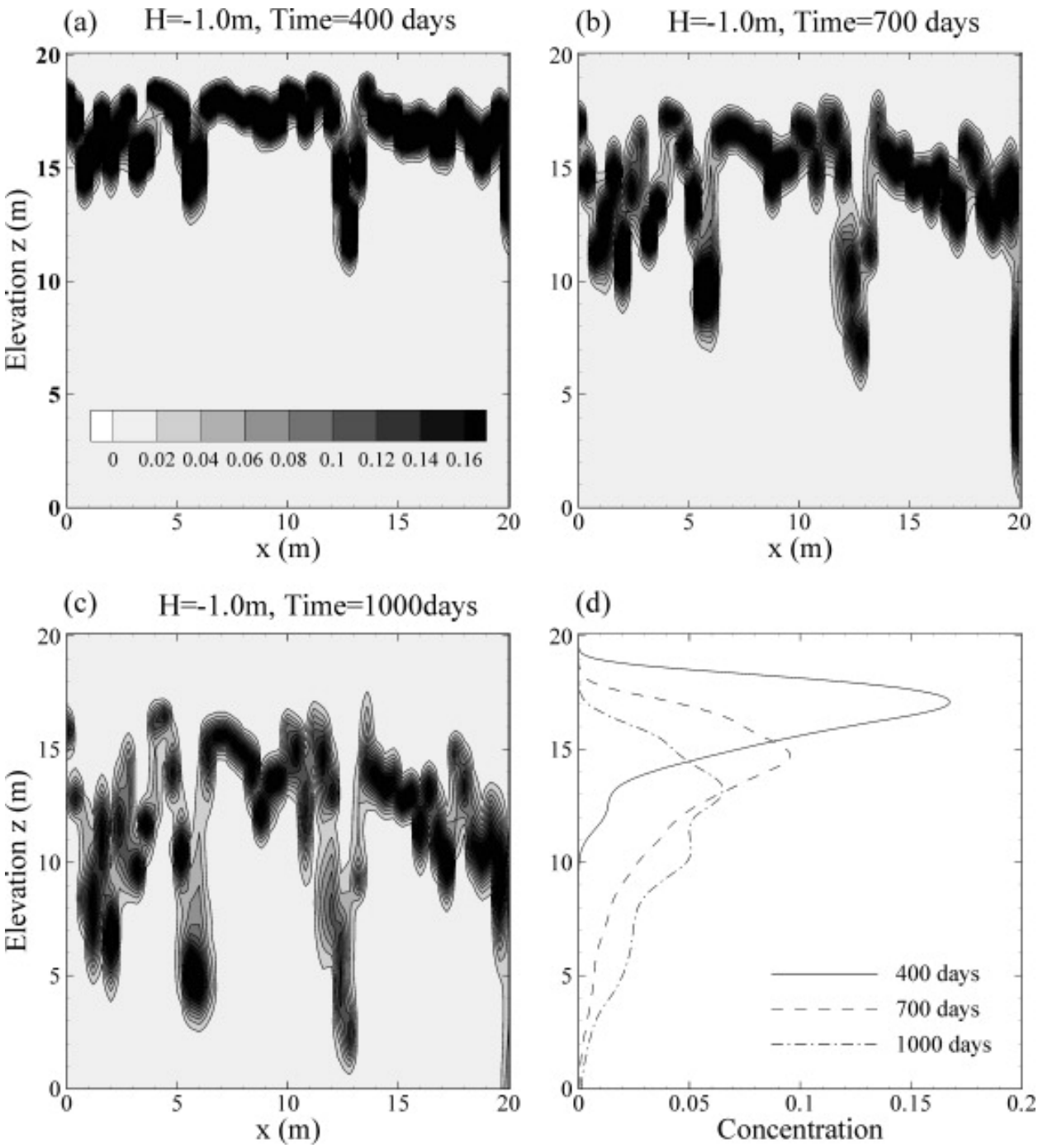

Source: Khaleel et al. 2002,"Upscaled Flow and Transport Properties for Heterogeneous Unsaturated Media"

Figure C-4. Unsaturated Hydraulic Conductivity Measurements for Sand-Dominated and Gravel-Dominated Samples (after Khaleel and Relyea 2001).

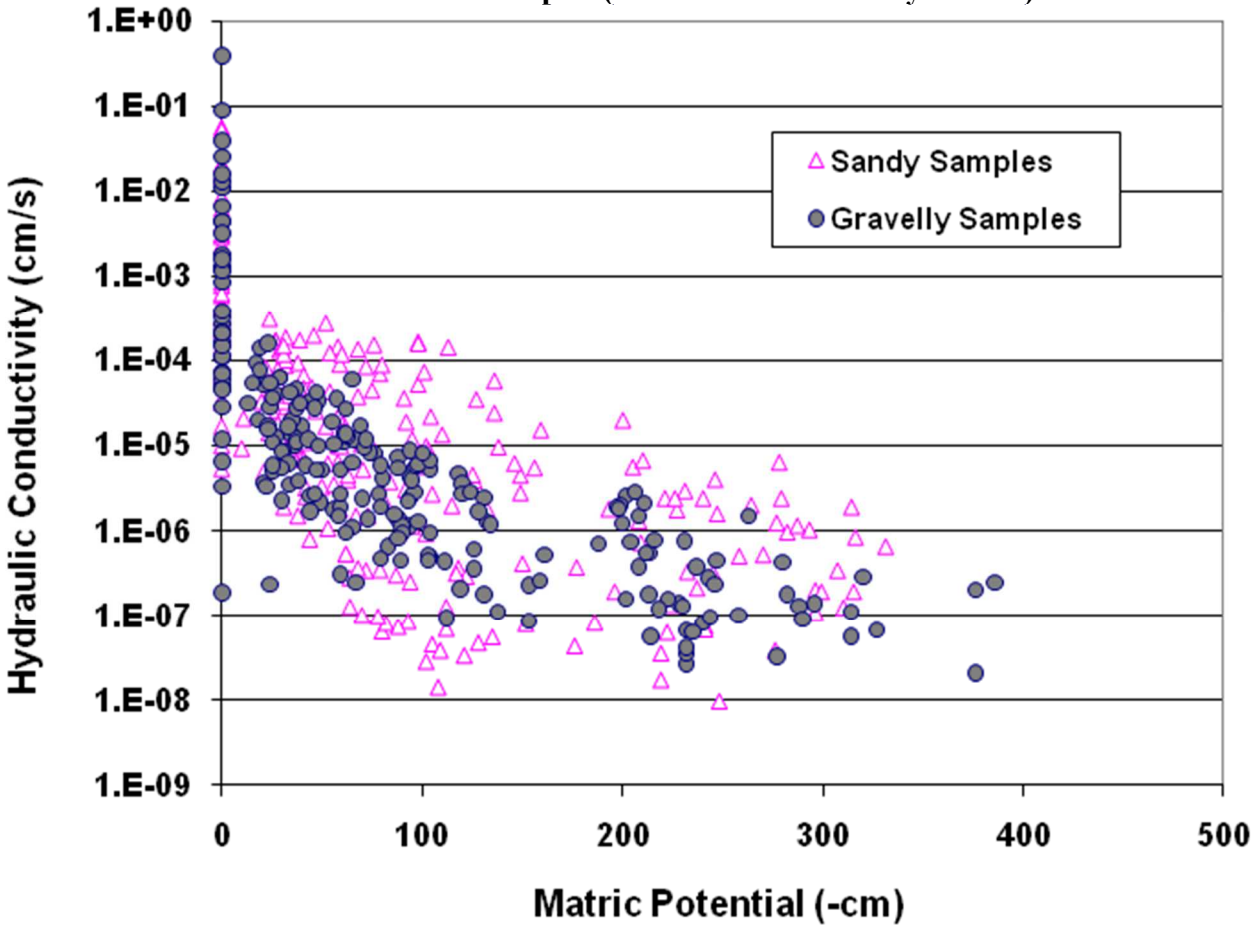

Source: Khaleel and Relyea 2001, "Variability of Gardner's α for coarse-textured sediments"

Figure C-5. Longitudinal Laboratory- and Field-Scale Dispersivities in Unsaturated Media as a Function of Overall Problem Scale.

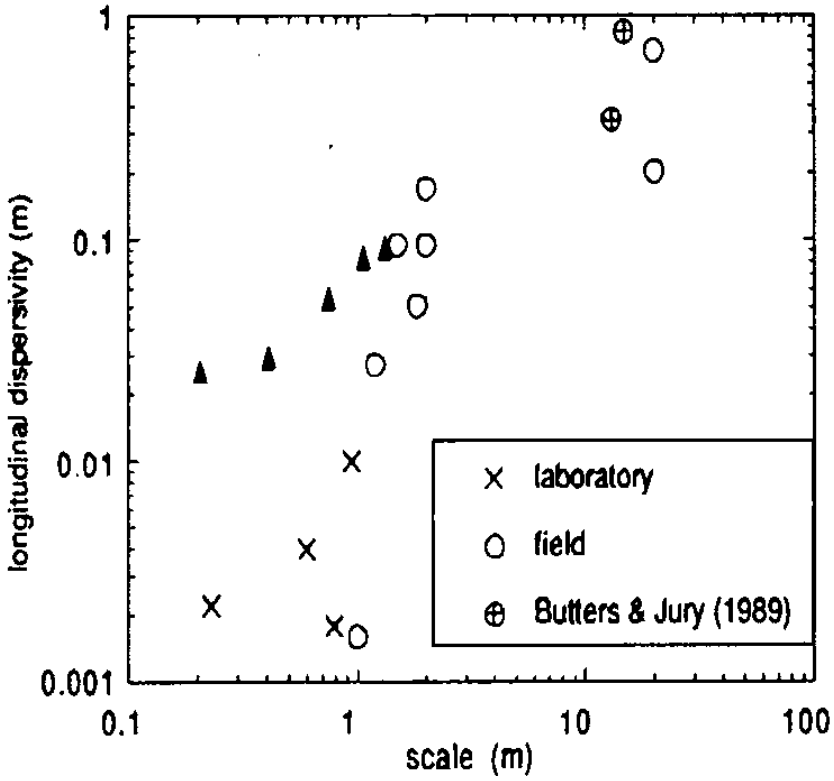

Note: The triangles are data from RPP-20621, *Far-Field Hydrology Data Package for the Integrated Disposal Facility Performance Assessment, Appendix E*, "Hanford Low-Activity Tank Waste Performance Assessment Activity: Determination of In Situ Hydraulic Parameters of the Upper Hanford Formation."

References:

Butters and Jury 1989, "Field Scale Transport of Bromide in an Unsaturated Soil, 2. Dispersion Modeling"

Gelhar 1993, *Stochastic Subsurface Hydrology*

Table C-1. Longitudinal Macrodispersivity Estimates (cm).

Hydrostratigraphic Unit	Numerical Simulation	Stochastic Theory (Russo and Mantoglou Equations 5 and 7)	200 Area Field Experiments
H2 Sand-Dominated Unit	25	~32[a] – 360[a]	~100[c]
H1, H3, and Backfill Gravelly Units	NA	~20[b] – 100[b]	NA

[a]Evaluated at a mean tension of 2 m.

[b]Evaluated at a mean tension of 4 m.

[c]Extrapolated experimental data (RPP-20621, "Far-Field Hydrology Data Package for the Integrated Disposal Facility Performance Assessment," Appendix E, "Hanford Low-Activity Tank Waste Performance Assessment Activity: Determination of In Situ Hydraulic Parameters of the Upper Hanford Formation").

NA = Not Available

References:

Mantoglou 1984, "Large-Scale Models of Transient Unsaturated Flow and Contaminant Transport Using Stochastic Methods"

Russo 1991, "Stochastic Analysis of Simulated Vadose Zone Solute Transport in a Vertical Cross Section of Heterogeneous Soil During Nonsteady Water Flow"

APPENDIX D

MODEL IMPLEMENTATION EXAMPLE TEST CASE

This page intentionally left blank.

Example Test Case Description.

For implementation of model described in Sections 3 and 4, a TC&WM EIS case was selected as the test case. The case considered is the same as TC&WM EIS Alternative 2B (i.e., 20 percent of I-129 is in ILAW, 80 percent in ETF secondary waste (9.55 Ci in ILAW and 33.6 Ci in ETF) [Appendix N, Section N.5.8, p. N-186]. For the test case, the release of I-129 from ETF-generated Secondary Solid Waste (ETF SSW) represents the source term. With the I-129 inventory being 33.6 Ci; ~2.5 Ci is released over 10,000 years based on the TC&WM EIS shrinking core diffusion model; the I-129 is considered to be non-sorbing with Kd=0. The release occurs from a 20 m x 20 m (65.6 ft x 65.6 ft) square footprint located under the currently completed portion of the IDF excavation at the liner elevation of 204-m NAVD 88.

The test case results are based on a recharge rate of 1.7 mm/yr (0.66 in./yr), whereas the EIS case (Appendix N) uses a recharge rate of 0.9 mm/yr (0.35 in./hr). Also, the EIS case used a molecular diffusion coefficient of 3.4E-2 m^2/yr; the same value was used for the test case in the STOMP Solute/Fluid Interactions Card, but it is different from the value (7.89E-2 m^2/yr) listed in Section 4. For the test case, only 5 m (16.4 ft) of saturated zone (elevation below 119.5 m [392 ft]) was modeled and the rest of the saturated zone was made inactive using the STOMP inactive node card. For this test case, a longitudinal dispersivity of 10.5 m (34.4 ft) and a transverse dispersivity of 0.1 m (0.328 ft) were used for the saturated zone transport calculations; the transverse dispersivity value is different from that cited in Table 4-1.

STOMP Modeling and Results.

Two model simulations were carried out in STOMP for steady state flow simulation for an arbitrary 3,000-yr long simulation to help define the initial condition for aqueous pressure distribution for a 1.7 mm/yr (0.66 in./yr) recharge for the model top boundary, and a 10,000-yr long flow and transport simulation with source introduced at model year 110.

Figures D-1 (a) and (b) illustrate the 3-D STOMP combined vadose zone and saturated zone model. The waste form release location, the 100 m (328 ft) boundary and the 5 m (16.04 ft) well screen locations are indicated in Figures D-1 (a) and (b). Figures D-1 (a) and (b) also show a streamline originating from the source release location for the aqueous flux obtained for the steady state flow model. This streamline plot helped in identifying the point of calculation to capture the maximum concentration at the 100 m (328 ft) downgradient location.

The modeling results are presented for the steady-state volumetric moisture content distribution (Figure D-2), vertical Darcy flux (Figure D-3), and the simulated matric potential distribution (Figure D-4.). These results are based on a uniform recharge rate of 1.7 mm/yr (0.66 in./yr) throughout the modeling domain. The vadose zone hydraulic properties are based on those listed in Table 4-1 as well as the aquifer properties for Hanford gravels and Ringold E. As expected, within the vadose zone, the simulated moisture for the H2 sand-dominated unit is slightly higher than the simulated moisture for the H3 gravel-dominated unit (Figure D-4.). Figure D-3 illustrates the condition that the recharge rate of 1.7 mm/yr (0.66 in./yr) is indeed maintained during the simulation. As expected, within the vadose zone, the simulated matric potential for the H2 sand-dominated unit is less negative than that for the H3 gravel-dominated unit (Figure D-4).

Figure D-5 illustrates the simulated breakthrough of I-129 at base of the source and the water table in terms of release rate, Ci/yr (left legend) and the cumulative release, Ci (right legend). The breakthrough curve is similar to that reported in TC&WM EIS Appendix N, Section N.5.8.

shows the breakthrough curve for I-129 at the point of calculation. The peak I-129 concentration occurs after 6,000 years of simulation and a peak concentration of 4.48 pCi/L is obtained at the point of calculation. Figure D-7 shows the I-129 concentration distribution for a plane parallel to the advective transport (i.e., the predominant transport direction within the saturated zone). Figure D-8 shows the distribution of I-129 concentration at the water table. Figures D-7 and D-8 show that the plume is migrating in the northeast direction as soon as it reaches the aquifer; as expected, the plume migration within the vadose zone is nearly vertical.

Figure D-1a. West-East Two-Dimensional Cross-Section through the Source Location.

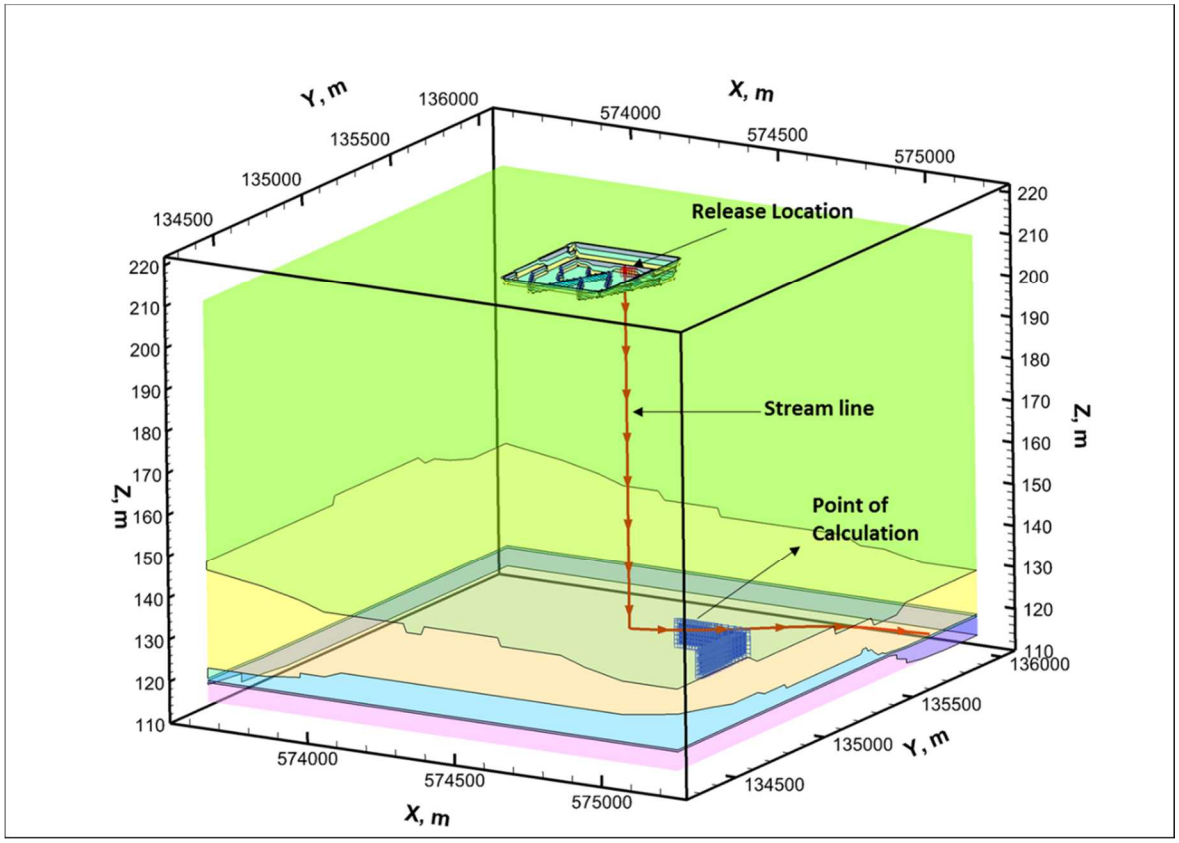

(a)

Figure D-1b. West-East Two-Dimensional Cross-Section Through the Source Location.

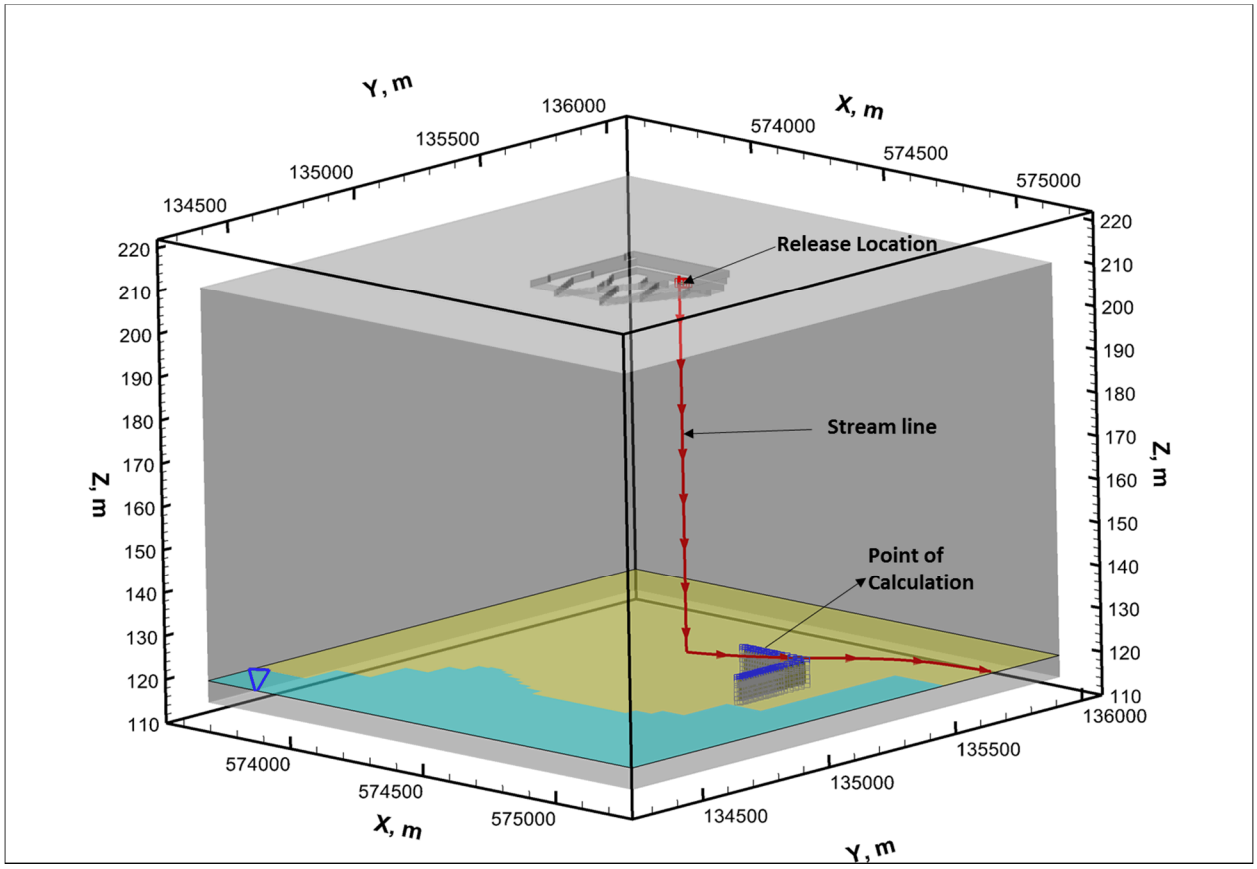

(b)

Figure D-2. Steady State Moisture Content Distribution for a Recharge Rate of 1.7 mm/yr (0.66 in./yr).

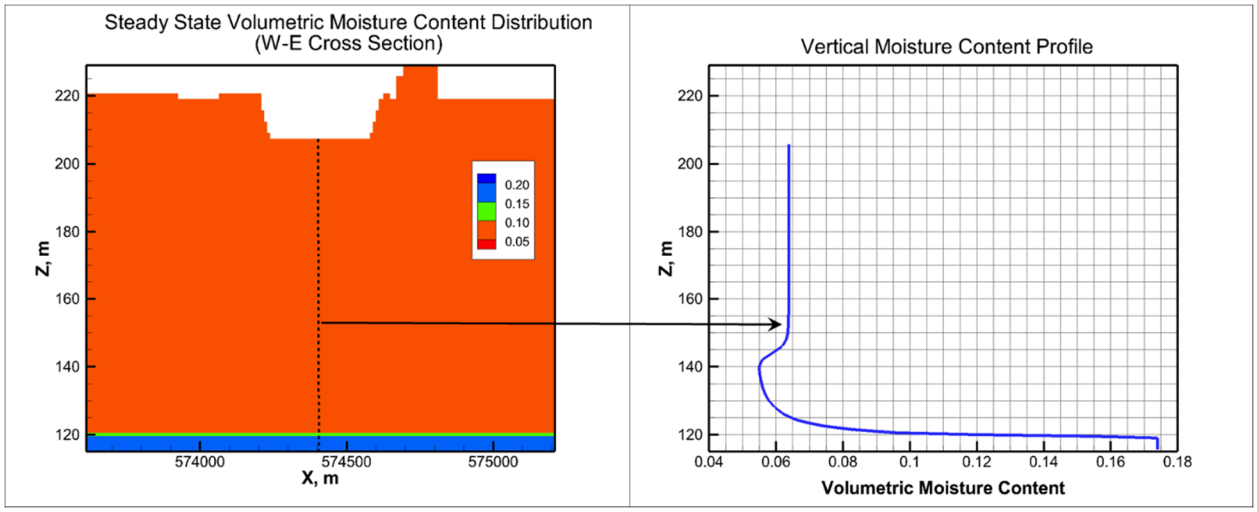

Figure D-3. Steady State Darcy Flux for a Recharge Rate of 1.7 mm/yr (0.66 in./yr).

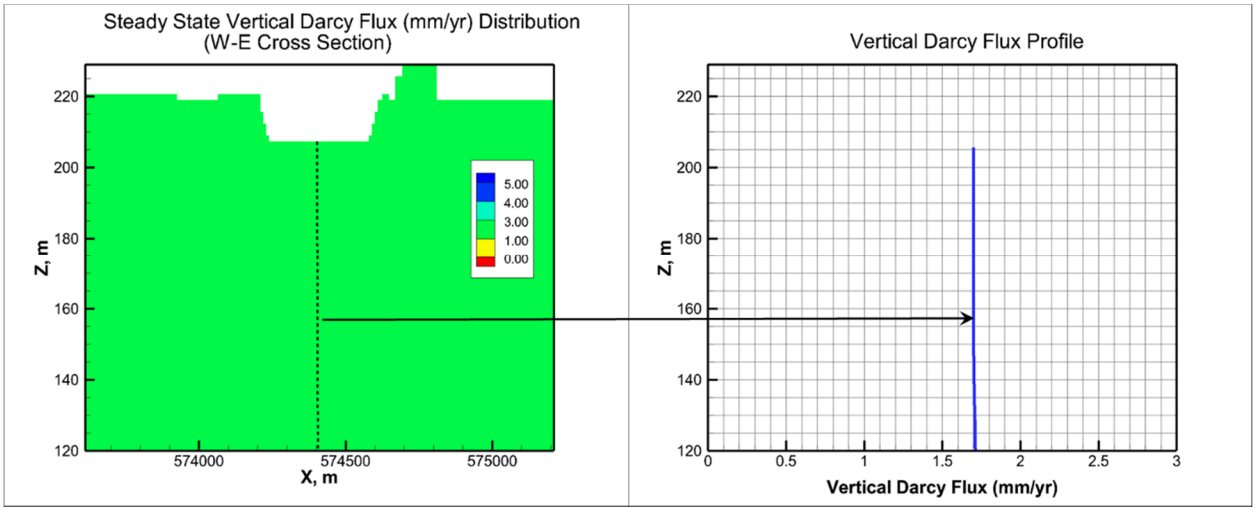

Figure D-4. Steady State Matric Potential Distribution for a Recharge Rate of 1.7 mm/yr (0.66 in./yr).

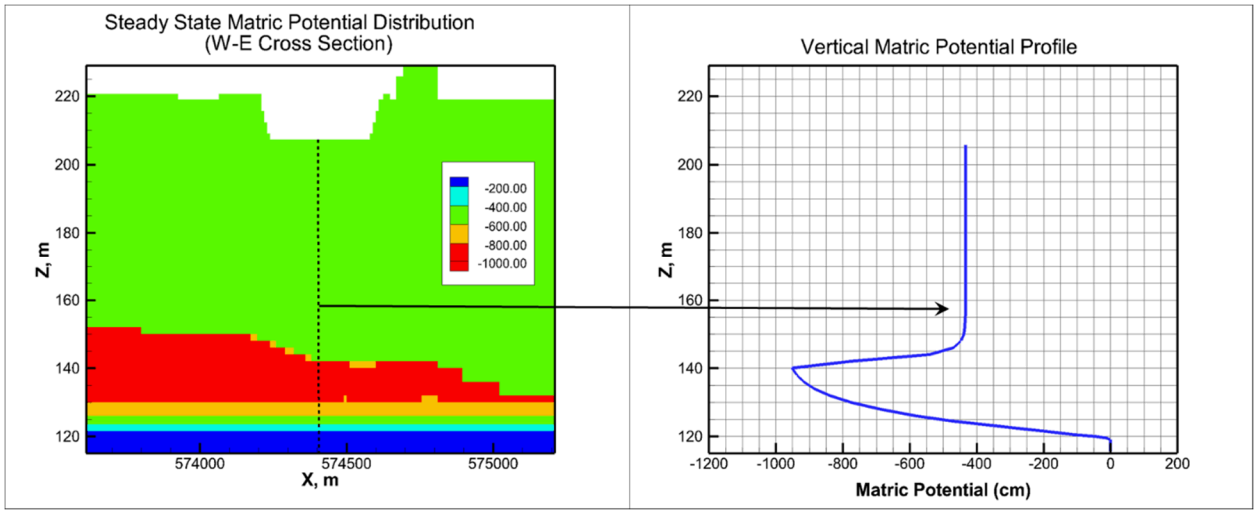

Figure D-5. Breakthrough of I-129 at Base of the Source and the Water Table.

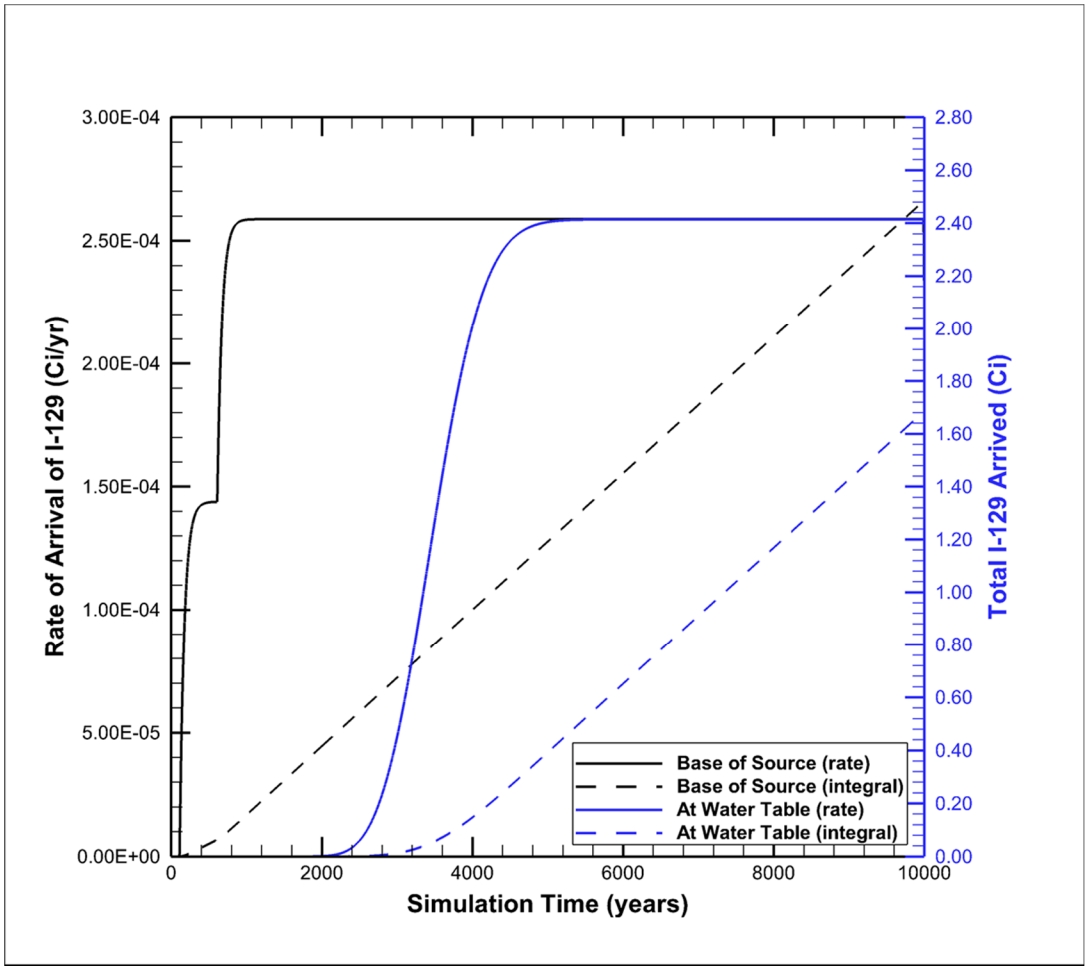

Figure D-6. I-129 Breakthrough Curve at the Point of Calculation.

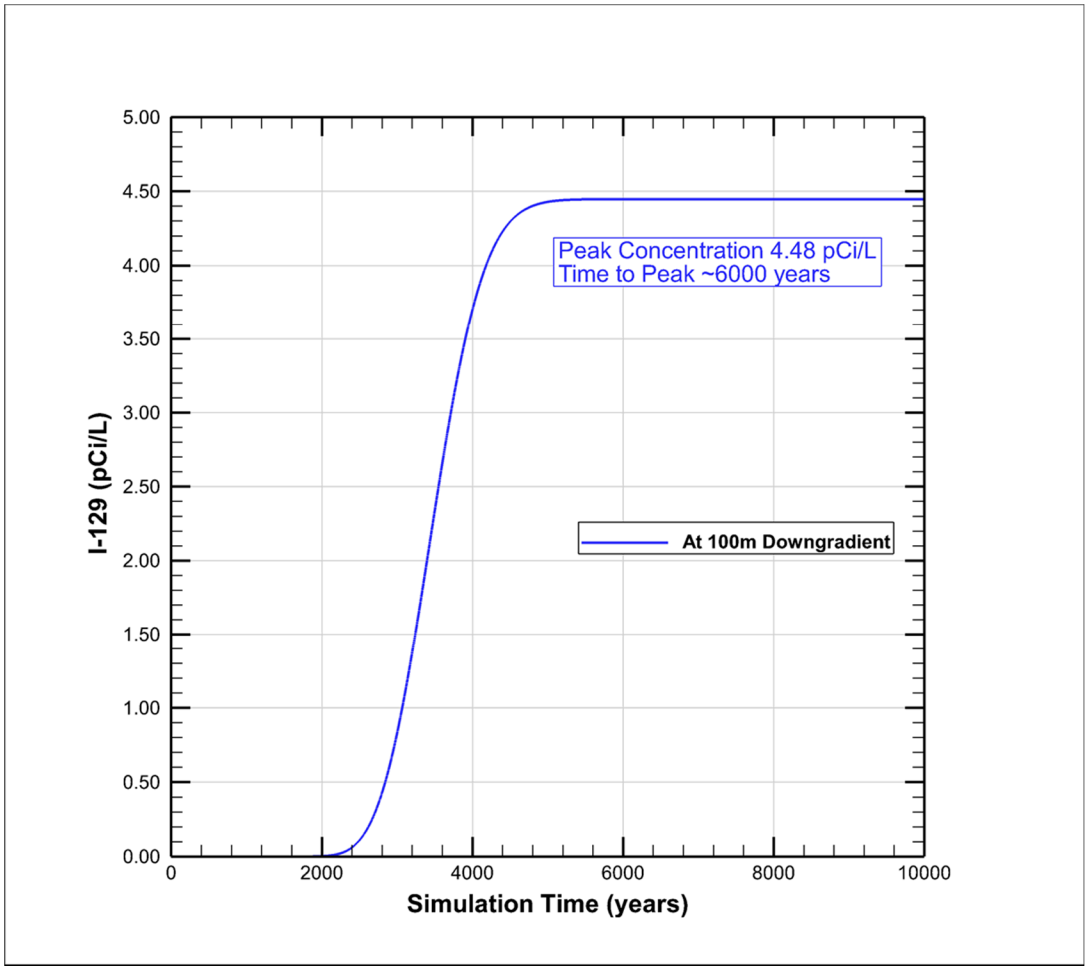

Figure D-7. Simulated I-129 Concentration Distribution at 6,000 Years.

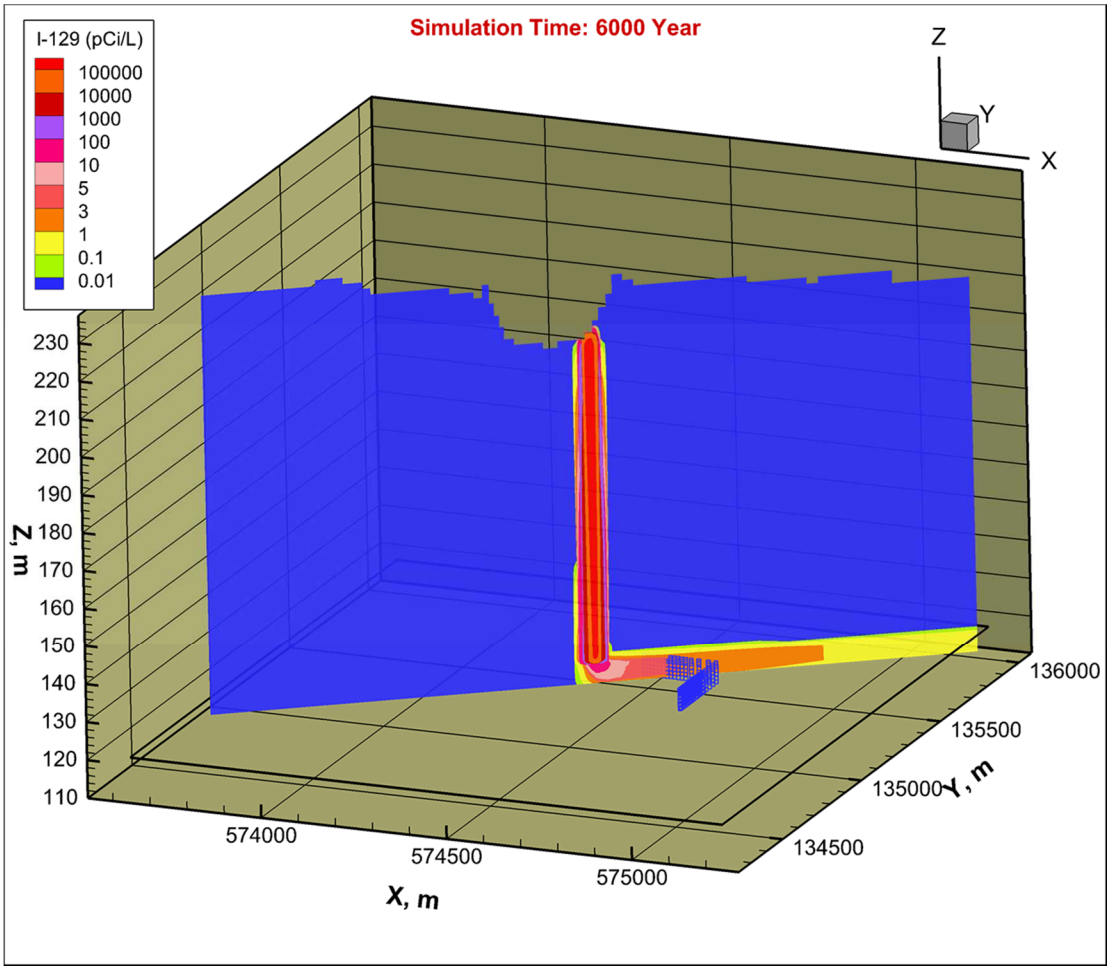

Figure D-8. Simulated I-129 Concentration Distribution at the Water Table at 6,000 Years.

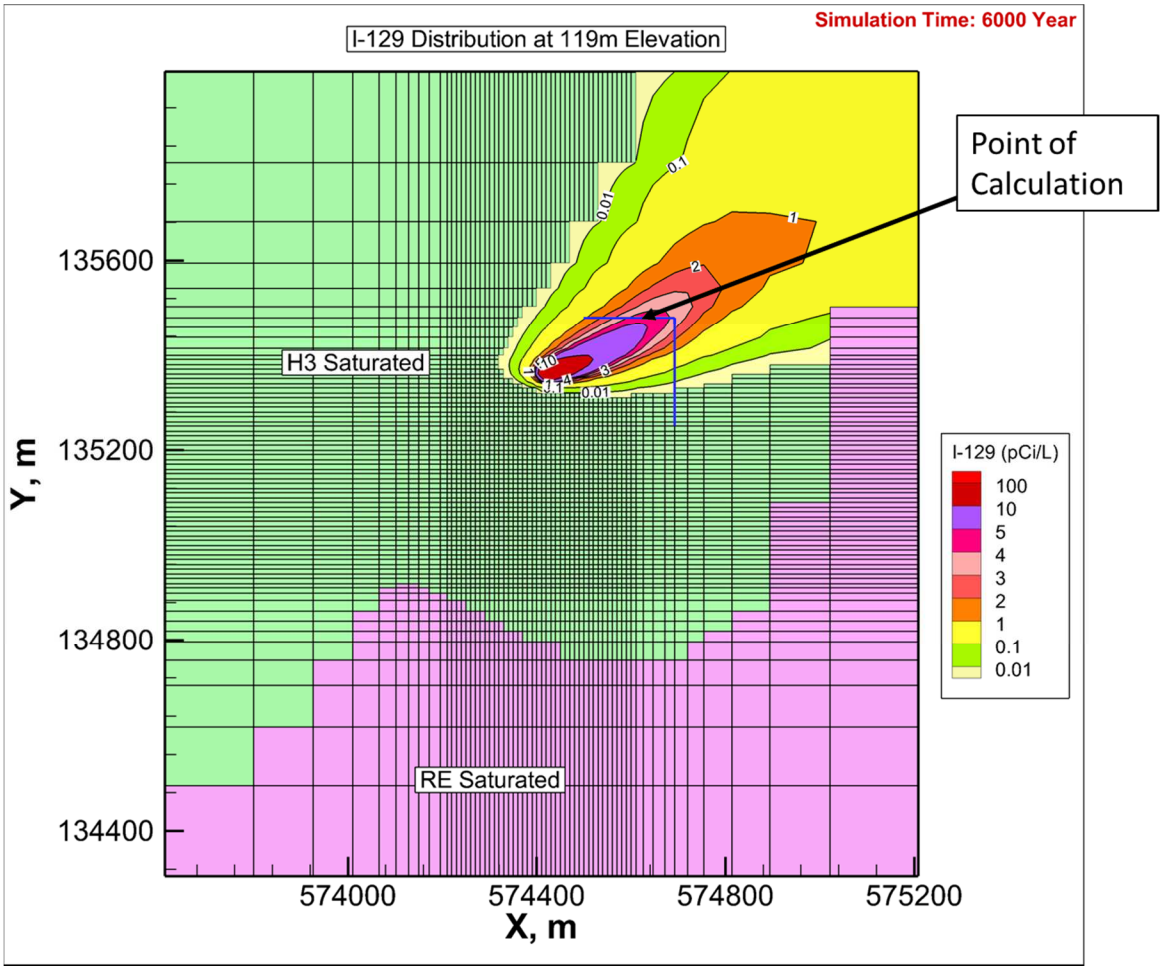

INFORMATION CLEARANCE REVIEW AND RELEASE APPROVAL

Part I: Background Information

Title: Integrated Disposal Facility Model Package Report: Vadose and Saturated Zone Flow and Transport

Publish to OSTI? ☐ Yes ☑ No

Information Category:
☐ Abstract ☐ Journal Article ☐ Summary
☐ Internet ☐ Visual Aid ☐ Software
☐ Full Paper ☑ Report ☐ Other

Trademark/Copyright "Right to Use" Information or Permission Documentation	Yes	NA
	☐	☑

Document Number: RPP-RPT-59344 Revision 0A Date: November 2016

Author: Lee, Kearn (Pat)

Part II: External/Public Presentation Information

Conference Name: Not Applicable

Sponsoring Organization(s): DOE-ORP

Date of Conference: Not Applicable Conference Location: Not Applicable

Will Material be Handed Out? ☐ Yes ☑ No Will Information be Published? ☐ Yes ☑ No *(If Yes, attach copy of Conference format instructions/guidance.)*

Part III: WRPS Document Originator Checklist

Description	*Yes*	*N/A*	*Print/Sign/Date*
Information Product meets requirements in TFC-BSM-AD-C-01?	☑	☐	Lee, Kearn (Pat) IDMS workflow data attached
Document Release Criteria in TFC-ENG-DESIGN-C-25 completed? (Attach checklist)	☑	☐	Lee, Kearn (Pat) IDMS workflow data attached
If product contains pictures, safety review completed?	☑	☐	Lee, Kearn (Pat) IDMS workflow data attached

Part IV: WRPS Internal Review

Function	*Organization*	*Date*	*Print Name/Signature/Date*
Subject Matter Expert	WRPS	07/18/2019	Lee, Kearn (Pat) Workflow data attached
Responsible Manager	WRPS	05/23/2019	Rutland, Paul L Workflow data attached
Other:			

Part V: IRM Clearance Services Review

Description	*Yes*	*No*	*Print Name/Signature*
Document Contains Classified Information?	☐	☒	If Answer is "Yes," ADC Approval Required Print Name/Signature/Date
Document Contains Information Restricted by DOE Operational Security Guidelines?	☐	☒	Reviewer Signature: Print Name/Signature/Date
Document is Subject to Release Restrictions? *If the answer is "Yes," please mark category at right and describe limitation or responsible organization below:*	☐	☒	Document contains: ☐ Applied Technology ☐ Protected CRADA ☐ Personal/Private ☐ Export Controlled ☐ Proprietary ☐ Procurement – Sensitive ☐ Patentable Info. ☐ OUO ☐ Predecisional Info. ☐ UCNI ☐ Restricted by Operational Security Guidelines ☐ Other (Specify)
Additional Comments from Information Clearance Specialist Review? *Reviewers approved Public; comments to be incorporated in future revision due to prior release in SPF.*	☒	☐	Information Clearance Specialist Approval APPROVED By Lynn M. Ayers at 10:34 am, Jul 18, 2019 Print Name/Signature/Date

When IRM Clearance Review is Complete – Return to WRPS Originator for Final Signature Routing (Part VI)

INFORMATION CLEARANCE REVIEW AND RELEASE APPROVAL

Part VI: Final Review and Approvals

Description	*Approved for Release*		*Print Name/Signature*
	Yes	*N/A*	
WRPS External Affairs	☒	☐	Roxburgh, Rob T - IDMS workflow data attached
WRPS Office of Chief Counsel	☒	☐	Cherry, Steve - IDMS workflow data attached
DOE – ORP Public Affairs/Communications	☒	☐	Levardi, Yvonne & Beeman, Melinda - Workflow data attached
Other: DOE Counsel	☒	☐	King, Grace J - IDMS workflow data attached
Other: DOE-ORP SME	☒	☐	Pyles, Gary L - IDMS workflow data attached

Comments Required for WRPS-Indicate Purpose of Document:

This model package report is being referenced by the Hanford Site hazardous chemical Cumulative Impact Evaluation. The authors of the CIE have requested that this report be added to the administrative record. A public release clearance process must be completed in order to fulfill that request.

Safety statement for photographic images: Photographic images are of rocks and soils.

APPROVED
By Lynn M. Ayers at 10:34 am, Jul 18, 2019

Approved for Public Release; Further Dissemination Unlimited

Information Release Station

Was/Is Information Product Approved for Release? ☒ Yes ☐ No

If Yes, what is the Level of Releaser? ☑ Public/Unrestricted ☐ Other (Specify) _____

Date Information Product Stamped/Marked for Release: 07/18/2019

Was/Is Information Product Transferred to OSTI? ☐ Yes ☒ No

Forward Copies of Completed Form to WRPS Originator

```
- <workflow name="(LMA) Normal - RPP-RPT-59344 Rev 0A" id="242783567">
  - <task name="Clearance Process" id="0" date-initiated="20190523T1513"
      performer="Lynn M Ayers" performer-id="212954838" username="h3998817">
      <comments>DUE: Thursday, June 13, 2019 - 2 PM Please review for public
        release, "Integrated Disposal Facility Model Package Report: Vadose and
        Saturated Zone Flow and Transport, submitted by Pat Lee for addition to
        the Administrative Record in support of the Hanford Site hazardous
        chemical Cumulative Impact Evaluation. Thank you, Lynn Ayers
        Information Clearance</comments>
    </task>
    <task name="Add XML" id="1" date-done="20190523T1514" />
    <task name="Manager Approval" id="41" date-due="20190528T1513" date-
      done="20190523T1521" performer="Paul L Rutland" performer-id="140633218"
      username="h4494439" disposition="Approve" authentication="true" />
    <task name="Document Reviewer1" id="54" date-due="20190528T1521" date-
      done="20190523T1609" performer="Rob T Roxburgh" performer-
      id="145327495" username="h6879768" disposition="Public Release"
      authentication="true" />
  - <task name="Document Reviewer2" id="53" date-due="20190528T1521" date-
      done="20190618T0629" performer="Stephen B Cherry" performer-id="1382719"
      username="h0374767" disposition="Public Release" authentication="true">
      <comments>Please correct a typo on page 15 of 128, the third paragraph
        under 3.1.1. Currently there is language that reads, "500
        0years ...."</comments>
    </task>
  - <task name="Doc Owner Clearance Review" id="13" date-due="20190619T0629"
      date-done="20190620T0827" performer="Kearn P Lee" performer-
      id="148796764" username="h8500694" disposition="Send On"
      authentication="true">
      <comments>The document has already been released in Smart Plant.
        Therefore, I cannot make editorial changes without a creating a new
        revision to the document. I would prefer not to expend the resources
        necessary to initiate a new revision to correct one typo. If ORP has
        additional comments and rejects the workflow, I will need to initiate a
        revision and will correct the typo at that time.</comments>
    </task>
    <task name="Milestone 1" id="24" date-done="20190620T0829" />
  - <task name="ORP Document Reviewer1" id="57" date-due="20190624T0829"
      date-done="20190717T0931" performer="Melinda C Beeman" performer-
      id="198738044" username="h5116897" disposition="Public Release"
      authentication="true">
      <reviewer performer="Gary L Pyles" performer-id="147601648"
        username="h6400308" />
      <reviewer performer="Grace J King" performer-id="211901436"
        username="h9807759" />
      <reviewer performer="Yvonne M Levardi" performer-id="185346745"
        username="h7131303" />
      <comments>Reviewer's Comments Date: 06/25/2019 01:47 PM Step Name:
        RPP-RPT-59344 Revision 0A Performer: Pyles, Gary (h6400308) No
        Comments Reviewer's Comments Date: 07/16/2019 08:38 AM Step
        Name: RPP-RPT-59344 Revision 0A Performer: Smith, Connie (h0035106)
        No comments. Reviewer's Comments Date: 07/17/2019 09:04 AM Step
        Name: RPP-RPT-59344 Revision 0A Integrated Performer: Levardi,
        Yvonne (h7131303) no comments ORP approved for release with the
```

consideration that changes requested by S Cherry are corrected.</comments>
</task>
<task name="**Doc Owner Reviews ORP Comments**" id="**61**" date-due="**20190718T0935**" date-done="**20190718T0858**" performer="**Kearn P Lee**" performer-id="**148796764**" username="**h8500694**" disposition="**Send On**" authentication="**true**" />
<task name="**Milestone 2**" id="**62**" date-done="**20190718T0858**" />
<task name="**Verify Doc Consistency**" id="**4**" date-due="**20190719T0858**" date-done="**20190718T0959**" performer="**Lynn M Ayers**" performer-id="**212954838**" username="**h3998817**" disposition="**Cleared**" authentication="**true**" />
</workflow>